

**SYNTHESIS AND KINETIC STUDY OF ZEOLITE Na-A
FROM THAI KAOLIN**

MS. JANJIRA WONGWIWATTANA

**A THESIS SUBMITTED IN PARTIAL FULFILLMENT OF THE REQUIREMENTS
FOR THE DEGREE OF MASTER OF SCIENCE IN CHEMISTRY
SURANAREE UNIVERSITY OF TECHNOLOGY
ACADEMIC YEAR 2002
ISBN 974-533-175-9**

การสังเคราะห์และการศึกษาจลนพลศาสตร์ของซีโอไลท์โซเดียมเอจากดินขาวของไทย

นางสาวจรรจิดา วงศ์วัฒนา

วิทยานิพนธ์นี้เป็นส่วนหนึ่งของการศึกษาตามหลักสูตรปริญญาวิทยาศาสตรมหาบัณฑิต

สาขาวิชาเคมี

มหาวิทยาลัยเทคโนโลยีสุรนารี

ปีการศึกษา 2545

ISBN 974-533-175-9

**SYNTHESIS AND KINETIC STUDY OF ZEOLITE Na-A
FROM THAI KAOLIN**

Suranaree University of Technology Council has approved this thesis,
submitted in partial fulfillment of the requirements for a Master's Degree.

Thesis Examining Committee

.....

(Asst. Prof. Dr. Malee Tangsathitkulchai)

Chairman

.....

(Asst. Prof. Dr. Kunwadee Rangriwatananon)

Thesis Advisor

.....

(Asst. Prof. Dr. Sutin Kuharuangrong)

Committee

.....

(Asst. Prof. Dr. Jatuporn Wittayakun)

Committee

.....

(Assoc. Prof. Dr. Tawit Chitsomboon)

Vice Rector for Academic Affairs

.....

(Assoc. Prof. Dr. Prasart Suebka)

Dean of Institute of Science

จรจรจิรา วงศ์วิวัฒนา: การสังเคราะห์และการศึกษาจลนพลศาสตร์ของซีโอไลต์โซเดียมเอจากดิน
ขาวของไทย (SYNTHESIS AND KINETIC STUDY OF ZEOLITE Na-A FROM THAI
KAOLIN)

อาจารย์ที่ปรึกษา: ผู้ช่วยศาสตราจารย์ ดร. กุลวดี รังษีวัฒนานนท์, 106 หน้า ISBN 974-533-175-9

ในงานวิจัยนี้ได้ศึกษาการสังเคราะห์และการศึกษาจลนพลศาสตร์ของการเกิดผลึกซีโอไลต์โซเดียมเอ (Zeolite Na-A) ด้วยดินขาวจากสามแหล่งของไทยคือ ลำปาง ระนองและนราธิวาส รวมทั้งศึกษาปัจจัยต่างๆที่มีผลต่อการสังเคราะห์ เช่น แหล่งของดินขาว การเผาดินขาว ความเข้มข้นของเบส อุณหภูมิและเวลาในการเกิดปฏิกิริยา เป็นต้น การสังเคราะห์ทำโดยนำดินขาวจากแหล่งต่างๆไปเผาที่อุณหภูมิ 600°C เป็นเวลา 1 ชั่วโมง และนำไปทำปฏิกิริยากับสารละลาย NaOH ที่ความเข้มข้น 10% w/v ที่อุณหภูมิ 100°C เพื่อให้ทราบถึงผลกระทบของชนิดดินขาว และได้้นำผลผลิตที่ได้ไปวิเคราะห์ด้วย X-ray Diffraction (XRD), Infrared Spectroscopy (IR) และ Scanning Electron Microscope (SEM) พบว่าองค์ประกอบของดินขาวมีผลกระทบต่อ การสังเคราะห์ กล่าวคือ ดินขาวจากลำปางให้ผลผลิตน้อย เนื่องจากประกอบด้วยควอร์ตซ์เป็นจำนวนมาก เมื่อเทียบกับแหล่งอื่น ๆ คือระนอง และ นราธิวาส ซึ่งให้ผลผลิตเป็นที่น่าพอใจ หลังจากนั้นได้เลือกดินขาวจากนราธิวาสเพื่อเป็นตัวแทนในการศึกษาปัจจัยอื่นๆ เพื่อเปรียบเทียบอุณหภูมิในการเผา เผาดินขาวที่อุณหภูมิต่าง ๆ คือ 500, 600, 700, 800 และ 900 °C และนำไปสังเคราะห์โดยใช้ NaOH 10% w/v ที่อุณหภูมิ 100°C พบว่าอุณหภูมิที่เหมาะสมที่สุดในการเผาดินขาวคือ 700 °C และได้ใช้อุณหภูมิดังกล่าวในการศึกษาจลนพลศาสตร์ โดยใช้ความเข้มข้นของเบส NaOH ต่างๆกันดังนี้คือ 10, 15, 20 และ 25% w/v ส่วนอุณหภูมิที่ใช้ในการสังเคราะห์คือ 70, 80, 90 และ 100°C ได้วิเคราะห์ผลการทดลองจากความสัมพันธ์ร้อยละของการเกิดผลึกกับเวลาพบว่า การเกิดผลึกขึ้นอยู่กับความเข้มข้นของ NaOH และ อุณหภูมิที่ใช้ในการสังเคราะห์ กล่าวคือ อัตราการเกิดผลึกเร็วขึ้นเมื่อเพิ่มความเข้มข้นของ NaOH หรือเพิ่มอุณหภูมิ อย่างไรก็ตาม การเกิดผลึกซีโอไลต์ได้ลดลงเมื่อความเข้มข้นของ NaOH และ อุณหภูมิในการสังเคราะห์สูงเกินไปเนื่องจากการเกิดโซคาไลต์ขึ้นแทน

สำหรับสภาวะที่เหมาะสมคือที่ความเข้มข้น NaOH 10-15% และอุณหภูมิ 70-80°C จะได้ผลิตภัณฑ์โอไลต์ 80-85% เมื่อวิเคราะห์ด้วยแปรจลนพลศาสตร์จากการทดลองโดยใช้สมการ Avrami พบว่า การเกิดผลิตภัณฑ์ได้เปลี่ยนไปตามเงื่อนไขต่างๆ โดยเลขยกกำลัง Avrami มีค่าในช่วง 3-6 พลังงานก่อกัมมันต์ในการตกผลึกมีค่าในช่วง 9.9-13.8 kcal/mol ซึ่งมีค่าค่อนข้างสูงเพราะเป็นผลเนื่องจากการเกิดโซดาไลต์ส่วนพลังงานก่อกัมมันต์ให้เริ่มเกิดเม็ดผลึกมีค่าในช่วง 12.7-16.7 kcal/mol

สาขาวิชาเคมี

ปีการศึกษา 2545

ลายมือชื่อนักศึกษา.....

ลายมือชื่ออาจารย์ที่ปรึกษา.....

ลายมือชื่ออาจารย์ที่ปรึกษาร่วม.....

ลายมือชื่ออาจารย์ที่ปรึกษาร่วม.....

JANJIRA WONGWIWATTANA: SYNTHESIS AND KINETIC STUDY OF
ZEOLITE Na-A FROM THAI KAOLIN

THESIS ADVISOR: ASST. PROF. KUNWADEE RANGSRIWATANANON, Ph. D.

106 PP. ISBN 974-533-175-9

In this work, the synthesis and kinetic study of hydrothermal formation of zeolite Na-A from Thai kaolin of Lampang, Ranong, and Narathiwat provinces have been examined. The factors affecting the synthesis such as source of kaolin samples, calcination of kaolin samples, concentration of alkalinity, reaction temperature and time were investigated. The kaolin samples were calcined at 600 °C to study the effect of kaolin source. The hydrothermal synthesis reactions of the calcined samples were accomplished in NaOH solution of 10% w/v at the reaction temperature of 100 °C. The products were characterized by x-ray diffraction (XRD), infrared spectroscopy (IR), and scanning electron microscopy (SEM). The results of the experiments showed that Lampang kaolin was not suitable for the synthesis of zeolite due to high quartz concentration. On the other hand, Narathiwat, and Ranong kaolin samples gave satisfactory synthesis results. To study the effect of calcination temperature, Narathiwat kaolin sample was used as the starting material. The synthesis reactions were prepared by calcining the kaolin samples at different temperatures of 500, 600, 700, 800, and 900 °C. The samples were treated with 10% w/v NaOH concentration and the reaction temperature of 100 °C. The results showed that the calcination of kaolin sample at 700 °C was the suitable condition for the synthesis of zeolite Na-A. The kinetic experiments were performed by calcining Narathiwat kaolin samples at 700 °C and hydrothermal reacted with various NaOH concentrations of 10, 15, 20, and 25%w/v at different temperatures of 70, 80, 90, and 100 °C. The analysis of the experimental results indicated that the crystallization of zeolite depended on the concentration of NaOH solution and reaction temperature. The rate of crystallinity increased with increasing NaOH concentration and reaction temperature. However, higher concentration of NaOH and reaction temperature produced lower percentage of zeolite crystallinity due to the stable phase of sodalite taking place.

Under suitable conditions, at NaOH concentration between 10, and 15% w/v and reaction temperature of 70, and 80°C , the ranges of percentage of crystallinity of the solid product were 80-85%. The kinetic parameters were deduced from the experiments using Avrami equation. The formation mechanisms of zeolite Na-A depended on the nature and condition of crystal growth. The Avrami exponent which related to the crystallization process were about 3-6. The activation energies of crystallization were 9.9-13.8 kcal/mol. The sodalite forming also accounted for the apparently high activation energy. The activation energies for nucleation were about 12.7-16.7 kcal/mol.

School of Chemistry
Academic Year 2002

Student.....
Advisor.....
Co-advisor.....
Co-advisor.....

Acknowledgements

I wish to express my deep appreciation to my thesis advisor, Assistant Professor Dr. Kunwadee Rangsiwatananon for her guidance and encouragement on each step of work. Also I would like to thank Assistant Professor Dr. Sutin Kuharuangrong and Assistant Professor Dr. Jatuporn Wittayakun for serving as the co-advisors in my thesis committee. I would like to thank Assistant Professor Dr. Malee Tungsathitkulchai for serving as the chairman of the committee. I am grateful to Assistant Professor Dr. Tritaporn Choosri for the support and the permission to use the standard reference materials for XRF analysis.

I wish to thank all lecturers at the school of chemistry for their good attitude and useful advice, all of the staffs at the Center for Scientific and Technological Equipment for their assistance and suggestion for the use of XRF, XRD, IR, AAS, and SEM, and all of my good friends for their kindness. At the end, I would like to thank my family for their understanding, encouragement and support during the whole period of my education.

Janjira Wongwiwattana

Contents

Abstract (Thai)	I
Abstract (English)	III
Acknowledgement	V
Contents	VI
List of Figures	IX
List of Tables	IV
List of Abbreviations	XV
Chapters	
I Introduction	1
1.1 Zeolite.....	2
1.2 Zeolite Na-A structure.....	5
1.3 Zeolite Na-A applications.....	6
1.3.1 Ion exchange.....	7
1.3.2 Catalysis.....	7
1.3.3 Adsorption and separation.....	7
1.4 Kaolinite.....	7
1.5 Mechanism of zeolite crystallization.....	9
1.5.1 Achievement of supersaturation.....	9
1.5.2 Nucleation	10
1.5.3 Crystal growth.....	10
1.6 Avrami theory.....	11
1.7 Characterization techniques.....	13
1.7.1 Atomic adsorption spectroscopy.....	13
1.7.2 X-ray fluorescence	14
1.7.3 Powder X-ray diffraction	15

Contents (Continued)

1.7.4 Fourier transform infrared spectroscopy.....	16
1.7.5 Scanning electron microscope.....	17
1.8 Literature reviews.....	19
1.9 Research objectives.....	21
II Materials, Instrumentation, and Methods.....	22
2.1 Material lists.....	22
2.1.1 Chemicals and Materials.....	22
2.1.2 Glass wares.....	23
2.1.3 Apparatuses	23
2.2 Instrumentation.....	24
2.2.1 X-ray fluorescence spectrometer.....	24
2.2.2 Atomic adsorption spectrometer.....	25
2.2.3 Powder x-ray diffractometer.....	25
2.2.4 Fourier transform infrared spectroscopy.....	27
2.2.5 Scanning electron microscopy.....	27
2.3 Experimental methods.....	27
2.3.1 Kaolin preparation	27
2.3.2 The zeolite Na-A synthesis method.....	28
2.3.3 Kinetic study.....	30
2.3.4 Ion exchange capability.....	30
III Results and Discussion.....	31
3.1 Kaolin composition analysis	31
3.2 Characterization of kaolin and metakaolinite.....	32
3.2.1 Kaolin characterization.....	32
3.2.2 Metakaolinite characterization.....	36
3.3 The synthesis of zeolite Na-A.....	40
3.3.1 The effect of kaolin source.....	40

Contents (Continued)

3.3.2 The effect of calcination temperature.....	53
3.3.3 The effect of alkalinity concentration and reaction temperature.....	56
3.4 Kinetic study result.....	66
3.4.1 Determination of the Avrami exponent.....	66
3.4.2 Determination of rate constant.....	68
3.4.3 Determination of activation energy(E_a) of zeolite Na-A crystallization...69	
3.4.4 Determination of activation energy(E_n) of nucleation zeolite Na-A.....	71
3.5 Ion exchange capability.....	73
IV Conclusions	75
References	76
Appendices	81
Appendix A Atlas of zeolite structure types.....	81
Appendix B Simulated XRD powder patterns for zeolites.....	85
Appendix C XRD powder patterns of the solid products.....	90
Curriculum Vitae	106

List of Figures

Figure	Page
1.1 Primary building unit of zeolite structure.....	3
1.2 Secondary building unit (SBUs) of zeolite structure.....	3
1.3 Framework of zeolite Linde type A.....	5
1.4 Representation of the structure of zeolite LTA and hydroxy-sodalite.....	6
1.5 Crystal lattice of kaolinite	8
1.6 The solubility-supersaturation diagram.....	9
1.7 (a) An atom in the ground state is excited by a photon with the same energy as the energy gap resulting in the final excited state. (b) A simplified diagram of AAS.....	13
1.8 The process of emission of characteristic X-ray.....	15
1.9 (a) Different crystal planes diffract X –ray at different angles (b) The diffraction spectra may be depicted by a plot of intensity and diffracted angle.....	16
1.10 A simplified diagram of SEM.....	18
2.1 (A) The apparatus of fusion machine and (B) sample disks.....	24
2.2 Apparatus set for powder XRD sample preparation.....	26
2.3 The apparatus for zeolite Na-A synthesis.....	29
3.1 Powder XRD patterns of Lampang, Narathiwat, and Ranong kaolin samples Compared with the standard pattern from JCPDS database.....	33
3.2 IR transmission spectra of kaolin from three provinces: Lampang, Ranong, and Narathiwat.....	34
3.3 SEM micrographs of the kaolin samples taken at 12 kV and 8,000 magnification....	35
3.4 Powder XRD patterns of kaolin samples after calcinations at 500, 600, 700, 800, And 900°C compared to the raw samples.....	37

List of Figures (Continued)

Figure	Page
3.5	IR transmission spectra of kaolin samples after calcinations at 500, 600, 700, 800, and 900°C compared to the raw samples.....39
3.6	Powder XRD patterns of solid phase samples obtained during the synthesis of zeolite Na-A from Lampang, Ranong, and Narathiwat samples.....41
3.7	Plot of XRD crystallinity of zeolite Na-A with time during the synthesis using kaolin from Lampang, Ranong, and Narathiwat..... 42
3.8	IR absorption bands of standard zeolite Na-A.....42
3.9	IR transmission spectra of solid sample obtained from the synthesis of zeolite Na-A from Thai kaolin at various times.....44
3.10	IR result for percentage of crystallinity of solid samples obtained from the synthesis of zeolite Na-A from Thai kaolinite at various times.....45
3.11	SEM micrographs of solid phases obtained in the synthesis of zeolite Na-A from Lampang kaolin activated at 600 °C with 10% w/v NaOH and reaction temperature 100 for various times.....46
3.12	SEM micrographs of solid phases obtained in the synthesis of zeolite Na-A from Ranong kaolin activated at 600 °C with 10% w/v NaOH and reaction temperature 100 for various times.....47
3.13	SEM micrographs of solid phases obtained in the synthesis of zeolite Na-A from Narathiwat kaolin activated at 600 °C with 10% w/v NaOH and reaction temperature 100 for various times.....48
3.14	XRD spectra of the synthetic products using Narathiwat kaolin calcined at 500 °C..... 49
3.15	SEM micrographs of the synthetic products using Narathiwat kaolin calcined at 500 °C.....50
3.16	Evolution of zeolite Na-A XRD peaks during the synthesis when using Narathiwat Kaolin activated at 600, 700, 800, and 900 °C..... 51
3.17	Percentage of crystallinity for different calcination temperature deduced from XRD.. 52

List of Figures (Continued)

Figure	Page
3.18	The evolution of IR spectra during the synthesis of zeolite Na-A from metakaolinite: The positions of adsorption bands are labeled. The bands evolution directions are indicated by arrows from metakaolinite to zeolite Na-A spectra. The synthesis condition was 10% w/v NaOH, with 70°C reaction temperature.....53
3.19	SEM micrographs of the solid phases obtained in the synthesis of zeolite Na-A from Narathiwat metakaolinite calcined at 700°C with 10% w/v NaOH and reaction temperature 100°C for various times.....54
3.20	The percentage of crystallinity of zeolite Na-A obtained from the reaction of Narathiwat kaolin activated at 700°C with NaOH concentration of 10, 15, 20, and 25% w/v at the reaction temperature of 70°C57
3.21	The percentage of crystallinity of zeolite Na-A obtained from the reaction of Narathiwat kaolin activated at 700°C with NaOH concentration of 10, 15, 20, and 25% w/v at the reaction temperature of 80°C57
3.22	The percentage of crystallinity of zeolite Na-A obtained from the reaction of Narathiwat kaolin activated at 700°C with NaOH concentration of 10, 15, 20, and 25% w/v at the reaction temperature of 90°C58
3.23	The percentage of crystallinity of zeolite Na-A obtained from the reaction of Narathiwat kaolin activated at 700°C with NaOH concentration of 10, 15, 20, and 25% w/v at the reaction temperature of 100°C58
3.24	The percentage of crystallinity of zeolite Na-A obtained from the reaction of Narathiwat kaolin activated at 700°C with reaction temperature of 70, 80, 90, and 100°C at 10% w/v NaOH concentration59
3.25	The percentage of crystallinity of zeolite Na-A obtained from the reaction of Narathiwat kaolin activated at 700°C with reaction temperature of 70, 80, 90, and 100°C at 15% w/v NaOH concentration60

List of Figures (Continued)

Figure	Page
3.26	The percentage of crystallinity of zeolite Na-A obtained from the reaction of Narathiwat kaolin activated at 700 ⁰ C with reaction temperature of 70, 80, 90, and 100 ⁰ C at 20% w/v NaOH concentration60
3.27	The percentage of crystallinity of zeolite Na-A obtained from the reaction of Narathiwat kaolin activated at 700 ⁰ C with reaction temperature of 70, 80, 90, and 100 ⁰ C at 25% w/v NaOH concentration61
3.28	The percentage of crystallinity of zeolite Na-A obtained from the reaction of Narathiwat kaolin activated at 700 ⁰ C with NaOH concentration of 10, 15, 20, and 25% w/v at the reaction temperature of 70 ⁰ C61
3.29	The percentage of crystallinity of zeolite Na-A obtained from the reaction of Narathiwat kaolin activated at 700 ⁰ C with NaOH concentration of 10, 15, 20, and 25% w/v at the reaction temperature of 80 ⁰ C62
3.30	The percentage of crystallinity of zeolite Na-A obtained from the reaction of Narathiwat kaolin activated at 700 ⁰ C with NaOH concentration of 10, 15, 20, and 25% w/v at the reaction temperature of 90 ⁰ C62
3.31	The percentage of crystallinity of zeolite Na-A obtained from the reaction of Narathiwat kaolin activated at 700 ⁰ C with NaOH concentration of 10, 15, 20, and 25% w/v at the reaction temperature of 100 ⁰ C63
3.32	XRD pattern of the solid phase obtained in the synthesis of zeolite Na-A from Narathiwat kaolin activated at 700 ⁰ C with 25% w/v NaOH at reaction Temperature 100 ⁰ C.....65
3.33	XRD results of the plot for ln(-ln(1- α)) versus ln t obtained in the synthesis of zeolite Na-A from Narathiwat kaolin activated at 700 ⁰ C with 10% w/v NaOH.....66
3.34	Plot of conversion factors and time for the hydrothermal experiment obtained from Narathiwat activated at 700 ⁰ C with 10% NaOH at different reaction temperatures.....68

List of Figures (Continued)

Figure		Page
3.35	The XRD measurement result of $-\ln k$ versus $1/T$ obtained in the synthesis of zeolite Na-A from Narathiwat kaolin activated at 700°C with 10, 15, and 20% w/v NaOH at different temperatures.....	70
3.36	The plot of $\ln t_0$ versus $1/T$ obtained in the synthesis of zeolite Na-A from Narathiwat kaolin activated at 700°C with 10, 15, and 20% w/v NaOH at different temperatures.....	72

List of Tables

Table	Page
1.1	Simple zeolite SBUs and their Shorthand notation.....4
1.2	Exponents n of the Avrami equation for different nucleation and growth mechanism..12
2.1	Process and heating programs for acid digestion method25
2.2	Sampling periods for various experiments30
3.1	The chemical compositions, LoI and Si/Al ratios of kaolin samples from three provinces determined by XRF.....31
3.2	The concentration of Si, Al, and Fe of kaolin samples from three provinces as determined by AAS.....32
3.3	Identifications of IR adsorption bands to specific vibrations..... 34
3.4	IR vibration bands of zeolite Na-A..... 43
3.5	The maximum yield of zeolite Na-A from various experiment conditions from XRD64
3.6	The maximum yields of zeolite Na-A from various experiment conditions from IR50
3.7	The analytical result of the Avrami exponents for the growth of zeolite Na-A from Narathiwat kaolin activated at 700°C at various conditions.....67
3.8	The analytical result of the rate constant, k, and fitting coefficient, R for the growth of zeolite Na-A from Narathiwat kaolin activated at 700°C at various conditions.....69
3.9	The analytical result of the apparent activation energy, E_a and fitting coefficient, R for the growth of zeolite Na-A from Narathiwat kaolin activated at 700°C at various conditions.....71
3.10	Activation energy of the nucleation process calculated from the induction periods..... 73
3.11	Calcium ion exchange capacity of the synthesis product, resin and standard zeolite Na-A.....74

List of Abbreviations

XRD	x-ray diffractometer
AAS	atomic absorption spectrometer
XRF	x-ray fluorescence
IR	Infrared
SEM	scanning electron microscope
$^{\circ}\text{C}$	degree celcius
K	degree kelvin
Å	angstrom
g	gram
ml	millilitre
mg	milligram
µm	micrometer
mm	millimetre
h	hour
min	minute
sec.	second
kv	kilovolt
mA	milliampare
cps	count per second
cm^{-1}	per centimeter
abs	absorbance
%T	percent transmittance
w/v	weight by volume
SBU	secondary building unit
HS	hydroxy-sodalite
e.g	for example
et al	et alia (and others)

Chapter I

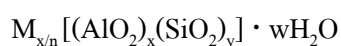
Introduction

Zeolite Na-A has gained a spot light attention from the chemical industries due to specialties in its properties. Since it is used as the main work horse in many applications, the productions of this kind of zeolite are on the massive scale in many countries. In general, it can be synthesized from kaolin. Therefore, the economical value of kaolin is elevated along with the popularity of zeolite Na-A. There are many reports published internationally about the synthesis zeolite Na-A due to high driving force from the industrial sector in the foreign countries especially in USA, Europe, and Japan. In general, locally obtained raw materials means the advantage in the reduction of operating budget thus improving the firm's competitiveness. In Thailand, historically, kaolin had found its main use in the production of ceramics. Geographically, kaolin was found in several parts of Thailand such as Lampang, Narathiwat and Ranong. The main question is weather Thai kaolin can be used as the raw material for the synthesis of zeolite Na-A. This research was set to investigate the possibility of using Thai kaolin as the starting material for the synthesis of zeolite Na-A. One can wish that the positive findings from this work may provide some valuable information and slightly pave the way for Thailand's large-scale zeolite production industry. Along the way, the scientific study on the kinetic of the crystallization process was also aimed.

This thesis is divided into four chapters: introduction, materials and methods, results and discussion and conclusion. In this chapter, the introduction, some basic pieces of information on zeolite Na-A and kaolin are described and the related literatures are reviewed to build the case for research objectives.

1.1 Zeolite

Zeolites are crystalline aluminosilicates with uniform pores, channels and cavities. The structure of zeolites contains aluminum, silicon, and oxygen in regular frameworks with cations and water in the pores. The silicon and aluminum are tetrahedrally coordinated with each other through shared oxygen atoms. Each AlO_4 tetrahedron in the framework bears a net negative charge which is balanced by a cation. The structure formula of zeolite is based on the crystallographic unit cell, the smallest unit of structure, represented as (King, R. B.1994, and Bekkum, V. H.,1991).



where M is an alkali or alkaline earth cation, n is the valence of the cation, w is the number of water molecules per unit cell, x and y are the total number of tetrahedra per unit cell, and the ratio y/x usually has values of 1 to 5. In the case of the high silica zeolite, y/x can be ranging from 10 to 100.

Zeolites have an open-structure framework consisting of many channels and interconnected voids which are occupied by cations and water molecules. The cations can be exchanged with other types of cations when aqueous passed through channels and voids. The ion exchange characteristic of zeolite has been used in water softening and water treatment processes. Na^+ ions in zeolite can be exchanged with Ca^{2+} ions, in hard water, hence softened the water. In addition, other heavy metal cations such as Hg^{2+} , Cd^{2+} , and Ag^+ can be also exchanged in the same manner. Zeolite has a reversible dehydration property. When zeolite is heated, the adsorbed water molecules will evaporate but the dehydrated structure will not be deformed or damaged. After dehydration the voids and channels can be refilled with water molecules again (King, R. B.1994, and Bekkum, V. H.,1991).

Each type of zeolite has specific uniform pore size, for instance, 3.5-4.5 Å for zeolite LTA, 4.5-6.0 Å for ZSM-5 and 6.0-8.0 Å for zeolite X, Y type. Therefore, zeolites are better molecular sieve than other adsorbents such as activated carbon, activated alumina, or silica gel in which pore sizes are not uniform and pore size distribution are broad (Bekkum, V. H.,1991).

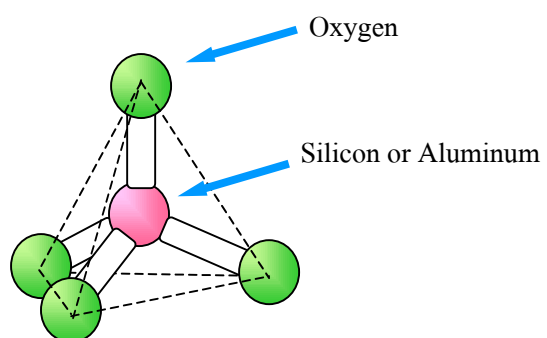


Figure 1.1 Primary building unit of zeolite structure.

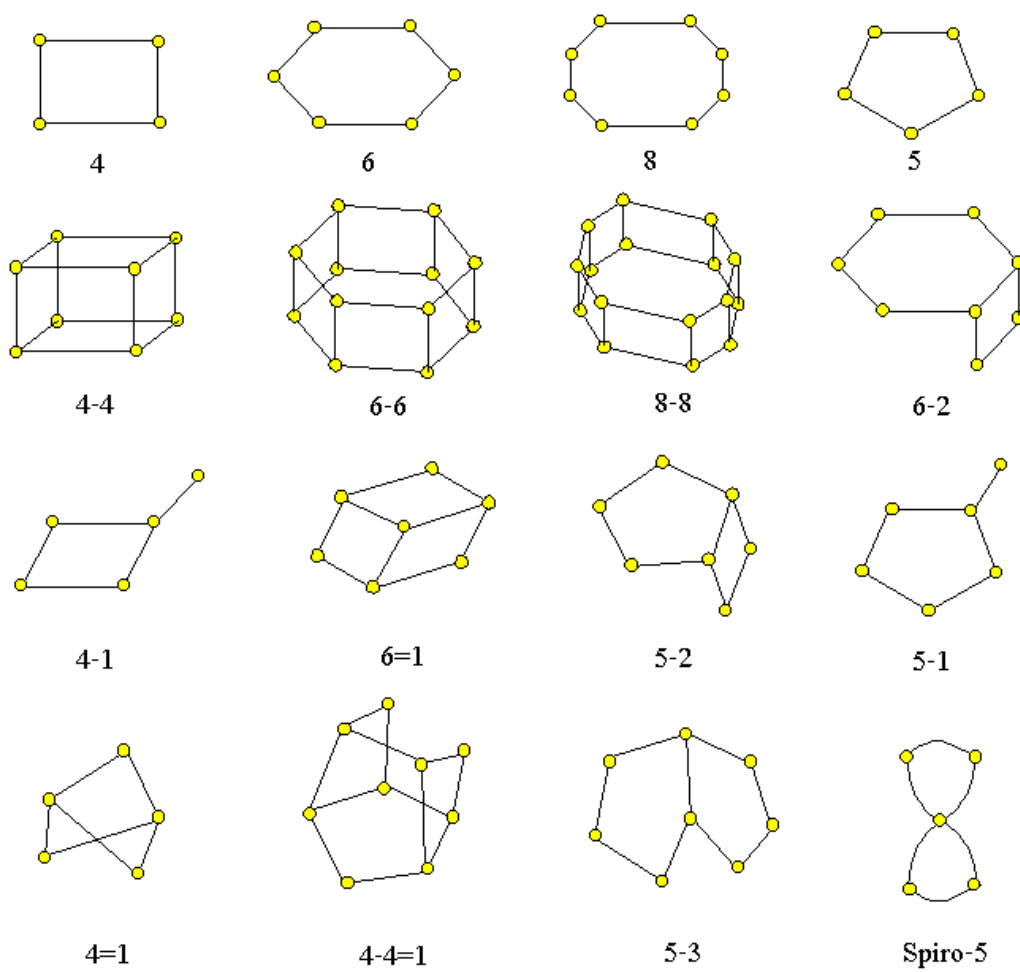


Figure 1.2 Secondary building unit (SBUs) of zeolite structure.

Zeolites primary structures are tetrahedra of SiO_4 and AlO_4 shown in figure 1.1. Each sub unit contains the pores and cavities within the frameworks, which were called secondary building units (SBUs) and illustrated in figure 1.2. The SBUs can be simple arrangements of tetrahedra such as four, six, or eight-membered ring or more complex structure. Some simple zeolite SBUs and their shorthand notations are given in table 1.1 (King, R. B 1994).

Table 1.1 Simple zeolite SBUs and their shorthand notations.

Number of linked tetrahedra	SBU created	Shorthand description ¹
4	4oxygen ring	S4R
5	5oxygen ring	S5R
6	6 oxygen ring	S6R
8	8 oxygen ring	S8R
8	4-4 oxygen rings	D4R
12	6-6 oxygen rings	D6R
16	8-8 oxygen rings	D8R

¹ S = single, D = double, R = ring.

There are two kinds of zeolite, natural and synthetic zeolite. Natural zeolites are processed from natural ore bodies. It is mainly found in the voids of basalt and volcanic rocks. The natural zeolite structure has more acid resistant so it does not break down in mildly acid environment. Therefore the natural zeolites are broadly used in the agricultural industry. Since the discovery of molecular sieve and ion exchange properties, they have been used as molecular sieve adsorbents in the natural gas industry, ammonia industry and water treatment. Natural zeolites have also found applications in paper, cements and concrete industries, which represent the major volume applications for natural zeolites. The examples of natural zeolites are Chabazite, erionite, mordenite and gmelinite etc.

Synthetic zeolites are mainly manufactured from energy consuming chemical. Zeolites can be synthesized from reactive starting materials such as freshly coprecipitated gels (sodium silicate and sodium aluminate), or amorphous solids (kaolinite, perlite, halloysite, etc.) by controlling the condition to form uniform growth of crystal such as (a) relatively high pH introduced in the form of an alkali metal hydroxide or other strong base (b) low temperature hydrothermal conditions with concurrent low autogeneous pressure at saturated water vapor or (c) a high degree of super-saturation of the components of the gel leading to the nucleation of a large number of crystals (Breck, D. W., 1974). The formation of zeolite can be influenced by several factors such as (a) the nature of the reactants and their pretreatment (b) the process in which the reactant mixture is made and pretreated and its overall chemical composition (c) homogeneity or heterogeneity of the mixture (d) pH of the mixture (e) low temperature aging of gels (f) seeding (g) addition of special additive or (h) temperature and pressure (Barrer, R. M., 1958). The examples of synthetic zeolites are zeolite A, X, Y, L, etc.

1.2 Zeolite Na-A structure

Zeolite Na-A is the simplest synthetic zeolite with a molecular ratio of one silicon to one aluminium to one sodium cation. Zeolite Na-A exhibits the LTA (linde type A) structure. It has a cubic structure as shown in figure 1.3 (Szostak, R. 1992, and Muller, J. C. M., 1998).

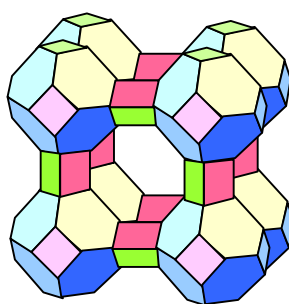


Figure 1.3 Framework of zeolite Linde Type A

The pseudo unit cell of zeolite Na-A consists of 12 SiO_2 and 12 AlO_2 unit , with enclosing a large cavity (α cage) with diameter 11.4 Å and small cavity (β cage) with diameter 6.6 Å, with a pore window opening of 4.1 Å. The chemical composition of pseudo unit cell is $\text{Na}_{12}[\text{Al}_{12}\text{SiO}_{12}\text{O}_{48}] \cdot 27\text{H}_2\text{O}$. It is 1/8 of the true unit cell.

Zeolite Na-A is constructed from structures of hydroxysodalite (SOD) sharing with bridging oxygen ion between oxygen four atoms and SOD structure is constructed from sodalite cage. The relatively simple structure of sodium zeolite LTA and the related hydroxysodalite (SOD) are shown in figure 1.4. The lines represent Al-O-Si linkages (Walton, R. I., 2001).

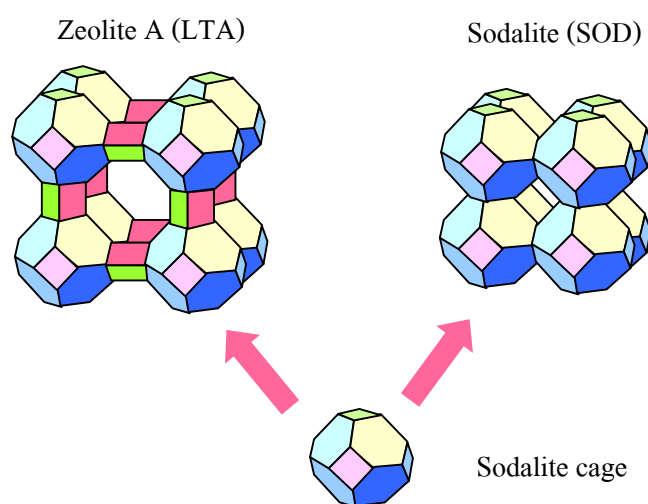


Figure 1.4 Representation of the structure of zeolite LTA and hydroxysodalite

1.3 Zeolite Na-A applications

The structure of zeolite consists of many channels, cavities and interconnected voids which are occupied by cation and water molecule. Some properties of zeolite are very interesting such as (a) high degree of hydration (b) low density and large void volume when dehydrated (c) stability of crystal structure (d) cation exchange properties (e) uniform molecular sized channels (f) special physical properties, i.e. high surface area, molecular sieve (g) adsorption for gas and vapor and (h) catalytic properties. Due to its unique and special properties which are suitable for various kinds of chemical reactions, zeolite has been widely used in many applications. Zeolite Na-A is of

much interest for various applications such as detergency, desiccant, adsorption and separation, catalysis, and ion exchange (King, R. B.1994, and Bekkum, V. H., 1991).

1.3.1 Ion-exchange

Zeolite Na-A is produced in the largest-scale industrial of all synthetic zeolite for use in the detergent industry. It is added to washing powders to exchange Ca^{2+} and soften water. The advantage of zeolite builders as a replacement for phosphate, hence reducing the release of phosphate to the environment. Zeolite Na-A has a high selectivity for Ca^{2+} . The ion exchange characteristic of zeolite Na-A are suitable for washing powder because of several properties such as non interaction with other substances in washing powder, non poison to human, animal and plant in the water and non pollutant. Industrial waste water containing heavy metals, and nuclear effluents containing radioactive isotopes can also be cleaned up using the similar process.

1.3.2 Catalysis

Zeolite has the ability to act as catalysts for chemical reactions which take place within the internal cavities of the material. Therefore the structure, shape, and chemical composition of pores and cage are important. In 1980, applications of zeolite and molecular sieves showed a growth in petroleum refining application. Also as catalytic support.

1.3.3 Adsorption and Separation

Zeolite has been used in adsorption and separation applications such as drying agent, gas purification. Also it was applied to important separation processes like the separation of n-paraffin from branched paraffin etc. Due to its high surface area and large pore, it is an ideal material for various novel processes such as the formation of special molecules in the cages. Advanced experiments have been performed using zeolite through out the world.

1.4 Kaolinite

Kaolin is a clay mineral consisted in the mineral kaolinite. The name kaolin comes from the Chinese term “ kaoling” meaning high ridge. In 1867, Johnson and Blake were apparently the

first to use the name kaolinite for the mineral of kaolin. Ross and Kerr in 1931 described that the kaolin minerals are not composed of a single mineral species.

Kaolin has long been mainly used in the ceramic industry, especially in fine porcelains because it can be easily molded, has fine structure, and is white when fired. Kaolinite has a color of white, pink or grey depended on their compositions. It is very soft with hardness of 2-2.5 (Grim, R. E. 1968, Velde, B. 1992).

The chemical formula of kaolinite is $\text{Al}_2\text{O}_3 \cdot 2\text{SiO}_2 \cdot 2\text{H}_2\text{O}$ and the composition expressed in oxides is 46.54% SiO_2 , 39.50% Al_2O_3 , 13.96% H_2O . Kaolinite is a layer aluminosilicate with a 1:1 uncharged dioctahedral layered structure. Each layer consists of a sheet of SiO_4 tetrahedra forming six-membered silicate rings connected via common oxygen atoms to a sheet of AlO_6 octahedra building four membered aluminate rings as shown in figure 1.5 (Bongear, D. 2000).

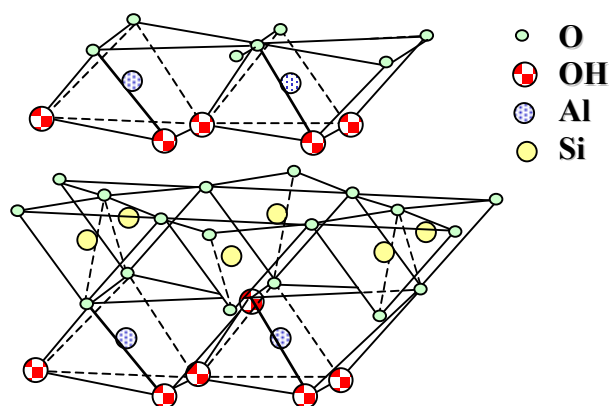


Figure 1.5 Crystal lattice of kaolinite

Kaolin has been found in many regions of the world. In Thailand, it is found mainly in Lampang, Narathiwat, and Ranong provinces. In the past, kaolin has been mainly used in ceramic industry. However, new applications of kaolin have been continuously discovered. Typical kaolin contains trace amount of iron, titanium, calcium, magnesium, etc. which are originally present in the natural kaolinite. Therefore zeolite prepared from natural kaolin is always contaminated with these elements. These elements may have some influence on the zeolite properties such as brightness, hardness, catalytic activity, electrical properties, etc. Nevertheless, kaolin is still a popular choice to be used as starting material for synthesis of zeolite. Presently, many researchers are working actively in various aspects on the synthesis of zeolite from kaolin.

1.5 Mechanism of Zeolite Crystallization

Hydrothermal synthesis of aluminosilicate zeolites involves a few basic steps by which a mixture of Si and Al species, metal cations, organic molecules and water is converted by an alkaline supersaturated solution into a microporous crystalline aluminosilicate (Feijen E.J.P, et al., 1994). The formation process of zeolite is thermally activated and usually takes place at elevated temperatures in order to achieve high yield of crystals in an acceptable period of time. On the basis of the chemical phenomena occurring during zeolite genesis, the process can be divided into three elementary steps: achievement of supersaturation, nucleation and crystal growth.

1.5.1 Achievement of supersaturation

During the induction period, the concentration of dissolved aluminosilicate species will increase in time by dissolution process. This increasing concentration of solute will transform a stable solution into a metastable solution and finally to a labile (transformable) one. This kind of transformation is denoted by an arrow in the solubility-supersolubility diagram of figure 1.6.

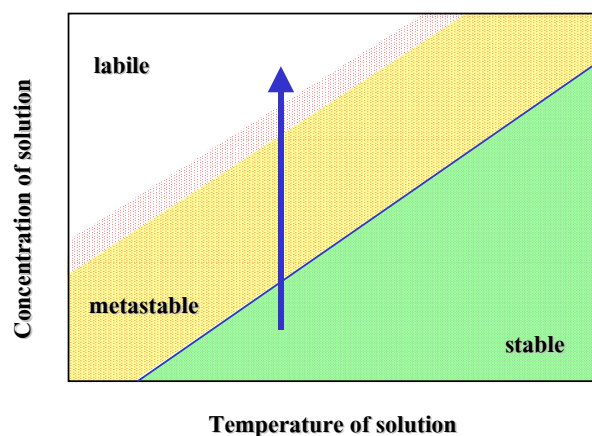


Figure 1.6 The solubility-supersaturation diagram. The arrow indicates the transformation of stable solution into labile solution by the increasing of solution concentration.

In general, a solution for a given concentration and temperature can be in a stable, metastable or labile regions. The stable and metastable regions are separated by a curve called the normal solubility curve while the boundary between the metastable and labile region is not always well-defined. The degree of supersaturation is depended on the ratio of the actual concentration to

the normal equilibrium concentration. In the stable region no nucleation or crystal growth can occur, while in the labile region nucleation as well as crystal growth are possible. In the metastable area, only crystal growth can occur.

1.5.2 Nucleation

Primary nucleation from a supersaturated solution can be divided into homogeneous and heterogeneous nucleation. The former occurs spontaneously, while the latter is induced by impurities or foreign particles present in the solution. The heterogeneous nucleation might be suppressed by filtration of the solutes. On the other hand, secondary nucleation is induced by crystals and is connected to the process of seeding. During the induction period, different kinds of embryos will form by chemical aggregations of precursor species and disappear again upon depolymerization. As a result of such fluctuations, the embryo will grow in time, and form eventually different kinds of nuclei, with dimension having the critical size on which crystal growth can occur spontaneously. The rate of nucleation could be derived from crystal size distribution measurement in the final crystallization product and size increment measurements of the large crystals during the crystallization. As nucleation and crystal growth are assumed to consume the same precursor species, the nucleation rate is expected to go through a maximum and decline again after a certain period when the consumption of precursor species by crystal growth limits the forming of new nuclei.

1.5.3 Crystal growth

After nucleation, crystal growth can start. The nuclei will grow by condensation of precursor species towards full-grown crystals. Experimental crystallization curves, giving the yield of crystalline material in time, usually exhibit a S-shape profile. The inflection points of these curves separate the period of autocatalytic increase of crystalline mass from the stage of delayed crystal growth. The autocatalytic nature of the first stage of the crystallization reflects the self accelerating behavior of a crystallization process. Presently, it is believed that the zeolite crystal growth occurs at the crystal plane-solution interface by the condensation of dissolved secondary units onto the growing crystal plane. In general, temperature and time have a positive influence on the zeolite formation process. Rising temperature will increase both the nucleation

rate and the growth rate. The crystallinity of the samples normally increases in time. Since the synthesis of zeolite is governed by the occurrence of the successive phase transformations, the thermodynamically least favorable phase will crystallize first, and will be replaced in time by more stable phases (Feijen E.J.P, et al., 1994). The next section describes a general theory of crystallization known as Avrami theory.

1.6 Avrami Theory

A general theory of crystallization kinetics was developed by Avrami in 1940. The theory describes that crystallization processes consist of nucleation and crystal growth.

1. Some nucleation and growth processes are:

- Spontaneous nucleation: During cooling of molten material to a fixed temperature nuclei appear randomly through out the volume.
- Time dependence of nucleation: Nuclei can appear instantaneously on cooling or during crystallization in the non-uniformed phase.
- Nature of growth process: Growth can proceed in one, two or three dimensions resulting in needles, discs or spheres. Growth stops when neighboring crystals merge.
- Time dependent of growth: Linear dimension of growing crystals increase in proportional to time.
- Density of the growing units: The transformed phase is not totally crystalline and assume that the density of the growing crystals is constant.

2. The Avrami exponent and the rate constant can be determined from the Avrami equation

$$-\ln (1-\alpha) = kt^n \quad \text{.....(1.1)}$$

where, α is the conversion factor, ranging from 0 to 1, $k = d\alpha/dt$ is the rate constant and the exponent n is the parameter which describes reaction mechanism .

3. The Avrami exponent value depends on the dimensionality of the growth process, and on the kinetic order of nucleation. In general case, where three dimensional growth is combined with the first order nucleation, the Avrami exponent $n = 3+1 =4$.

The Avrami exponents for different nucleation and growth mechanisms are shown in table 1.2

Table 1.2 Exponents n of the Avrami equation for different nucleation and growth mechanism.

n	Growth mechanism
3+1=4	3 dimension growth + random nucleation
3+0=3	3 dimension growth + instantaneous nucleation
2+1=3	Disc-like growth + random nucleation
2+0=2	Disc-like growth + instantaneous nucleation
1+1=2	Rod-like growth + random nucleation
1+0=1	Rod-like growth + instantaneous nucleation

To study the kinetic of crystal formation, the Avrami equation can provide a good empirical fit of the kinetic curves. It can be used for the calculation of the rate constant and Avrami exponent. If we consider Avrami equation as shown in equation (1.1). Taking logarithms of equation (1.1), gives

$$\ln(-\ln(1-\alpha)) = n \ln t + \ln k \quad \text{.....(1.2)}$$

Thus, a plot of $\ln(-\ln(1-\alpha))$ versus $\ln t$, the slope of the regression lines, n, is related to the mechanism of reaction.

The rate constant k can be expressed using Arrhenius equation as

$$k = A \exp(-E_a/RT) \quad \text{.....(1.3)}$$

where E_a represents the activation energy, A is a constant, R is gas constant and T is the absolute temperature. Similarly the time used in the nucleation process can be expressed as

$$1/t_0 = B \exp(-E_n/RT) \quad \text{.....(1.4)}$$

where t_0 is called inductive period, E_n represents activation energy for nucleation, and B is a constant.

1.7 Characterization techniques

In this study, various characterization techniques were used to analyze the properties of kaolin and the synthetic products. In this section, a brief overview of the characterization techniques is described.

1.7.1 Atomic Absorption Spectroscopy

Atomic Absorption Spectroscopy (AAS) is one of the analytical techniques that give precision measurement result for the elemental concentration of the sample.

The atom is made up of a nucleus surrounded by electrons. Every element has a specific number of electrons which are associated with the atomic nucleus in an orbital structure which is unique to each element. The electrons occupy orbital positions in an orderly and predictable way. The lowest, most stable electronic configuration of an atom, known as the “ground state”, is the normal orbital configuration for an atom. If energy of the right magnitude is applied to an atom, the energy will be absorbed by the atom, and an outer electron will be promoted to a less stable configuration or “excited state”. As this state is unstable, the atom will immediately and spontaneously return to its ground state configuration. If light of just the right wavelength impinges on a free, ground state atom, the atom may absorb the light as it enters an excited state in a process known as atomic absorption as shown in figure 1.7.

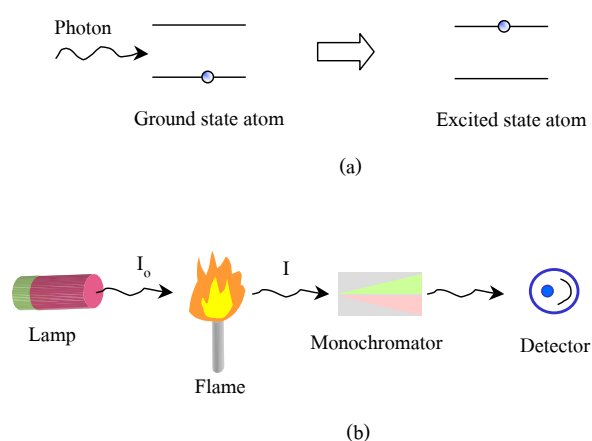


Figure 1.7 (a) An atom in the ground state is excited by a photon with the same energy as the energy gap resulting in the final excited state. (b) A simplified diagram of AAS

The quantity of interest in AAS is the amount of light at the resonance wavelength which is absorbed as the light passes through a cloud of atoms. As the number of atoms in the light path increases, the amount of light absorbed in a predictable way. By measuring the amount of light absorbed, a quantitative determination of the amount of analyte element present can be made.

The atom cloud required for AAS is produced by supplying enough thermal energy to the sample to dissociate the chemical compound into free atom. Aspirating a solution of the sample into a flame aligned in the light beam serves this purpose. Under the proper flame conditions, most of the atoms will remain in the ground state form and are capable of absorbing light at the analytical wavelength from a source lamp. The ease and speed at which precise and accurate determinations can be made with this technique have made AAS one of the most popular methods for determination of metals.

1.7.2 X-ray Fluorescence

The X-ray fluorescence (XRF) is widely used to measure the elemental composition of materials. Since this method is fast and non-destructive to the sample, it is the method of choice for field applications and industrial production for control of materials. Depending on the application, XRF can be performed by using not only X-rays but also other primary excitation sources like alpha particles, protons or high energy electron beams.

When a primary X-ray excitation source from an X-ray tube or a radioactive source strikes a sample, the X-ray can either be absorbed by the atom or scattered through the material. The process in which an X-ray is absorbed by the atom by transferring all of its energy to an innermost electron is called the photoelectric effect. During this process, if the primary X-ray had sufficient energy, the electron is ejected from the inner shell, creating a vacancy. The vacancy presents an unstable condition for the atom. As the atom returns to its stable condition, electron from the outer shell is transferred to the inner shell and in the process give off a characteristic X-ray whose energy is the difference between the two binding energies of the corresponding shells. Because each element has a unique set of energy levels, each element produces X-rays at a unique set of energies, allowing one to non-destructively measure the elemental composition of a sample. The process of emissions of characteristic X-rays is called "X-ray Fluorescence," or XRF. The process is illustrated in figure 1.8.

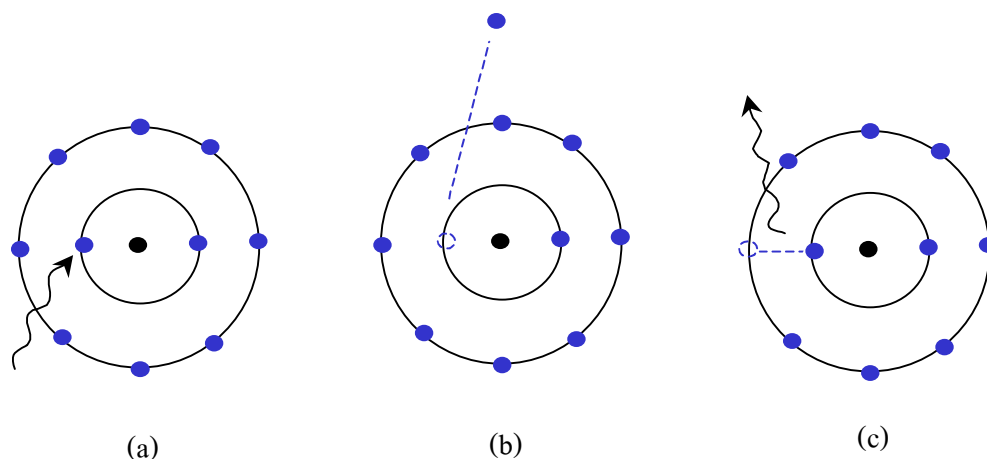


Figure 1.8 The process of emission of characteristic X-ray: (a) a x-ray photon is absorbed by an inner shell electron (b) the electron is ejected from the atom creating a vacancy (c) an outer shell electron moves to the inner shell and emits the characteristic x-ray.

Analysis using X-ray fluorescence is called "X-ray Fluorescence Spectroscopy." In most cases the innermost K and L shells are involved in XRF detection. A typical X-ray spectrum from an irradiated sample will display multiple peaks of different intensities. The identification of atom can be done by comparing the spectrum with the standard valued stored in the look-up table. Also, the quantitative analysis can be done using the intensities of the peaks.

1.7.3 Powder X-ray Diffraction

X-rays are electromagnetic radiation of wavelength about 1 \AA (10^{-10} m), which is about the same size as atomic distances in solid thus it can be used to probe the crystalline structure at atomic level. X-ray diffraction has been used in two main areas, for the fingerprint characterization of crystalline materials and the determination of their structure. Each crystalline solid has its unique characteristic X-ray powder pattern which may be used as a "fingerprint" for its identification. Once the material has been identified, X-ray crystallography may be used to determine its structure, i.e. how the atoms pack together in the crystalline state and what the inter-atomic distance and angle are. These unique properties made X-ray diffraction one of the most important characterization tools used in solid state chemistry and material science.

An important equation for X-ray diffraction is Bragg's equation which shows a relationship between X-ray wavelength (λ) with lattice point distance (d) and the incident diffraction angle (θ).

$$n\lambda = 2d\sin\theta \quad \dots(1.5)$$

As illustrated in figure 1.9, different crystal plane in the crystal will diffract X-ray at different angle according to the Bragg's equation. Therefore, by rotate the sample plane with respect to the incident X-ray, the diffracted angles can be recorded by a detector and the diffraction pattern is obtained. The identification of the sample structure can be done by comparing the spectrum with the pattern stored in the database.

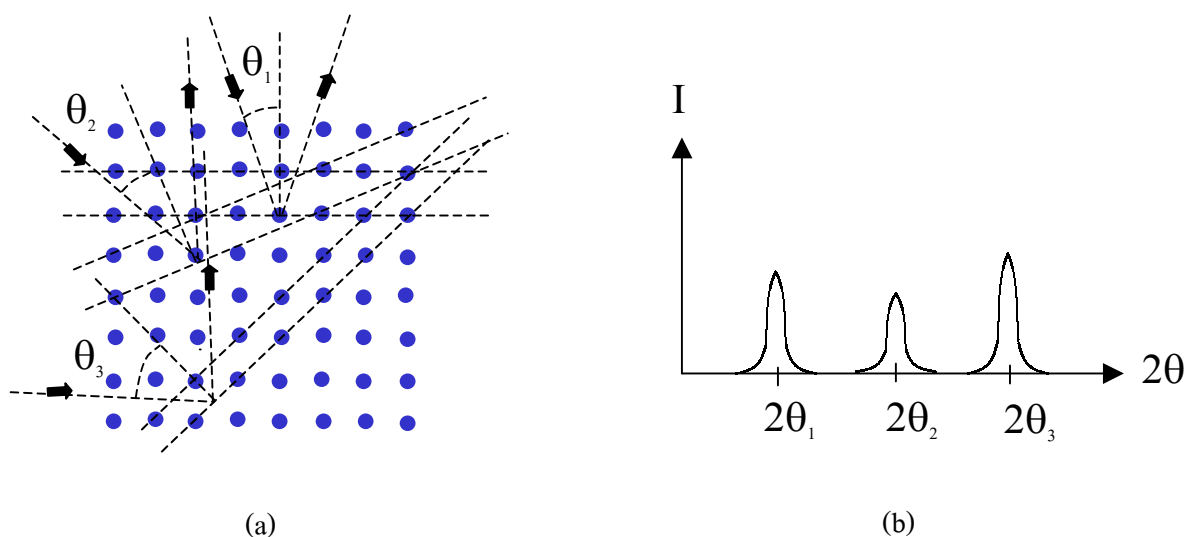


Figure 1.9 (a) Different crystal planes diffract X-ray at different angles (b) The diffraction spectra may be depicted by a plot of intensity and diffracted angle

1.7.4 Fourier Transform Infrared spectroscopy

The region of the infrared spectrum which is of great interest to most of the chemists is the wavelength range 2.5 to 15 μm . In practice, units proportional to frequency, (wave number in units of cm^{-1}) rather than wavelength, are commonly used and the region 2 to 15 μm corresponds to approximately 4000 to 400 cm^{-1} .

The atoms in a molecule are constantly oscillating around average positions. Bond lengths and bond angles are continuously changing due to this vibration. A molecule absorbs infrared radiation when the vibration of the atoms in the molecule produces an oscillating electric field with the same frequency as the frequency of incident IR radiation when they are in resonance. Each molecule has its own characteristic spectrum. The bands that appear depend on the types of bonds and the structure of the molecule.

Fourier transform infrared (FTIR) spectroscopy measures dominantly vibrations of functional groups and highly polar bonds. Thus these chemical fingerprints are made up of the vibrational features of all the samples components. FTIR spectrometer records the interaction of IR radiation with experimental samples, measuring the frequencies at which the sample absorbs the radiation and the intensities of the absorptions. Determining these frequencies allows identification of the sample's chemical makeup, since chemical functional groups are known to absorb light at specific frequencies. FTIR experiments generally can be classified into the following two categories: (a) qualitative analysis, where the aim is to identify the sample and (b) quantitative analysis, where the intensity of absorptions are related to the concentration of the component.

1.7.5 Scanning Electron Microscopy

Scanning electron microscope (SEM) is a type of microscope that uses electrons rather than light to form an image. There are many advantages to using the SEM instead of a light microscope. The SEM has a large depth of field, which allows a large amount of the sample to be in focus at one time. The SEM also produces images of high resolution, which means that small spaced features can be examined at a high magnification. Preparation of the samples is relatively easy since most SEM instruments only require the sample to be conductive. The combination of higher magnification, larger depth of focus, greater resolution, and ease of sample observation makes the SEM one of the most heavily used instruments in present-day research.

By using the wave-particle duality, SEM creates the magnified images by using electrons instead of light waves. The SEM shows very detailed 3-dimensional images at much higher magnifications than is possible with a light microscope. The images created without light waves are rendered black and white. By the nature of electron beam, the vacuum is required during the

operation, therefore the sample has to be prepared carefully to withstand the vacuum inside the microscope. The samples must be conductive material in order to be able to interact with electron, SEM samples are coated with a very thin layer of gold by a machine called a sputter coater. The sample is placed inside the microscope's vacuum column through an air-tight door. A simplified diagram of SEM is illustrated in figure 1.10.

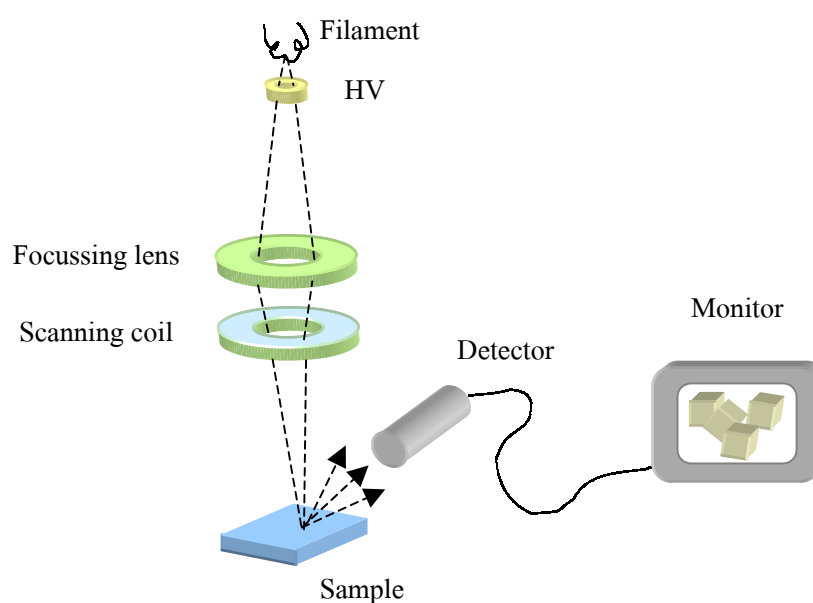


Figure 1.10 A simplified diagram of SEM

After the air is pumped out of the column, an electron gun emits a beam of high energy electrons. This beam travels downward through a series of magnetic lenses designed to focus the electrons to a very fine spot. Near the bottom, a set of scanning coils moves the focused beam back and forth across the specimen, row by row. As the electron beam hits each spot on the sample, secondary electrons and back scattered electrons are knocked loose from its surface. A detector counts these electrons and sends the signals to an amplifier. The final image is built up from the number of electrons emitted from each spot on the sample. By this way the morphology of the sample can be seen directly from the micrograph.

1.8 Literature reviews

Modification of clay minerals by converting them to zeolites was reported as early as 1935 according to Breck (Breck, D.W., 1974). Such studies are still relevant when zeolites with specific properties are prepared for certain industrial applications (Barrer, R. M., 1978). The kaolinite mineral with a Si/Al ratio of approximately 1 can be conveniently used as raw material for the synthesis of silica zeolite. Synthesis of zeolite Na-A from kaolin was reported as early as 1964 (Ruiz, R., 1997). Later, various aspects of the synthesis have been reported from several researchers.

Kerr, G. T. (1965) studied the factors affecting the formation of zeolite A, and found that the rate of formation of zeolite A increased as the concentration of alkali in the aqueous phase increased.

Madami, A. et al. (1990) studied the zeolite formation from alkali-leached kaolinite and the influence of thermal preactivation and found that the synthesis of zeolite (Si/Al > 1) required the previous polymerization of dissolved silica species, and amount of incorporated Si depended on the temperature of pretreatment of kaolinite.

Rocha, J. et al. (1991) studied the synthesis of zeolite Na-A from metakaolinite and found that the synthesis usually involved the treatment of clay with strong base such as NaOH at elevated temperature. Upon treatment with strong base the aluminous matrix of metakaolinite transformed very rapidly even at room temperature. They found that the aluminous matrix of metakaolinite prepared by calcining kaolinite at 700 °C had higher reactivity of metakaolinite than metakaolinite prepared at other calcination temperatures. The mechanism involved the slow dissolution of metakaolinite in the alkali to a solution containing monomeric silicate ions with reactive SiOH groups which condensed with aluminate ions to give a crystal of aluminosilicate.

Gualtieri, A. et al. (1997) studied the kinetics of formation of zeolite Na-A from natural kaolinites activated at 800 °C with 4M NaOH concentration at reaction temperature 70-100 °C, by time resolved synchrotron powder diffraction techniques. They found that the formation of zeolite Na-A depended on the calcination of starting material but not the number of defects of the starting material. Also, the n values obtained from Avrami method decreased when reaction temperature increased and the range of n were between 5 and 7.

Demortier, A. et al. (1999) studied the formation of intermediate compound during the synthesis of zeolite Na-A from metakaolinite by infrared technique. IR spectra showed that intermediate compound was synthesized and zeolite Na-A was formed only when metakaolinite has been totally transformed.

Hu, H. C. et al. (1990) studied the kinetic of formation of zeolite from sodium metasilicate and sodium aluminate. They found that the kinetic of nucleation and crystallization were correlated to the initial concentration and temperature. The activation energies of the nucleation and crystallization were 15.0 and 10.9 kcal/mol, respectively.

Walton R. I. et al. (2001) studied on the influence of the reaction condition of the hydrothermal crystallization and the transformation of zeolite Na-A into sodalite by time resolved in situ energy dispersive x-ray diffraction. They found that the crystallization of zeolite Na-A depended on both NaOH concentration and reaction temperature. At the highest NaOH concentrations and when the amount of water was low, zeolite Na-A was only present for a short time and hydroxy sodalite was the sole product on continue heating. The n values obtained from Avrami's model increased when the NaOH concentration was increased and the range of n were in between 2-5.

As mentioned earlier, the introduction and the literature reviews have been guided by the principal that synthesis of zeolite Na-A from kaolin depends on calcination of starting material, strong base concentration, temperature and duration of the synthesis. Generally, there are two steps involving in the zeolite forming reaction from kaolin (1) thermal activation (metakaolinisation) of the kaolin to get a dehydroxylated product called metakaolinite and (2) hydrothermal reaction (zeolitisation) of metakaolin in alkaline medium [Chandrasekhar, S. 1999].

Kaolinite is one of the convenient starting materials for the synthesis of zeolite because of its structure and chemical composition is suitable for the synthesis of zeolites [Rocha, J. 1991]. Kaolinite has been found in many parts of Thailand, especially in Lampang, Ranong and Narathiwat provinces. However, there are some limited number of reports on the synthesis of zeolite Na-A from Thai kaolin and the detail of kaolinite transformations to crystalline zeolite has not been investigated. Furthermore, it is well-known that Thai kaolin is mainly used in ceramic industry, thus it is useful to utilize Thai kaolin as a starting material to produce new materials

which are expensive and applicable to many industrial organizations such as in environmental sectors, detergent industry and catalyst industry.

1.9 Research objectives

The main objective of this study is to synthesize zeolite Na-A from locally available Thai kaolin from Lampang, Ranong, and Narathiwat provinces. Several factors that influence the synthesis were investigated such as metakaolinisation temperature, concentration of NaOH, reaction temperatures and time. The most suitable synthesis condition was found and reported. Also, the reaction kinetic of hydrothermal formation of zeolite Na-A was investigated using IR, and XRD techniques. The results were modeled based on the Avrami's method and the research findings are summarized and concluded.

Chapter II

Materials, Instrumentation, and Method

This chapter is divided into three main parts. In the first part, lists of materials, glassware and apparatus are provided. In the second part, the characterization routines using analytical instruments such as x-ray fluorescence (XRF), atomic absorption spectrometer (AAS), x-ray diffractometer (XRD), Fourier transform infrared spectrometer (FTIR) and scanning electron microscope (SEM) are described. The third part of the chapter describes about the experimental methods. This part is divided into four topics. The first topic is the analysis of kaolin chemical composition. The second topic is the procedure for the synthesis of zeolite Na-A. There are two steps described in this topics. The first step is the thermal activation of kaolin to get a product called metakaolinite. The second step is the hydrothermal reaction of metakaolinite in alkaline medium. The third topic is kinetic study. Finally, the fourth topic describes the procedure to demonstrate the ion exchange capability of the synthetic zeolite Na-A product.

2.1 Material Lists

2.1.1 Chemicals and Materials

- (a) Washed clay, Thai kaolin samples of Lampang, Ranong, and Narathiwat, The Center for Ceramic Industry Development
- (b) Anhydrous Sodium hydroxide pellets (NaOH), Analytical reagent, Carlo Erba, Italy
- (c) Standard powder of Kaolin, MBH reference materials 1998-99, UK
- (d) Standard reference material 600(Bauxite), National Institute of Standard and Technology, USA
- (e) Standard reference material 98b(Plastic clay), National Bureau of Standard, USA
- (f) Standard reference material 679 (Brick clay), National Bureau of Standard, USA
- (g) Standard reference material 2709(Soil), National Institute of Standard and Technology, USA

- (h) Silicon, Aluminium, Iron standard solution, 1000mg/l, Merck, Germany
- (i) CaCl_2 , Laboratory reagent APS Ajax, Finechem, Australia
- (j) Anhydrous, fused, Lithium tetraborate ($\text{Li}_2\text{B}_4\text{O}_7$), Claisse, Canada
- (k) Lithium bromide (LiBr), Analytical reagent, Claisse, Canada

2.1.2 Glasswares

- (a) Condenser for reflux procedure
- (b) Round bottom flask 250ml with two neck
- (c) Watch glass
- (d) Polyethylene pasteur pipettes
- (e) Utility clamp
- (f) Glass stirring rod
- (g) Beakers 50ml, 100ml
- (h) Volumetric flasks 100ml
- (i) Mortar and pestle
- (j) Platinum crucible and mold

2.1.3 Apparatuses

- (a) Thermometer
- (b) Heating mantle with stirrer (Horst)
- (c) Vacuum filtration apparatus
- (d) Oven for drying sample (Binder, ED)
- (e) Furnace chamber for kaolin calcination, (Honeywell, UDC 2000)
- (f) Fusion machine for sample preparation XRF analysis, (Claisse, Fluxer Bis)
- (g) Desiccator

2.2 Instrumentation

2.2.1 X-ray fluorescence spectrometer (XRF)

XRF is one of the techniques, widely used to determine elemental compositions of solid samples especially in soil or powder samples. In this work, XRF (Phillip, MagiX Pro) was used to measure the composition of kaolin samples and synthetic products. The samples were prepared for the measurement by Borate-fusion technique as follow:

1. Mix 1g of the sample with 7 g of flux ($\text{Li}_2\text{B}_4\text{O}_7$) in the platinum crucible.
2. Add LiBr about 0.03g to the mixed sample.
3. Transfer the platinum crucible to the fusion machine.
4. Program the fusion machine for power and fusion time according to the instruction.
5. Start the fusion machine to allow the the mixture to melt. After cooling, solidification and casting, the flat lower surface of the disk can be used for XRF analysis.

The apparatus of fusion machine and disk of the sample as show in figure 2.1.



A



B

Figure 2.1 A The apparatus of fusion machine and B sample disks.

The tube high voltage was 40 kV with the tube current of 30 mA. Each sample was measured using standard procedure suggested by the instrument manufacturer. The measurement time was about 5 min./sample. The results were reported in the form of oxide percentage compared with standard powder of kaolin, MBH reference material 1998-99 and standard reference materials.

2.2.2 Atomic absorption spectrometer (AAS)

AAS is one of the techniques used for measurement of concentration of elements containing in samples. This method can give high accuracy result for elemental concentrations. The samples were digested by acid using microwave digestion which is similar to the suggested sample digestion procedure using Mar 5 CEM microwave. In each measurement, 0.5 g of the sample was put to the HP-500 Plus PFA vessels. The temperature was elevated and controlled by the amount of microwave power provided to the reaction vessels. The process and heating programs are shown in table 2.1.

Table 2.1 Process and heating programs for acid digestion method: (a) Step 1: Add Hydrofluoric acid (48%) 7 ml, Hydrochloric acid (37%) 3 ml, and Nitric acid (65%) 1 ml, respectively and (b) Step2: Add Boric acid 4% 30 ml.

Max. Power	% power	Ramp time(min)	Pressure (psi)	Temp.(°C)	Hold(min)
Step1: 600w	100	15	130	210	10
Step2: 600w	100	10	100	210	5

After acid digestion, the samples were transformed to clear solutions. Then the clear solutions were diluted to a proper level covered by the calibration curves. The concentrations of Si, Al, and Fe in the solutions were measured by a Perkin-Elmer, AAS, analyst 100 machine. The calibration curve for each element was prepared from a series of 4 reference solutions. Si and Al measurements were done using graphite furnace technique. Fe measurement was done using flame technique. The results were reported in the form of weight percentage.

2.2.3 Powder X-ray diffractometer (XRD)

XRD is a popular technique used for the analysis of the structural properties and the identifications of mineral in solid state and material science. A Bruker D5005 Powder X-ray diffractometer with Ni-filtered Cu K_α radiation was used to record all of the diffraction spectra.

Prior to the measurement, each sample was prepared using a standard method for powder sample preparation.

Sample preparation procedure for XRD

The apparatus set used for powder XRD sample preparation is illustrated in figure 2.2.

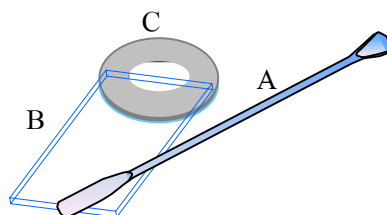


Figure 2.2 Apparatus set for powder XRD sample preparation (A= spatula, B= glass slide, C= sample holder)

1. Dry the sample in the oven at 100 °C.
2. Grind about 1 g of each solid sample to fine powder as homogeneous as possible, then load into the Polymethyl metaacrylate (PMMA) sample holder.
3. Tap the powder gently and evenly to uniformly cover the holder cavity.
4. Gently press the powder sample into the cavity using a glass slide.
5. Gently lift off glass slide to reveal the sample surface.

Each diffraction spectrum was recorded with condition: 2θ angle of between 5° and 50° . Cu-target, 35 kV, 35 mA., and scan speed of 0.3 degree/ 0.02 second. Typically, the data was expressed in the plot between intensity of diffraction peaks and 2θ angle. The positions of diffraction peaks were compared with a reference data base and the identifications of compounds could be obtained. The percentage of crystallinity was obtained by the area of 12 strong diffraction peaks of the sample compared to the pattern of standard zeolite which was set to be 100% (Hu, H. C., 1990)

$$\text{Percent of crystallinity} = \frac{\text{Total area of 12 strong peaks of the sample} \times (100\%)}{\text{Total area of 12 strong peaks of the standard}}$$

2.2.4 Fourier transform infrared spectroscopy (IR)

A Perkin-Elmer spectrum GX FTIR Spectrophotometer, infrared spectra were used to take the mid IR spectra of samples ($2000\text{--}370\text{ cm}^{-1}$) with the KBr pellet technique. The solid sample and KBr pellet were dried at $120\text{ }^{\circ}\text{C}$ for 1 h before to obtain spectra. Approximately 0.5 mg of each sample was mixed with 300 mg dried KBr powder and ground to very fine powder with a mortar and pestle. The ground powder was pressed into a transparent disk using a hydraulic pressing machine with an equivalent weight of about 10 tons for 1 minute. The spectra were obtained using an average of 12 scans with 4 cm^{-1} resolution. To compare several spectra together, the normalization was done using one fixed point at 1500 cm^{-1} . The percent of crystallinity of each sample was determined by comparing the ratio of the areas under two pre-selected absorbance bands of sample to the ratio from standard zeolite which was set to be 100%.

2.2.5 Scanning electron microscope (SEM)

Morphology of the solid sample could be seen through the use of SEM. Crystal shape and size of the crystalline solid phase could be identified from the micrograph. The observation was done using a JEOL scanning electron microscope model JSM6400. To prepare for the observation, the solid sample was placed on a brass stub sample holder using double stick carbon tape. Then, the sample was dried using infrared light for five minutes. After that, the sample was coated with a layer of gold approximately $20\text{--}25\text{ \AA}$ thick using a Balzer sputtering coater. The micrographs were recorded with 12kV, 8000x magnification.

2.3 Experimental methods

2.3.1 Kaolin preparation

Thai kaolin samples collected from three provinces were ground in a gate mortar and sieved with mesh number 120, 125 micron aperture. Prior to the XRF analysis, the Loss on Ignition (LoI) values of kaolin samples were determined. The kaolin samples were characterized by XRF and AAS to find the composition prior to the calcination. The calcination temperatures were carried out from $500\text{ }^{\circ}\text{C}$ to $900\text{ }^{\circ}\text{C}$. Then the calcined kaolin samples were used as starting materials for the synthesis of zeolite Na-A.

LoI determination procedure

Place a crucible in the oven at a temperature of 105 °C and leave it for at least 2 hours. Then place it in a desiccator and let it cool down to room temperature. Weigh the empty crucible (A). Weigh at least 2 g of sample in the crucible and weigh again (B). Place the crucible overnight in the oven at 105 °C. Transfer the crucible to the desiccator and allow to cool to room temperature. Finally weigh the crucible again (C). The moisture content can be calculated using equation :

After drying, place the crucible in the ignition oven and allow the sample to warm up gradually to 900 °C. Ignite for at least four hours. Allow the oven to cool down to 100 °C. Then, transfer the crucible to the desiccator and allow it to cool down to room temperature. Finally, weigh the crucible again (D). Loss on ignition (LoI) could be calculated from

$$\text{LoI} = 100\% (C-D)/(C-A).$$

2.3.2 The zeolite Na-A synthesis method

1. Kaolin samples were calcined in the furnace chamber at different temperatures (500, 600, 700, 800, 900 °C) for 1 h. After the calcination process, kaolinite samples were transformed to metakaolinite. The resulting metakaolinite samples from each temperature were used to in the next zeolite Na-A synthesise step.
2. The procedure for hydrothermal reaction of metakaolinite in alkaline medium are described as followings.
 - 2.1 Metakaolinite samples were treated with different concentrations of NaOH solution (10%, 15%, 20%, 25%, w/v) , Metakaolinite : NaOH solution = 1g : 5 ml.

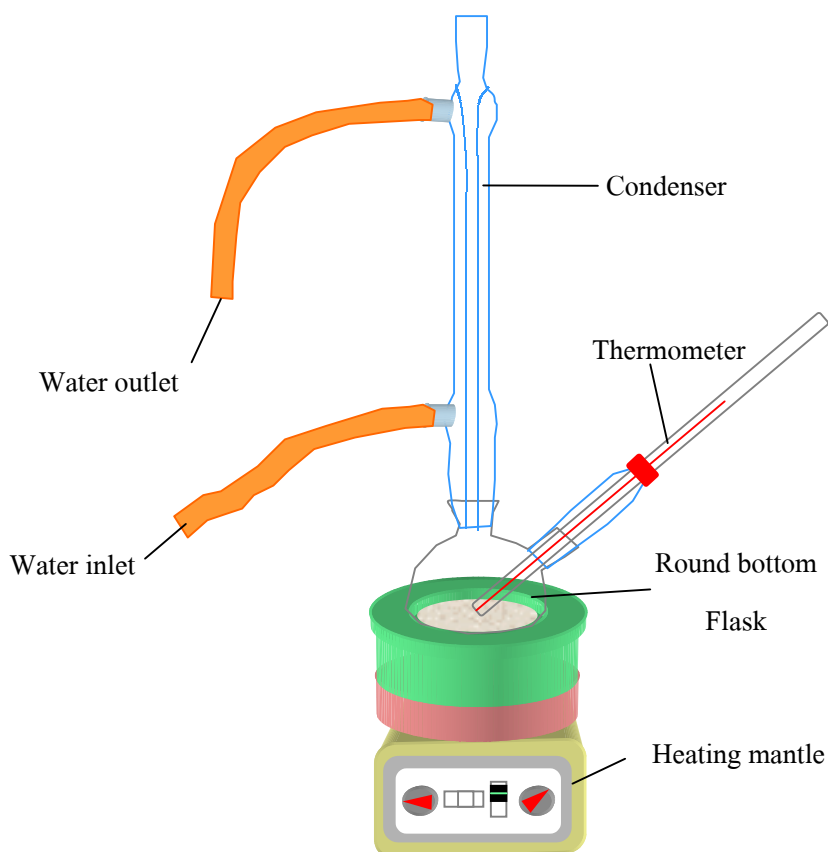


Figure 2.3 The apparatus for zeolite Na-A synthesis.

- 2.2 Zeolite Na-A was synthesized in a 250 ml glass round-bottom flask with two necks: one neck fitted with a water-cooled reflux condenser and the another neck for temperature measurement. The apparatus for zeolite synthesis is shown in figure 2.3
- 2.3 The stirred bath reactions were carried out at ambient pressure.
- 2.4 The reactions were carried out at various temperatures (70, 80, 90, 100 °C).
- 2.5 During hydrothermal treatment, samples were collected from the reaction vessel by pipetting out 5 ml portions of reaction mixture at various periods as shown in the table 2.1.
- 2.6 The solid phase samples were filtered, washed with distilled water, and then dried at 120 °C for 5 hours.
- 2.7 The solid products were characterized by XRD, IR, and SEM techniques.

Temp.(°C) [NaOH] w/v	70	80	90	100
10%	30 min	20 min	15 min	10 min
15%	15 min	15 min	10 min	10 min
20%	15 min	10 min	10 min	5 min
25%	10 min	10 min	5 min	5 min

Table2.2 Sampling periods for various experiments.

2.3.3 Kinetic study

The kinetic of reaction was investigated by using the data from XRD and IR. The percentage of crystallinity of zeolite Na-A were determined from IR spectra and x-ray diffraction patterns of solid phase samples at various times and at different experiment conditions. The relationship between the percentage of crystallinity and time at different NaOH concentrations and different temperatures provides the information on kinetic study. Rate of reaction were extracted from slope of the plot between crystallinity and time. The rate constant (k) and the value of Avrami exponent (n) which is related to mechanism of reaction were deduced from Avrami equation. Finally, the apparent activation energies were obtained using Arrhenius plot.

2.3.4 Ion exchanger capability

In order to demonstrate the ion exchanged capability of the synthetic zeolite Na-A, the following procedure steps were used.

1. Prepare CaCl₂ solution at various concentrations [600, 1000, 1400, 2000 mg/l].
2. Put 1 g of zeolite into 100 ml of each CaCl₂ solution.
3. Keep stirring the mixture solutions for three days.
4. Filter the solutions to remove solid phase.
5. Determine the concentration of Ca ions in each solution using AAS technique.
6. The ion exchange capability can be approximated from the AAS result.

Chapter 3

Results and Discussion

In this chapter, the experimental results are discussed. Firstly, the analytical result for kaolin composition is shown. Secondly, the characterization results for kaolinite and metakaolinite are compared. Thirdly, the result for the synthesis of zeolite Na-A is reported. The effects of kaolin source, calcination, alkalinity concentration and reaction temperature are discussed in this part. Fourthly, the kinetic study of the synthesis reaction is discussed. The kinetic parameters based on Avrami model are reported in this part. Finally, the ion exchange capability of the synthesis product is demonstrated.

3.1 Kaolin composition analysis

The chemical compositions of kaolin samples from Lampang, Ranong and Narathiwat provinces were determined by XRF as given in the table 3.1. The main compositions of kaolinite samples are oxides of Si and Al. The Si/Al ratio of Lampang kaolin is 2.81, compared to 1.15 and 1.13 for Ranong and Narathiwat samples. High Si/Al ratio is the signature of high SiO₂ content as verified by XRD. Significantly, the kaolin from three provinces contains mineral impurities of iron, titanium, calcium, magnesium, etc. Therefore zeolite prepared from these kaolin samples are always contaminated with these elements [Chandrasekhar, P. N. 2001]. Those impurities may also effect the crystallization mechanism.

Table 3.1 The chemical compositions, LoI and Si/Al ratios of kaolin samples from three provinces determined by XRF

Chemical content (% weight)	Lampang	Narathiwat	Ranong
SiO ₂	67.08	46.72	45.63
Al ₂ O ₃	21.12	35.75	35.75
Fe ₂ O ₃	0.79	0.70	0.77
TiO ₂	0.03	0.64	0.04
MnO ₂	0.10	0.01	0.01
CaO	0.18	0.03	0.02
MgO	0.08	0.05	0.04
K ₂ O	2.87	0.43	0.99
LoI (%)	6.27	13.86	13.38
Si/Al ratio	2.81	1.15	1.13

To confirm the XRF data, AAS was used to determine the concentration of Si, Al and Fe contained in the kaolin samples. The AAS result is shown in table 3.2. The AAS data agrees well with the XRF data ensuring the chemical compositions data. It has been shown in the literature that kaolin material with a Si/Al ratio closed to unity is suitable for the synthesis of zeolite. At this stage, it may be speculated that Lampang kaolin would not give a good synthesis result.

Table 3.2 The concentration of Si, Al, and Fe of kaolin samples from three provinces as determined by AAS.

Elemental Content (%weight)	Lampang	Narathiwat	Ranong
Si	32.11	22.02	21.9
Al	10.99	19.24	19.52
Fe	0.66	0.52	0.69
Si/Al ratio	2.92	1.14	1.12

3.2 Characterization of kaolin and metakaolinite

Prior to the zeolite synthesis, kaolin samples must be prepared by calcination process to transform them to metakaolinite. In order to know the effect of calcination, one may analyze the characteristics of the samples before and after the process. Therefore XRD and IR spectra were recorded for comparison.

3.2.1 Kaolin characterization

The powder XRD spectra of kaolin samples from three provinces were recorded as shown in figure 3.1. The identifications of different crystalline phases were realized by using diffraction pattern files provided by Joint Committee on Powder Diffraction Standards (JCPDS). All of the samples showed clear diffraction peaks exhibiting some degree of crystallinity. Significantly, the major composition of Lampang kaolin is quartz mixed with a minority amount of kaolin. On the other hand, the XRD characteristics of Narathiwat and Ranong kaolin samples indicate the kaolin majority. Nevertheless, the precise ratios between quartz and kaolin phases in the samples have not been determined.

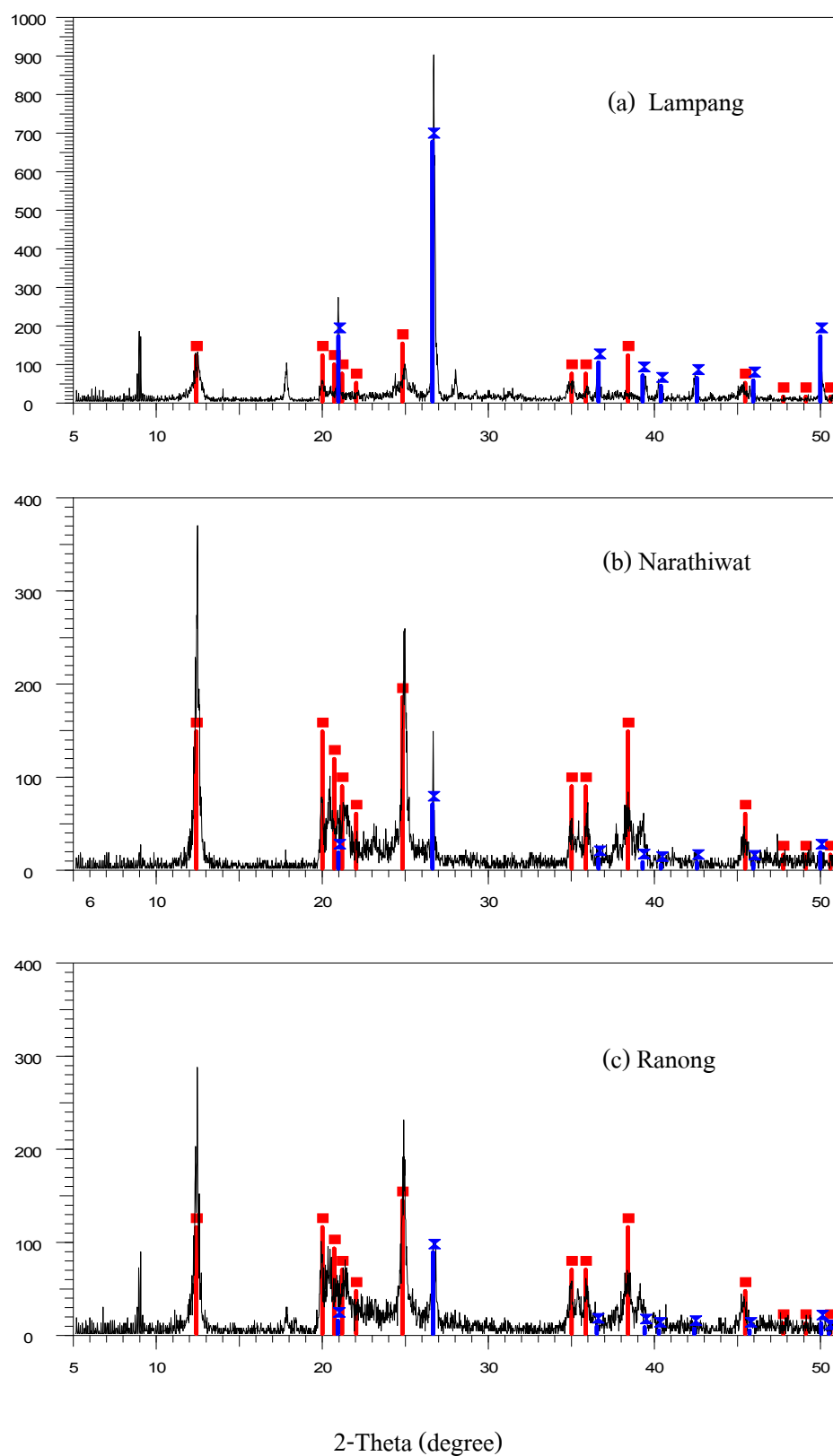


Figure 3.1 Powder XRD patterns of Lampang (a), Narathiwat (b), and Ranong (c), kaolin samples compared with the standard pattern from JCPDS database.

(\times quartz and \blacksquare kaolin).

IR spectra of natural kaolin samples were also recorded as shown in figure 3.2. In general, an absorption bands is related to the vibration at a specific configuration of chemical bonding. The interpretation of the spectra has been guided by the data published in literatures (Madani, A. et al., 1990. Bougeard, D. et al., 2000). The identifications of IR absorption bands to the related vibrations are shown in table 3.3. Since the major compositions of all samples are oxides of Si and Al, therefore the IR spectra exhibit the similar series of absorption bands as expected.

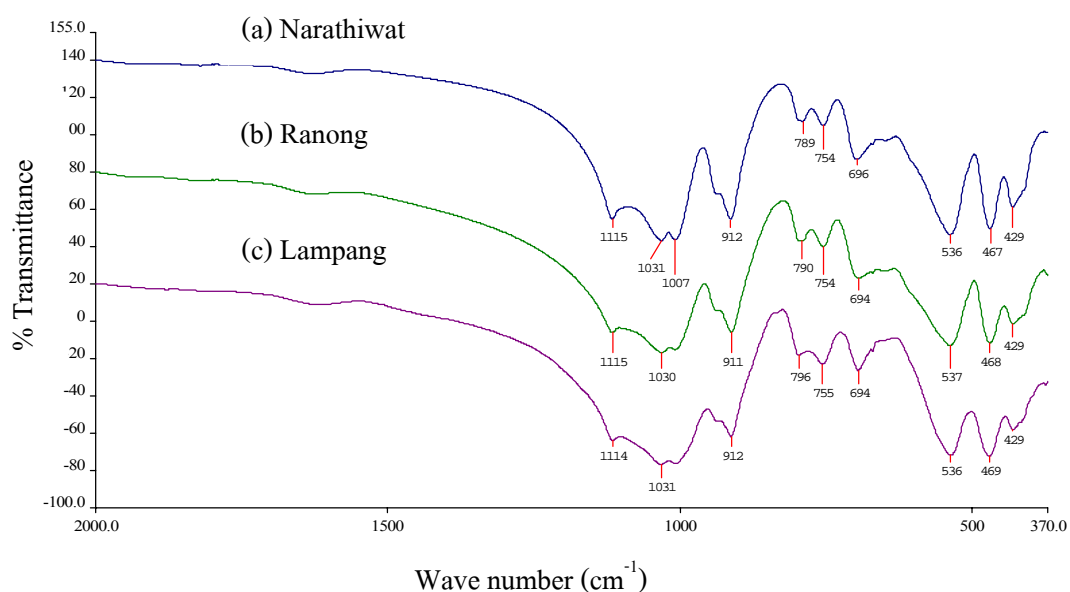


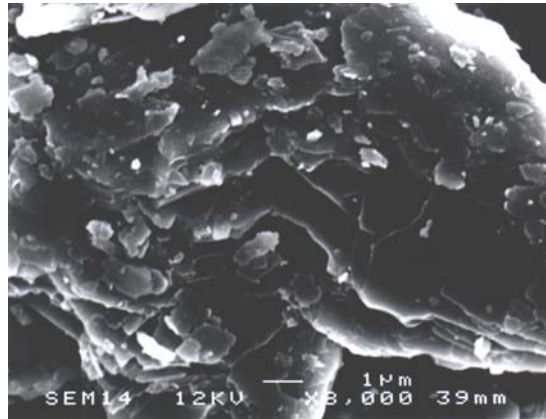
Figure 3.2 IR transmission spectra of kaolin from three provinces:

(a) Narathiwat, (b) Ranong, (c) Lampang

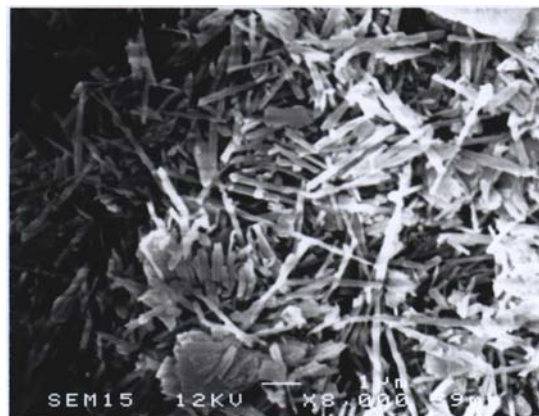
Table 3.3 Identifications of IR absorption bands to specific vibrations.

Wave number (cm ⁻¹)	Vibrations
1115, 1030, 1007	Asymmetric Si-O stretching
912, 936	O-H bending
789	Si translation
696, 755	Symmetric Si-O stretching
537	Coordinated Al octahedral
468	O-Si-O, O-Al-O bending, stretching
429	O-Al-O bending

Lampang kaolinite



Ranong kaolinite



Narathiwat kaolinite



Figure 3.3 SEM micrograph of the kaolin samples with 12kv and 8,000 magnification.

All of the kaolin samples from three provinces were examined by SEM. The micrographs are shown in figure 3.3. Each micrograph was taken at the electron energy of 12 kV with a magnification of 8000 or an area coverage of about 12x10 μm .

From the micrographs, at this scale, the structures of the kaolin samples appear to be different. Lampang kaolin shows layer-structure with the period of about 0.3 μm per layer. There are some small grains, $\sim 0.5 \mu\text{m}$ size, dispersed over the layers. This may be the indication of the mixing between kaolin and quartz in this sample. For the case of Ranong sample, some needle-like structure with irregular orientation is observed. Shape and size of the needles appear to be uniform about 30 μm long and 2 μm thin. Different structure is observed for Narathiwat sample. The sample has a layer-structure with uniform period of about 2 μm and the layers are well oriented.

After the characterizations by XRF, AAS, XRD, IR and SEM, the kaolin samples were calcined at 500, 600, 700, 800 and 900 $^{\circ}\text{C}$ to investigate about the activation temperature. At high enough temperature kaolin can be transformed into metakaolinite which is a suitable form for the synthesis of zeolite Na-A.

3.2.2 Metakaolinite characterization

The x-ray diffraction patterns of kaolin samples after calcination at different temperatures are shown in figure 3.4. In general, at the activation temperature of 500 $^{\circ}\text{C}$, no major structural change has been observed. However, when activated at 600, 700, 800 and 900 $^{\circ}\text{C}$, the crystalline kaolinite related peaks gradually disappeared and the amorphous phase appeared as evidenced by the very broad diffraction hills. The result suggested the transformation of crystalline phase of kaolinite into the amorphous phase called metakaolinite. Nevertheless, the SiO_2 related peaks remained apparently distinguishable in all of the samples suggesting the high thermal stability of crystalline quartz phase. This implies some difficulties in the use of the high quartz contained kaolin sample in the synthesis of zeolite.

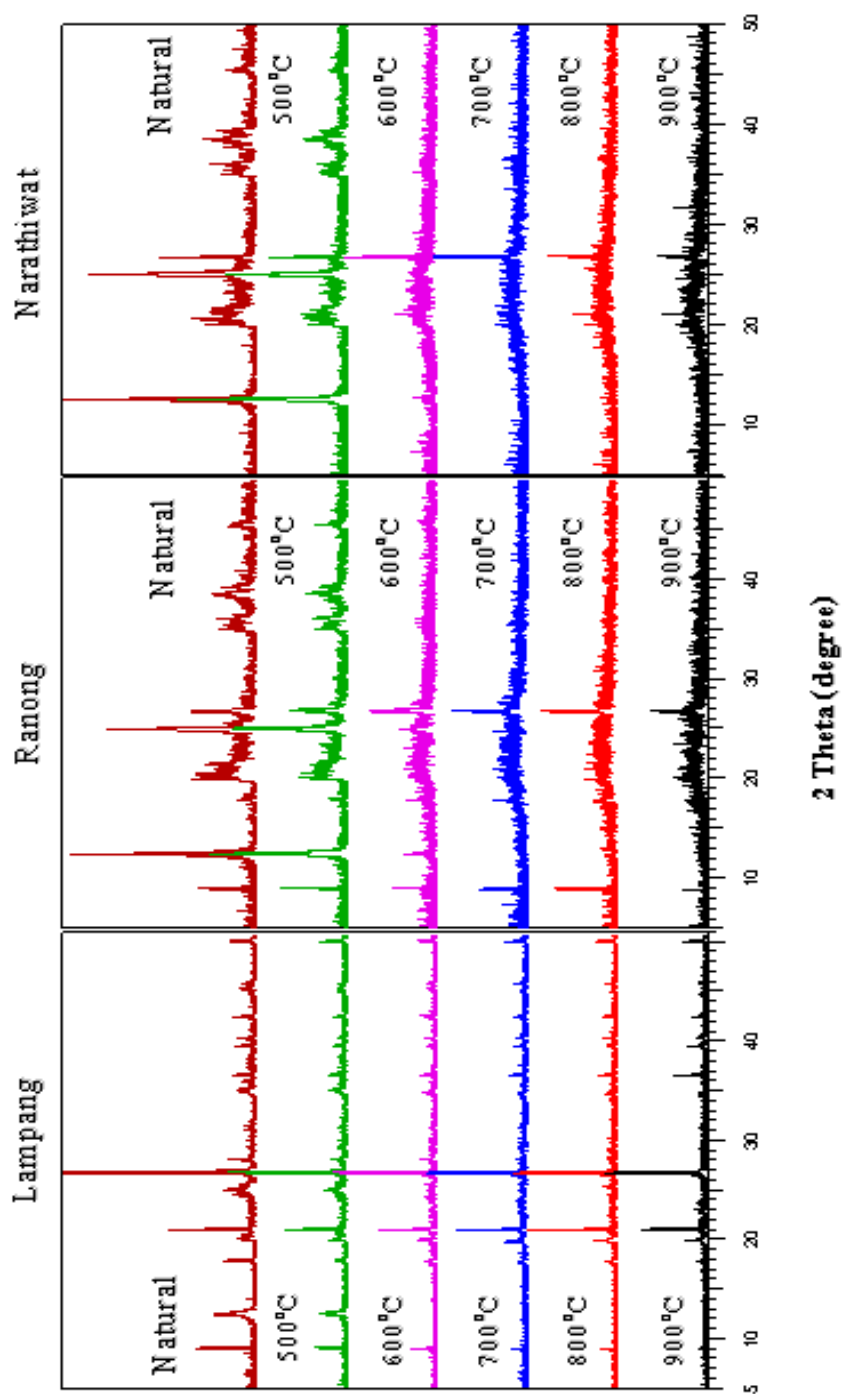


Figure 3.4 Powder XRD spectra for kaolin samples after calcination at 500, 600, 700, 800 and 900°C compared to the raw samples.

From the XRD result, it could be expected that Lampang samples would give a lower zeolite yield than the Ranong and Narathiwat samples because of the high concentration of quartz phase which is very stable.

Not only the kaolinite structure is altered by the calcination but also some chemical bondings as shown by IR measurement.

IR transmission spectra for kaolin samples after calcination at 500, 600, 700, 800 and 900°C were compared to the raw samples in figure 3.5. At the calcination temperature of 500°C, the IR spectra of the samples were similar to the unheated samples. Referring to table 3.3, at the calcination temperature rising from 600-900°C, the antisymmetric Si-O stretching bands merged to be a broad band and shifted to 1030-1090 cm⁻¹. The OH bending bands were eliminated indicating the complete dehydroxylation process. The coordination of Al changed from octahedral at 537 cm⁻¹ to the lower one at 803-810 cm⁻¹. This was indentified as the Al-O bond in the Al₂O₃ part of metakaolinite. In the case of Lampang kaolin, the absorption band at 536 cm⁻¹ which is related to Al at octahedral sites was visible even after being calcined at 900 °C.

Generally, the calcination temperature is chosen in the range that enable the complete transformation of crystalline kaolin into the amorphous phase of metakolinite. From thermodynamics point of view, the higher calcination temperature, the better transformation can occur. However, there should be some balance from the economic reason. Therefore, the calcination temperature of 600°C was chosen for the following experiment since it is high enough for the transformation and uses the lower amount of electrical power.

3.3 The synthesis of zeolite Na-A

3.3.1 Effect of the kaolin source

To study the effect of kaolin source in the synthesis of zeolite Na-A, the calcination temperature of 600°C for 1 h was selected since the amorphous kaolin can be obtained at this temperature. The synthesis condition was 10% w/v of NaOH concentration, and the reaction temperature of 100°C. To follow the reaction processes, the solid phases were regularly sampled until 300 min of reaction time. XRD was used to measure the structural property of the collected solid samples. The XRD patterns of the solid samples from three series are shown and compared to the pattern of standard zeolite in figure 3.6

From the figure, the zeolite Na-A XRD peaks started to appear gradually. Similar results were obtained for Narathiwat and Ranong samples. During the induction period, up to 30 min, no crystalline products were formed or in the other word the amount of nucleated crystals were under the detection limit. However, after 60 min, the characteristic peaks of zeolite Na-A started to appear over the broad peak of amorphous metakaolinite phase, indicating the transformation process. After 120 min, the XRD characteristic peaks of the samples were similar to the standard zeolite Na-A product. At this stage, a high fraction of the metakaolinite has transformed into zeolite Na-A.

Considering the Lampang product a different result was obtained. Only a limited amount of the Lampang product showed the characteristic of zeolite Na-A even after 300 min, indicating difficulties in the transformation. The characteristic peaks of quartz were visible all the time. This demonstrated the rigidity of quartz phase against the transformation to the other phases.

The plots between the percentage of zeolite Na-A crystallinity obtained in the synthesis of zeolite Na-A from different sources of kaolinite and reaction time are shown in figure 3.7. The individual point is defined as the ratio of the total area of 12 strong XRD peaks of each sample to the reference standard zeolite Na-A sample which is set to be 100% (Hu, H. C. et al., 1990). From the data, within the expectation, Lampang sample gave a small yield of only 28%, while Narathiwat and Ranong samples gave satisfactory yields which are 77% and 73% respectively.

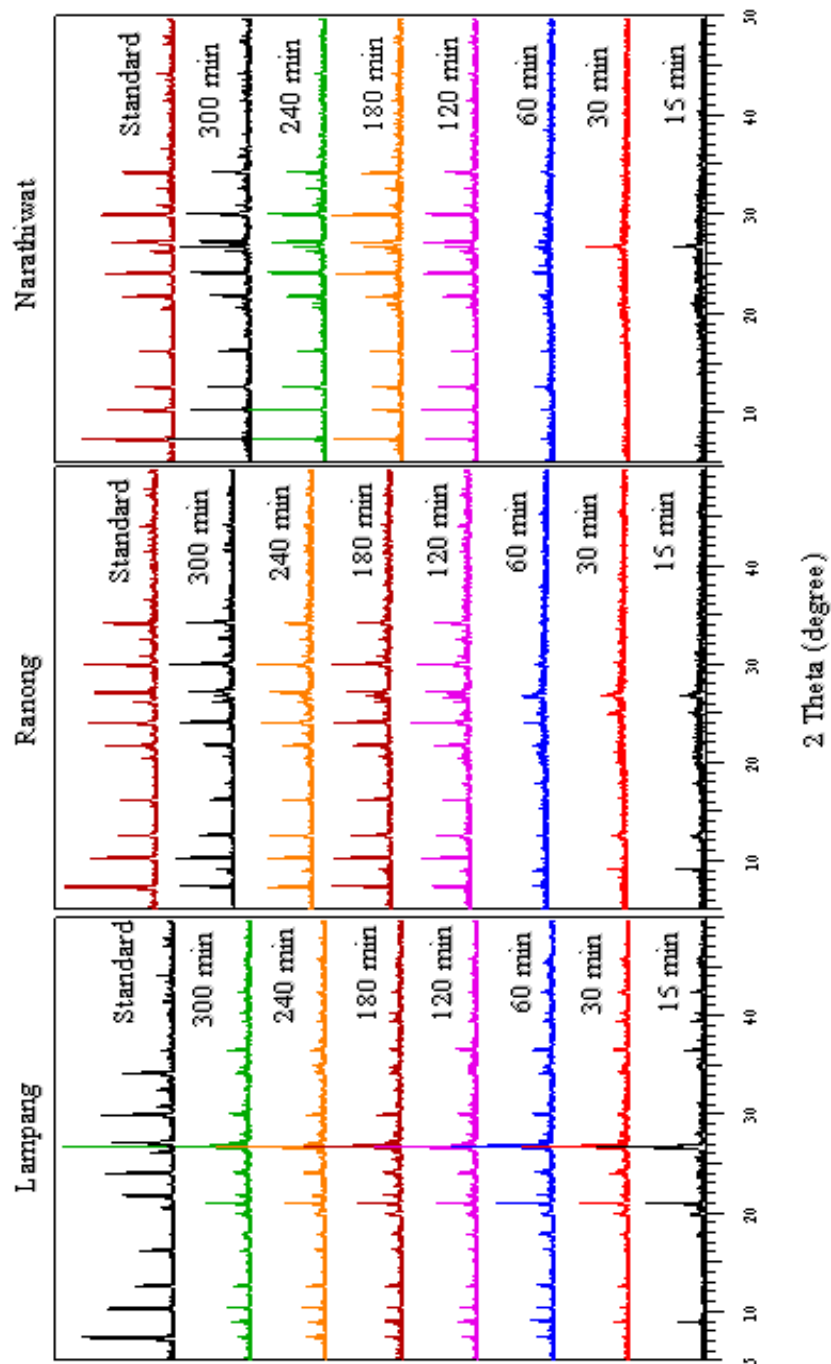


Figure 3.6 Powder XRD patterns of solid phase samples obtained during the synthesis of zeolite Na-A from Lampung, Ranong and Narathiwat samples.

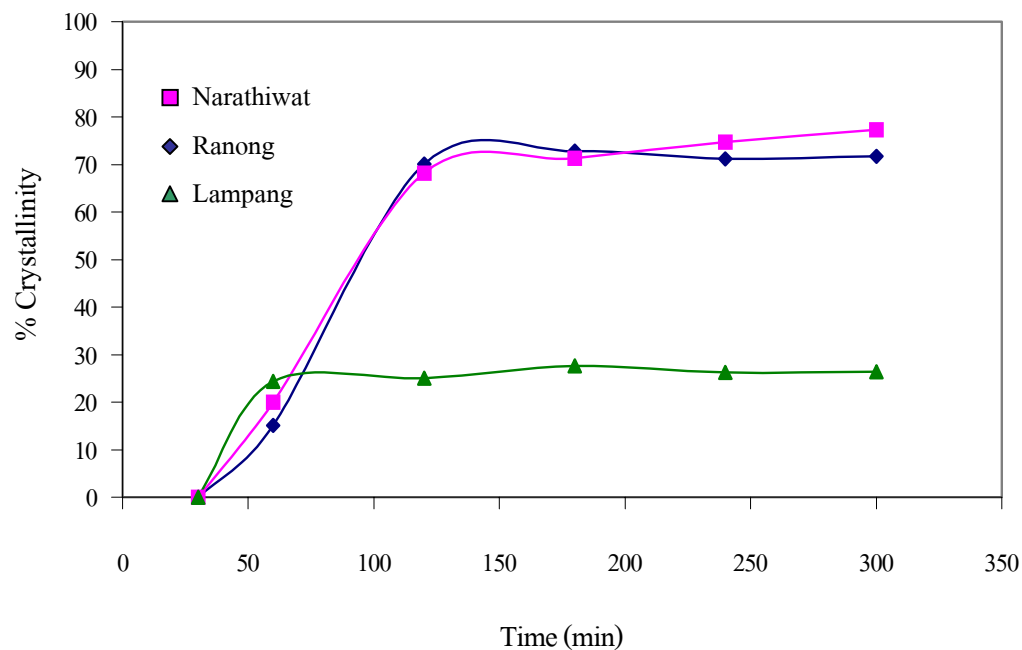


Figure 3.7 Plot of XRD crystallinity of zeolite Na-A with time during the synthesis using kaolin from Lampung, Ranong and Narathiwat

IR measurements were done for to verify the XRD result. IR absorption bands for standard zeolite Na-A is shown in figure 3.8. Table 3.4 summarizes the IR absorption bands for zeolite Na-A and the related vibrations (Rocha J. et al., 1991, Deortier, A et al., 1997)

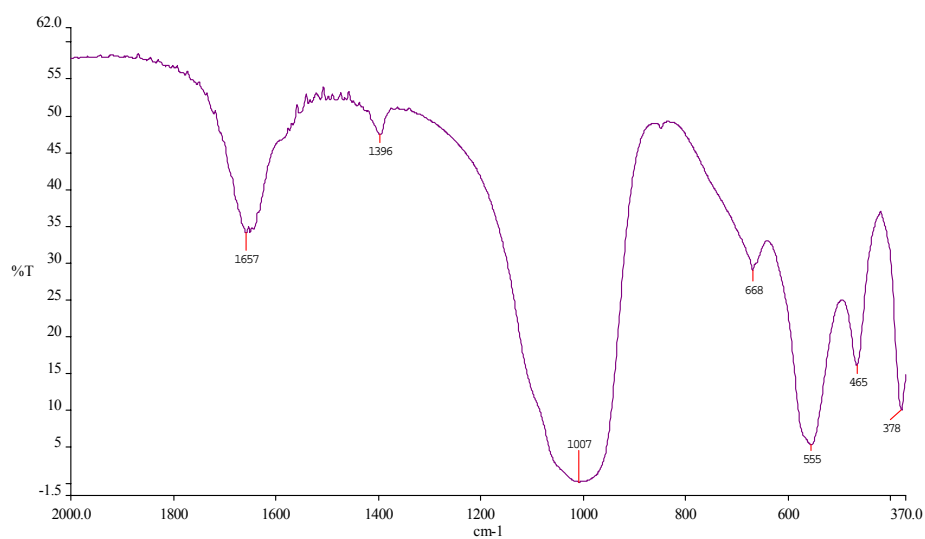


Figure 3.8 IR absorption bands of standard of zeolite Na-A.

Table 3.4 IR Vibration bands of zeolite Na-A.

Absorption band (cm^{-1})	Vibration
378	Opening of pore
465	Si-O, Four-coordinated Al-O bending
555	Double four member ring
1007	Assymmetric stretching Si-O, Al-O

Figure 3.9 shows the IR spectra of solid samples obtained at various times during the synthesis of zeolite Na-A from kaolin compared with the standard zeolite Na-A. The broad band of metakaolinite located at 800 cm^{-1} assigned to the Al-O bonds in Al_2O_3 was not observed. The vibration band at 1090 cm^{-1} for metakaolinite assigned to the stretching of Si-O bond in SiO_2 is shifted to 1007 cm^{-1} after 60 min of reaction. At 120 minutes of reaction, several bands started to appear. The band at 554 cm^{-1} is closed to the value of cubic crystal band of zeolite Na-A. The band at 467 cm^{-1} is related to SiO and four coordinated AlO bending. The band at 1007 cm^{-1} is identified as antisymmetric stretching of Si-O or Al-O bonds. The band at 387 cm^{-1} is related to the opening of pores. This result verified the high degree crystallization of zeolite Na-A in Ranong and Narathiwat samples. Different result was obtained in the synthesis from Lampang kaolin. The band at 553 cm^{-1} is related to double- four membering in zeolite Na-A, however the band at 465 cm^{-1} which related to Si-O and four coordinated Al-O bending in zeolite Na-A is not visible. We may conclude that only small portions of the Lampang kaolin can be transformed to zeolite Na-A. The plot of percentage of crystallinity with time is shown in figure 3.10. Each data point represents the ratio of peak areas at 555 cm^{-1} and 465 cm^{-1} and the ratio is compared with the standard zeolite Na-A. The 72% and 70% of crystallinity were obtained from Narathiwat and Ranong samples while only 24% was obtained for Lampang sample.

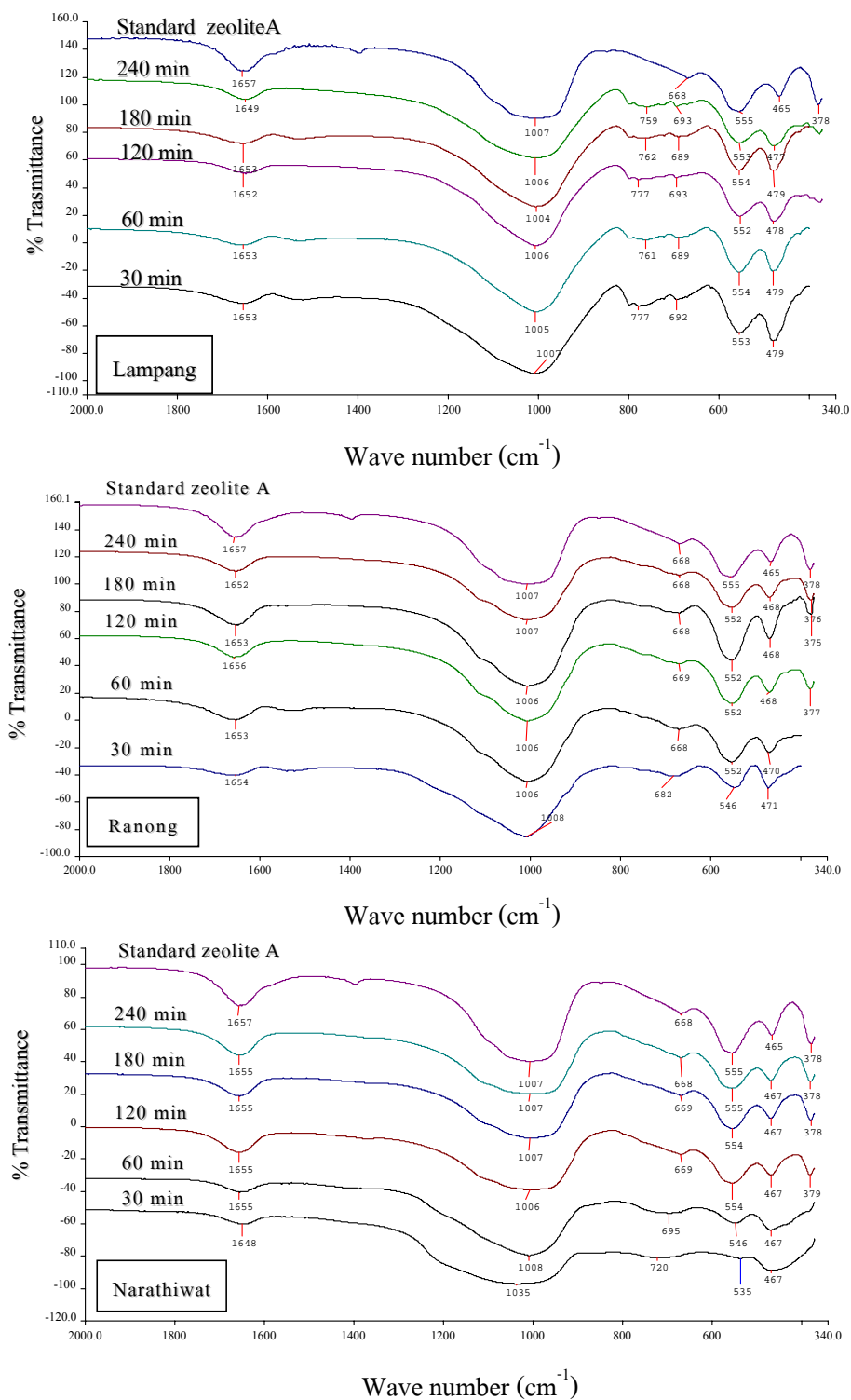


Figure 3.9 IR transmission spectra of solid sample obtained from the synthesis of zeolite Na-A from Thai kaolin at various times.

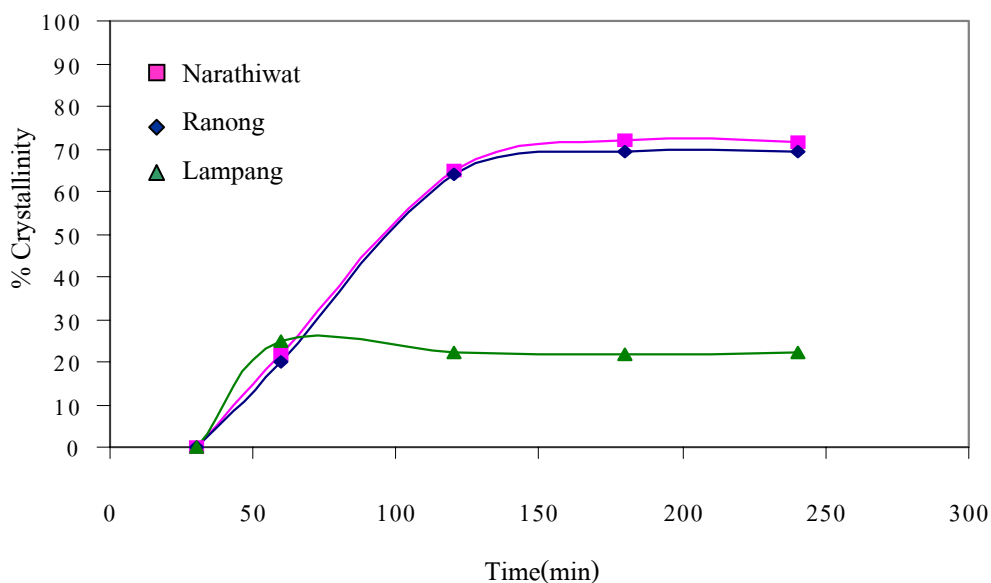
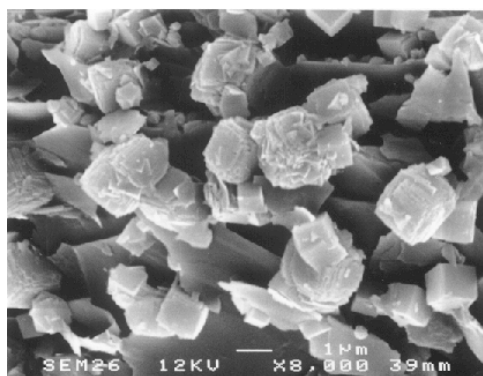


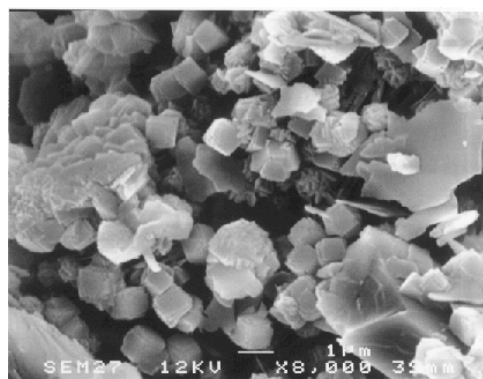
Figure 3.10 IR result for percentage of crystallinity of solid samples obtained from the synthesis of zeolite Na-A from Thai kaolin at various times.

Figures 3.11-3.13 show the SEM micrographs taken from the synthetic product from Lampang, Ranong, and Narathiwat samples, respectively. Zeolite Na-A crystal has cubic shape, therefore the good product should contain uniformly distributed cubic-shape crystals. In Lampang series, some cubic-shape crystals size $\sim 0.8 \mu\text{m}$, were observed to mix with the other platelet phase. This is consistent with XRD and IR that the majority quartz phase is contained in the Lampang samples. In the other hand, with the same synthesis condition, the cubic-shape crystals of size $1.0\text{-}1.5 \mu\text{m}$ were observed to distribute uniformly over the space for Ranong and Narathiwat samples. It is quite clear from the micrographs that the cubic crystals started to grow out of the metakaolinite structures. Even though the starting materials had different out-looks but resulting in a similar form of cubic crystals. This is the indication of high conversion ratio of metakaolinite to zeolite Na-A in Ranong and Narathiwat samples.

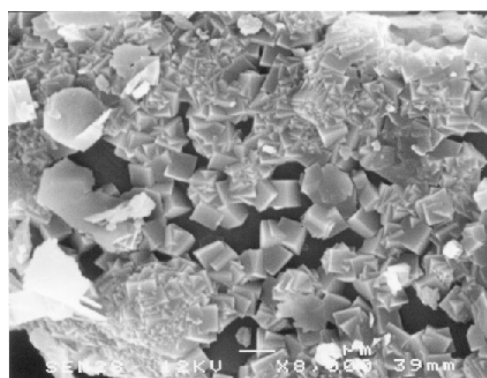
Since, the Narathiwat sample gave the highest yield, slightly over the Ranong samples, it was selected to be the starting material for the next experiment.



120 min

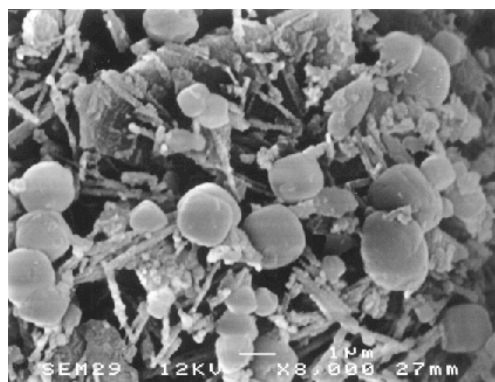


180 min

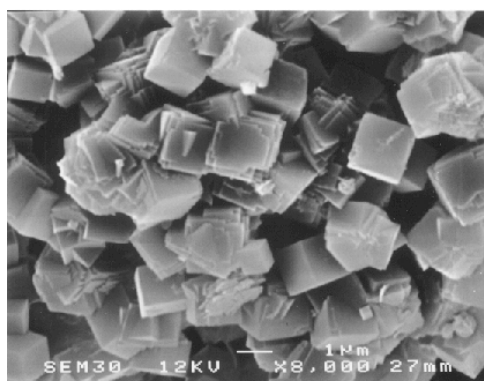


300 min

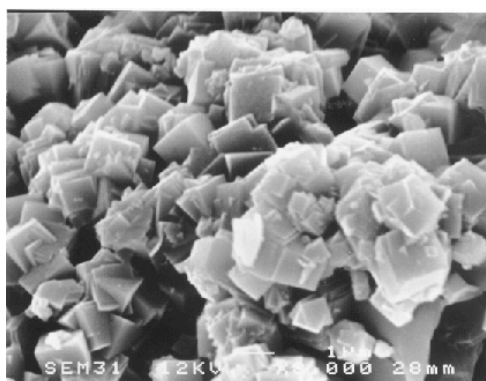
Figure 3.11 SEM micrographs of solid phases obtained in the synthesis of zeolite Na-A from Lampang kaolin activated at 600 °C with 10% w/v NaOH and reaction temperature 100 °C for various times.



120 min

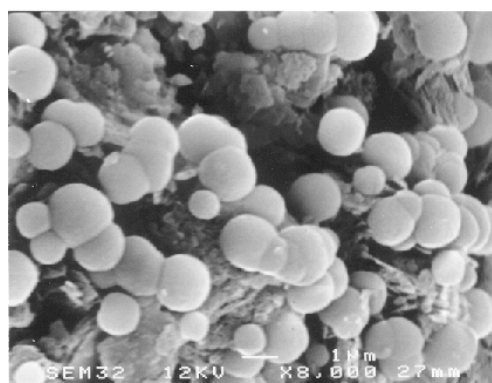


180 min

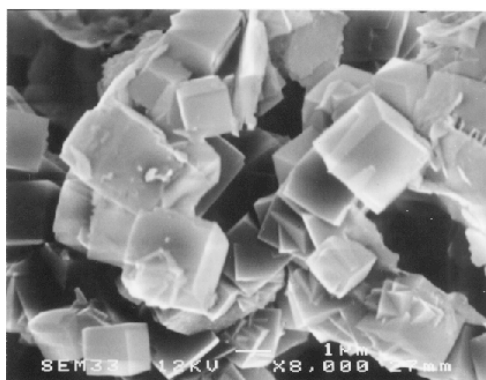


300 min

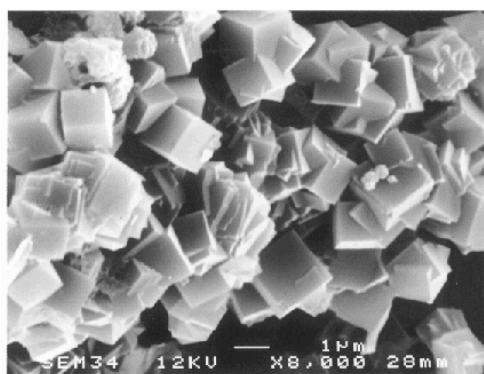
Figure 3.12 SEM micrographs of solid phases obtained in the synthesis of zeolite Na-A from Ranong kaolin activated at 600 °C with 10% w/v NaOH and reaction temperature 100 °C for various times



120 min



180 min



300 min

Figure 3.13 SEM micrographs of solid phases obtained in the synthesis of zeolite Na-A from Narathiwat kaolin activated at 600 °C with 10% w/v NaOH and reaction temperature 100 °C for various times.

3.3.2 The effect of calcination temperature

To study closer on the effect of kaolin calcination temperature, Narathiwat kaolin was selected to be the starting material. The samples were activated at the temperatures of 500, 600, 700, 800, and 900°C for 1 h and the calcined kaolin samples were used for synthesis zeolite Na-A with the condition NaOH 10%, 100°C.

From the previous studies, if the calcination temperature is too low, kaolin can not be transformed in to the amorphous form and resulting in no conversion into zeolite Na-A in the synthesis. As shown in figure 3.14, at the calcination temperature of 500 °C and kaolin was in the crystalline phase, even though some phase has occurred but no zeolite Na-A was observed by XRD.

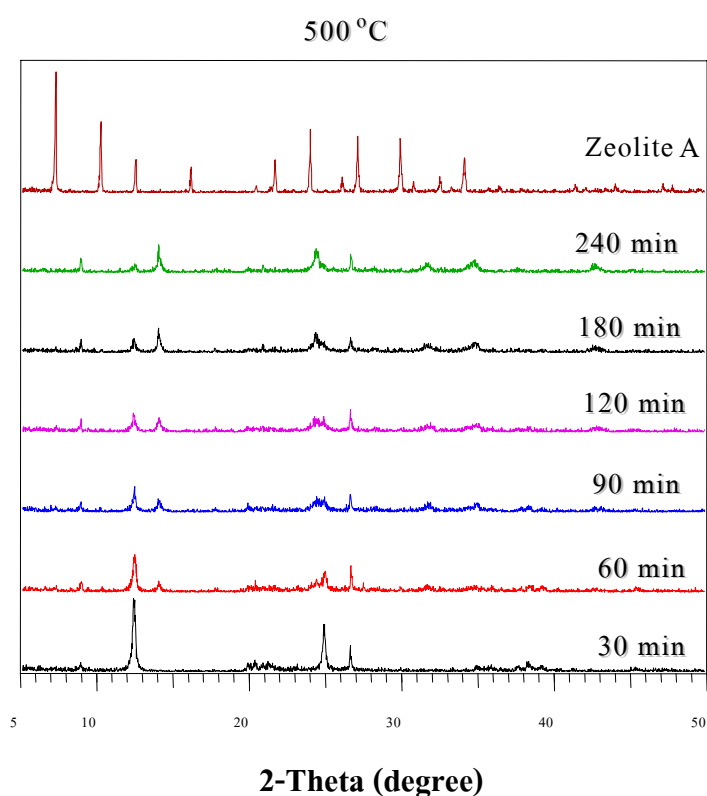


Figure 3.14 XRD spectra of the synthetic products using Narathiwat kaolin calcine at 500°C

The SEM observation as confirmed the XRD finding. As shown by the micrograph in figure 3.15, some round shapes buds have grown over the calcined kaolin structure but no cubic shape crystal seen in the micrographs.

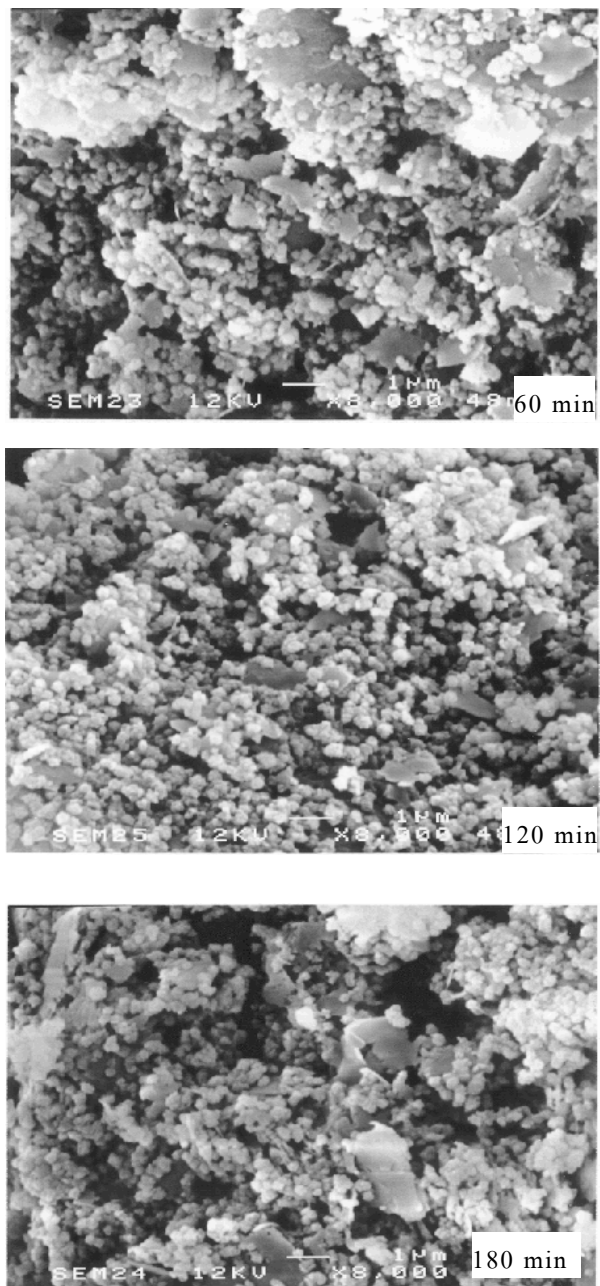


Figure 3.15 SEM micrographs of the synthetic products using Narathiwat kaolin calcine at 500°C

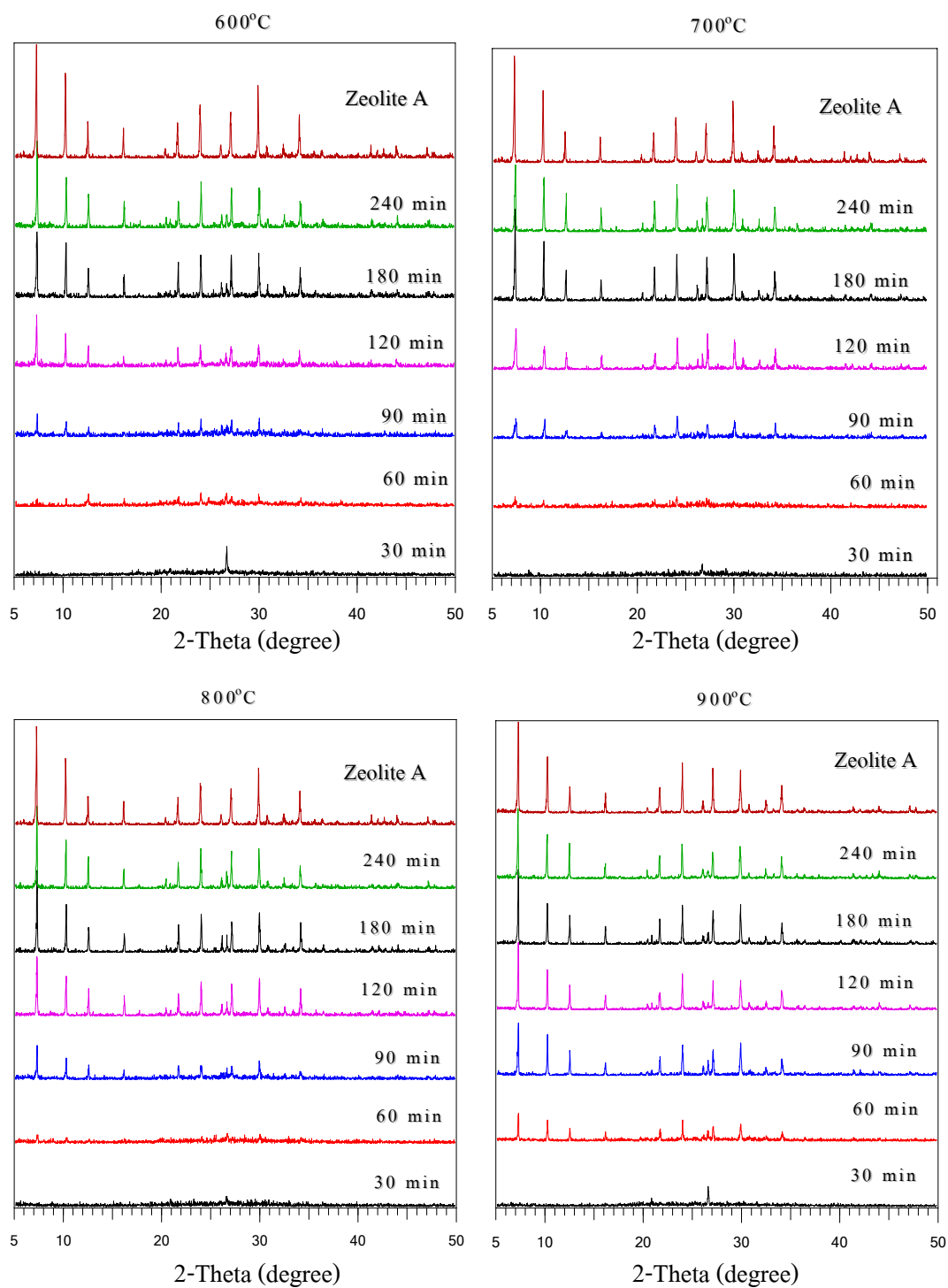


Figure 3.16 Evolution of zeolite Na-A XRD peaks during the synthesis when using Narathiwat kaolin activated at 600°C, 700°C, 800°C and 900°C.

On the other hand, when calcined at higher activation temperature (600-900 °C), kaolin can be transformed to metakaolinite, and the zeolite Na-A peaks can be synthesized. As shown in figure 3.16, the XRD shows the evolution of zeolite peaks during the synthesis.

After the induction period, the zeolite peak appeared at around 90 min of reaction time. The rate of growth tends to increase with the calcination temperature. At the activation temperature of 900 °C, we observed that zeolite peak appeared at 60 min which is faster when compared with 90 min. for the activation temperatures of 600-800 °C.

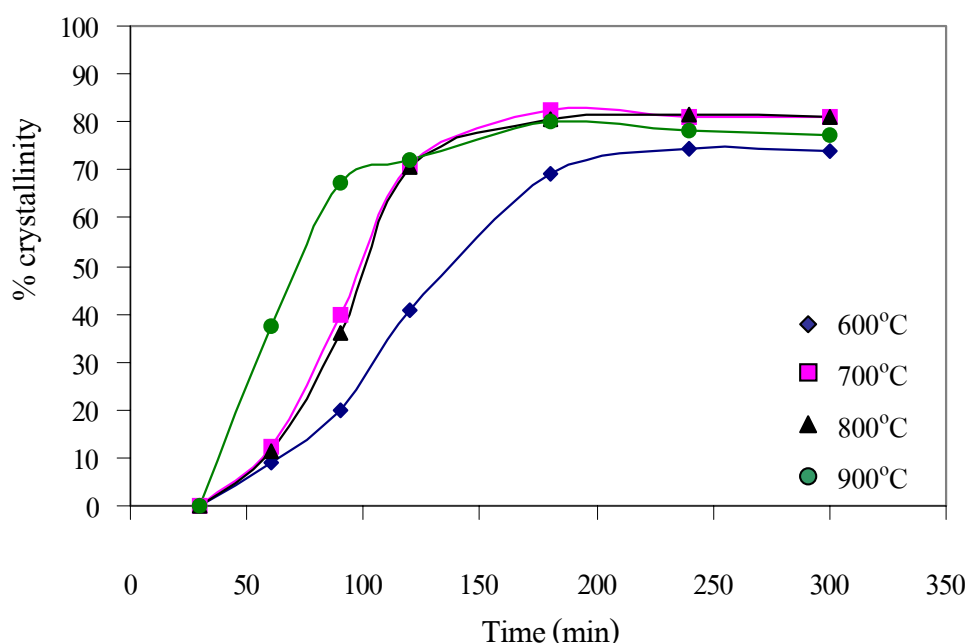


Figure 3.17 Percentage of crystallinity for different calcination temperature deduced from XRD.

The percentage of crystallinity for different calcination temperatures are shown in figure 3.17. In the beginning, the crystal in 900°C sample grew at the fastest rate until the reaction time reached 120 min, the 800°C and 700°C samples caught up. At 300 min, crystallinity of 900°C dropped down below the level of 800°C and 700°C. While 600°C, the crystal grew at the slowest rate but tended to catch up at the end. The calcination temperature of 700°C had the highest crystallinity which reached 82% after 300 min. Therefore, the calcination temperature of kaolin for the next experiment was selected to be 700°C.

3.3.3 The transformation of metakaolinite into zeolite Na-A

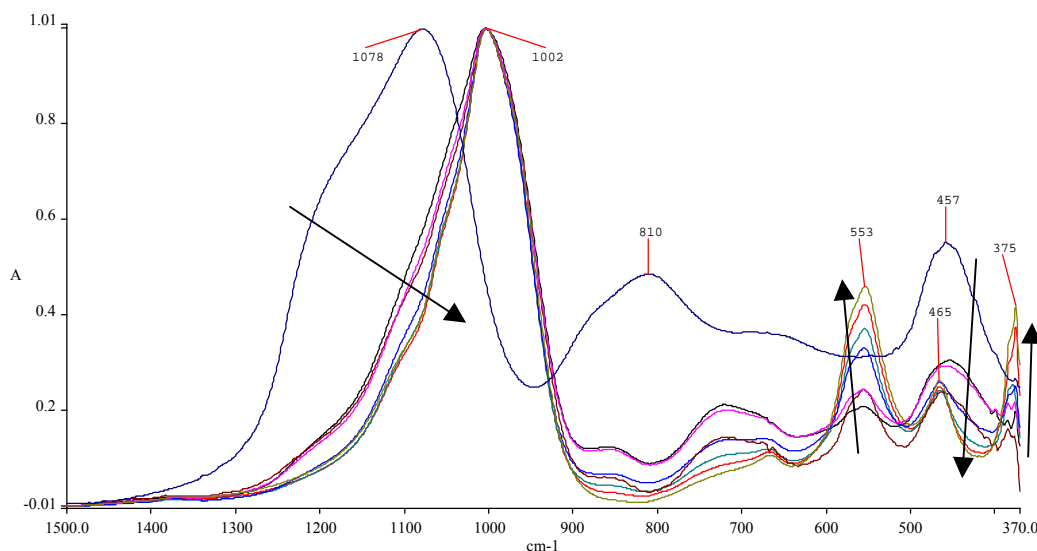


Figure 3.18 The evolution of IR spectra during the synthesis of zeolite Na-A from metakaolinite: The positions of absorption bands are labeled. The bands evolution directions are indicated by arrows, from metakaolinite to zeolite Na-A spectra. The synthesis condition was 10% w/v NaOH, with 70°C reaction temperature.

In a similar manner to XRD measurement, the IR spectra can be used to obtain the crystallinity of the product. As shown in figure 3.18, the directions of evolution of IR absorption bands during the synthesis of zeolite A from metakaolinite are indicated by arrows. The IR characteristic bands evolved from those of metakaolinite to the bands of zeolite Na-A, recalling table 3.3 and 3.4. For comparison, all base line spectra were normalized with zero absorbance taken at 1500 cm^{-1} and a maximum absorbance was set to be 1.0. From IR spectra, the intensity of the band at 555 cm^{-1} which is the characteristic of zeolite Na-A increased with increasing reaction time. The broad vibration band at 1078 cm^{-1} for metakaolinite, assigned to the stretching of Si-O bond in SiO_2 shifted to 1002 cm^{-1} and the band became narrow band. The broad band of metakaolinite located at 810 cm^{-1} , assigned to the Al-O bonds in Al_2O_3 was not observed in the final product. From the IR result, the high intensities, zeolite Na-A characteristic, band at 555 cm^{-1} was used to be the indication of zeolite formation. The zeolite Na-A crystal growth can be visually observed through SEM micrographs as shown in figure 3.19.

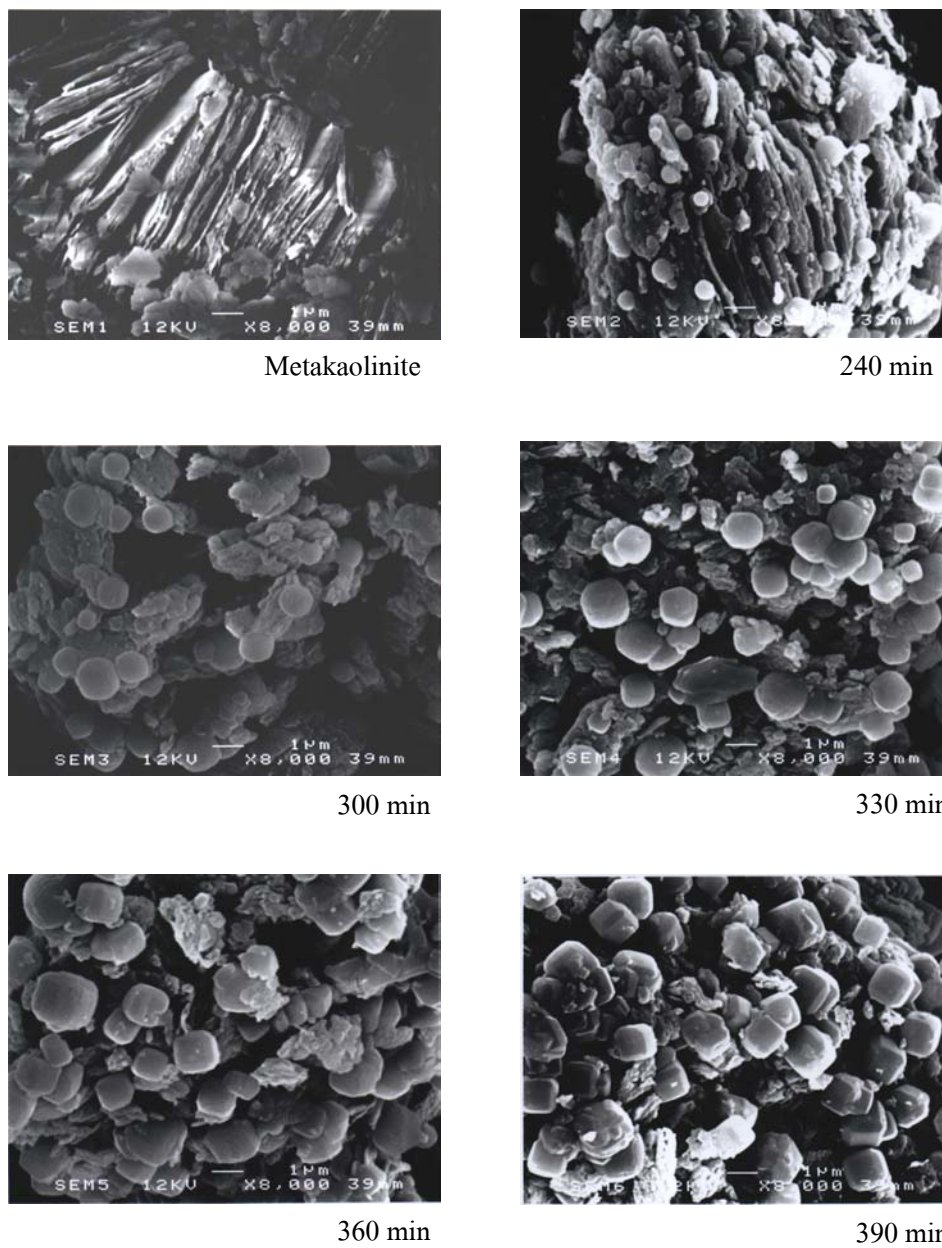
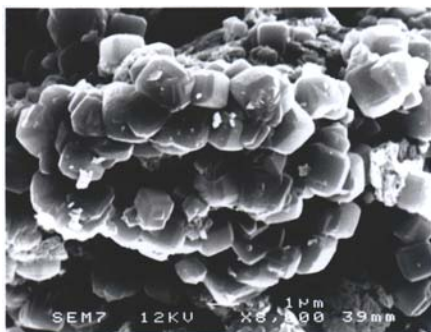
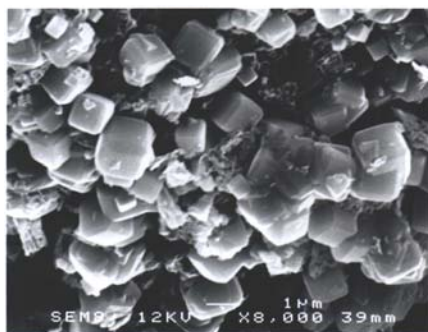


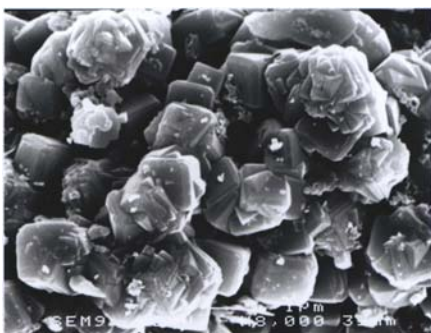
Figure 3.19 SEM micrographs of the solid phases obtained in the synthesis of zeolite Na-A from Narathiwat metakaolinite activated at 700⁰C with 10% w/v NaOH and reaction temperature 100⁰C.



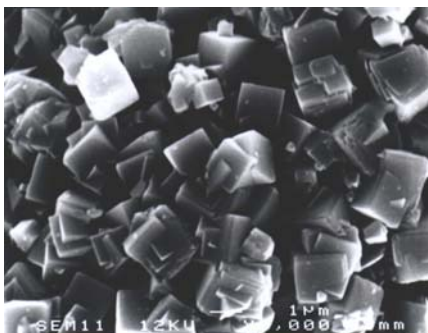
420 min



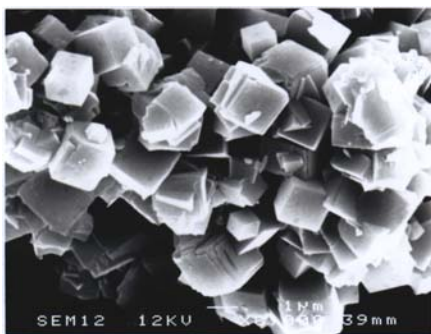
480 min



540 min



660 min



720 min

Figure 3.19 (Continued).

The 70°C reaction temperature was select to allow more convenient observation of the crystal growth. From the SEM micrographs, small round crystals of size ~0.2-0.5 µm started to appear on the metakolinite framework around 240 min. From XRD and IR data, these spheres are related to the first stage of the crystal growth. Then small sphere grew larger in size to be about 0.8-1.0 µm at 300 min. The number of crystal per area was also increased indicating the ongoing nucleation. At 330 min, the crystals started to evolve from round shape toward the cubic shape. The size of crystals were about 1.0-1.2 µm. At 330 min half of the crystals had cubic shape. This implied changing in the growth mechanism toward the preference of surface diffusion. At 480 min the crystal sizes were about 1.2-1.5 µm. From this time, the size of crystal grew slower but number of crystal per area still increased. However, the cubic crystals appeared to be very well defined, sharpen edges. This was the indication for higher surface diffusion mechanism. Therefore, the rate of crystallinity was more or less altered. This suggested that there were more than one growth mechanisms involving in the experiment.

3.3.3 The effect of alkalinity concentration and reaction temperature

In this section, the effect of reaction temperature and NaOH concentration on the synthesis of zeolite Na-A were investigated. Narathiwat kaolin activated at 700 °C was chosen to be the starting material. The synthesis conditions were varied on NaOH concentrations 10%, 15%, 20%, 25% and reaction temperatures 70 °C, 80 °C, 90 °C, and 100 °C. XRD and IR were used to determine the crystallinity at various times during the reaction.

The plots of the percentage of crystallinity of the solid products with reaction time from various experiment conditions deduced from XRD technique are shown in figures 3.20-3.23. Each figure represents the plots for one reaction temperature and various NaOH concentrations. In general, the higher NaOH concentration, the faster the reaction. At the NaOH concentration 10% and 15%, the percentages of crystallinity were high in the range of 78-85% at all reaction temperatures. On the other hand, at 20% and 25% NaOH, at 90°C and 100°C reaction temperatures, the crystallinity percentages remarkably decreased to be in the range of 45-70%. Therefore, it may be concluded that the suitable concentration of NaOH for the synthesis is about 10-15 %.

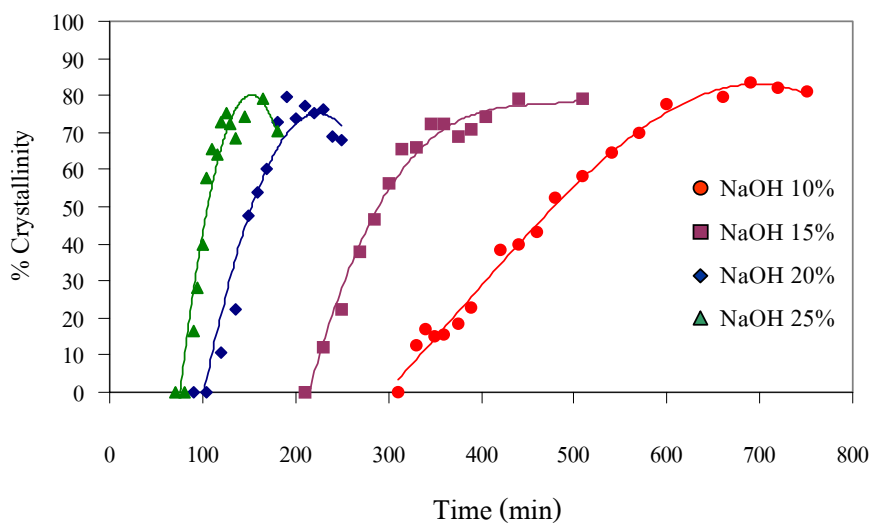


Figure 3.20 The percentage of crystallinity of zeolite Na-A obtained from the reaction of Narathiwat kaolin activated at 700 °C with NaOH concentrations of 10, 15, 20, and 25% at the reaction temperature of 70 °C.

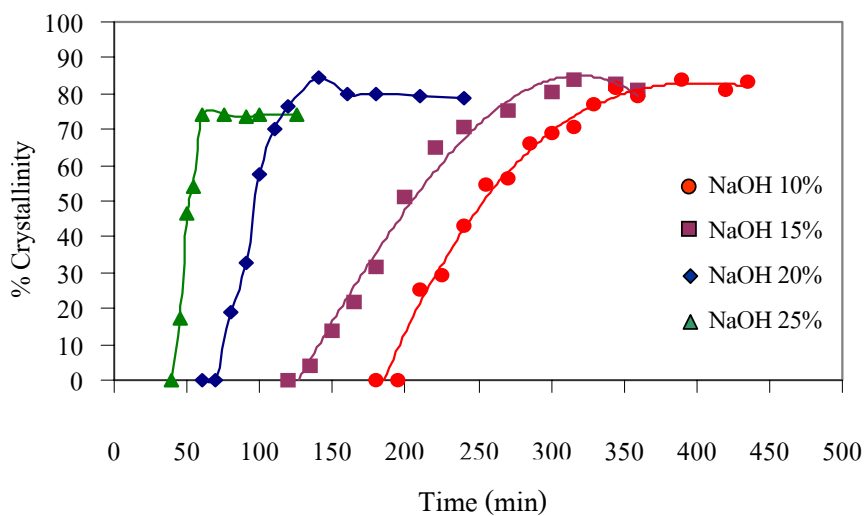


Figure 3.21 The percentage of crystallinity of zeolite Na-A obtained from the reaction of Narathiwat kaolin activated at 700 °C with NaOH concentration of 10, 15, 20, and 25% at the reaction temperature of 80 °C .

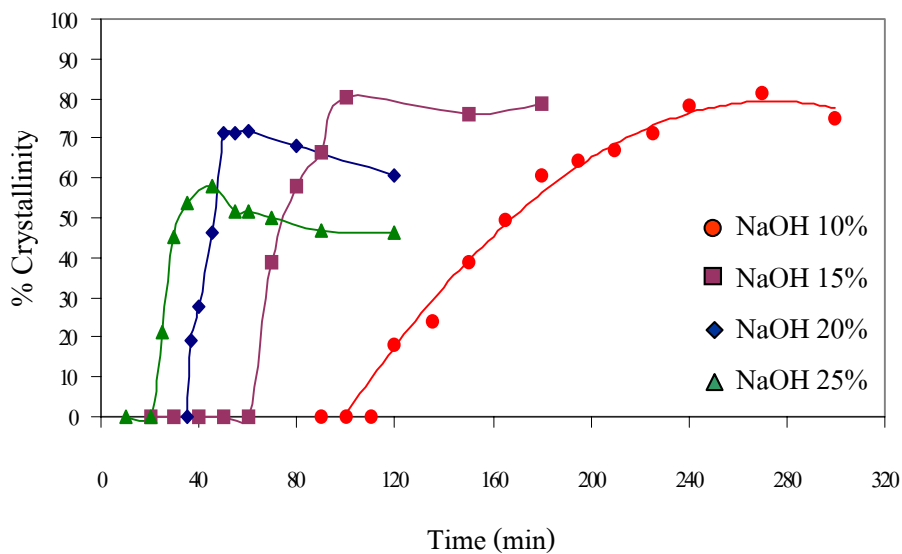


Figure 3.22 The percentage of crystallinity of zeolite Na-A obtained from the reaction of Narathiwat kaolin activated at 700 °C, with NaOH concentrations of 10, 15, 20, and 25% at the reaction temperature of 90 °C.

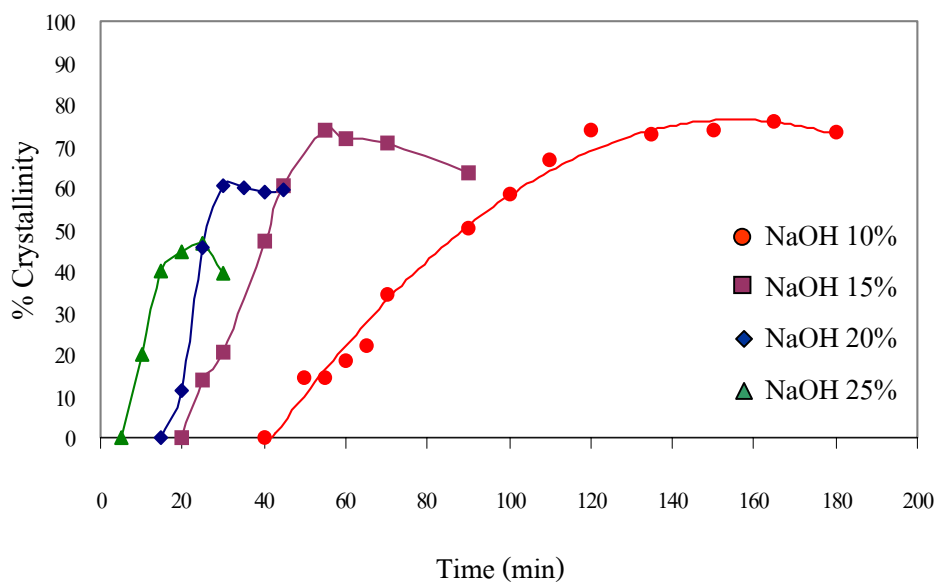


Figure 3.23 The percentage of crystallinity of zeolite Na-A obtained from the reaction of Narathiwat kaolin activated at 700 °C with NaOH concentration of 10, 15, 20, and 25% at the reaction temperature of 100 °C.

The reaction temperature has the similar effect on the synthesis. The plots of the percentage of crystallinity of the solid products with reaction time deduced from XRD technique when reaction temperature varied, are shown in figures 3.24-3.27. The data implied that, at the beginning of reaction, the rate of reaction increased with increasing reaction temperature.

At the reaction temperature 70 °C and 80 °C for all NaOH concentrations the average percentage of crystallinity of the solid products reached about 80%. For higher reaction temperature of 90 °C and 100 °C at high NaOH concentrations (20% and 25%), the reaction occurred faster at the beginning however the percentage of crystallinity decreased rapidly. Therefore the suitable reaction temperature is about 70-80°C.

From the data discussed so far, we may summarize that rate of crystallinity depends on the NaOH concentration and reaction temperature. The rate of crystallinity increases with increasing of NaOH concentration and reaction temperature. However, the percentage of crystallinity decreases at very high NaOH concentration and reaction temperature. The decreasing was due to the competition from the growth of sodalite phase, which will be discussed later. In summary, to obtain high yield, the synthesis condition must meet the requirements for NaOH concentration and reaction temperature.

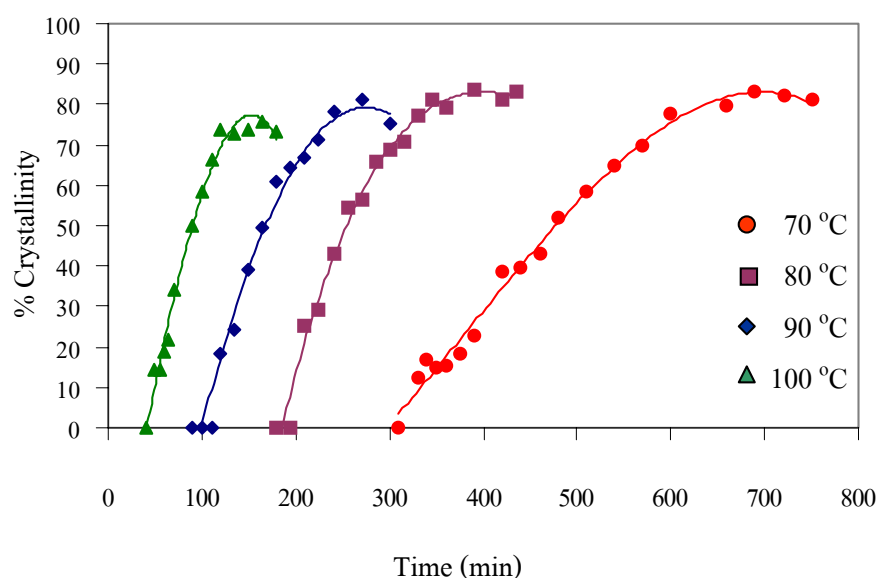


Figure 3.24 The percentage of crystallinity of zeolite Na-A obtained from the reaction of Narathiwat kaolinite activated at 700 °C with reaction temperatures of 70, 80, 90, and 100 °C at 10 % w/v NaOH concentration.

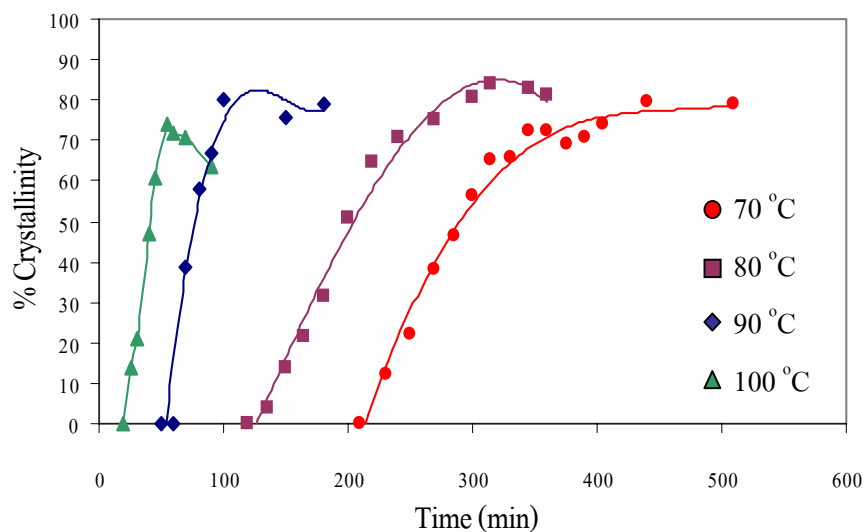


Figure 3.25 The percentage of crystallinity of zeolite Na-A obtained from the reaction of Narathiwat kaolinite activated at 700 °C with reaction temperatures of 70, 80, 90, and 100 °C at 15 % w/v NaOH concentration.

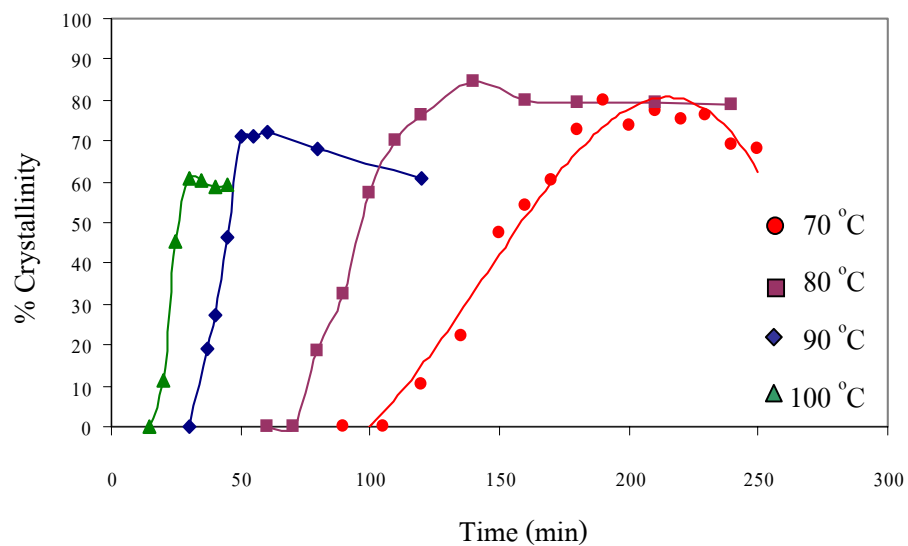


Figure 3.26 The percentage of crystallinity of zeolite Na-A obtained from the reaction of Narathiwat kaolinite activated at 700 °C with reaction temperatures of 70, 80, 90, and 100 °C at 20 % w/v NaOH concentration.

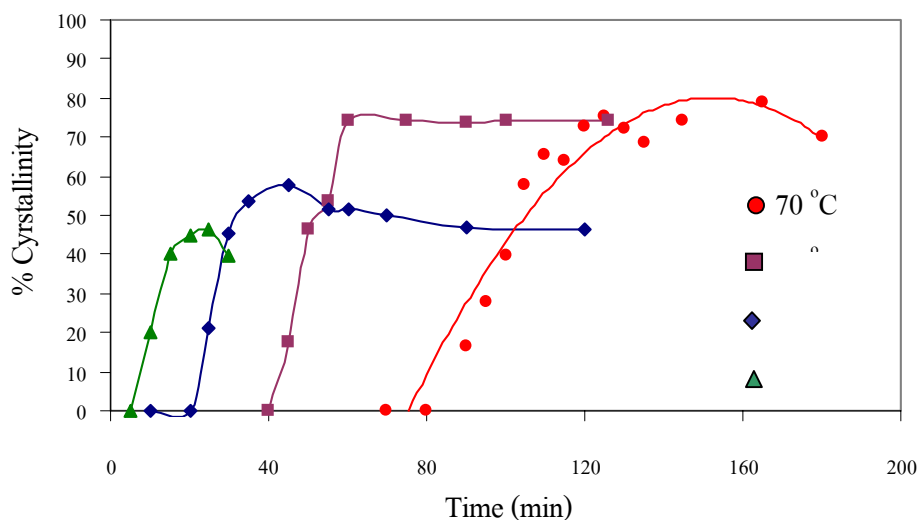


Figure 3.27 The percentage of crystallinity of zeolite Na-A obtained from the reaction of Narathiwat kaolinite activated at 700 °C with reaction temperatures of 70, 80, 90, and 100 °C at 25 % w/v NaOH concentration.

The IR measurement confirmed the XRD results. The data are shown in figure 3.28-3.31.

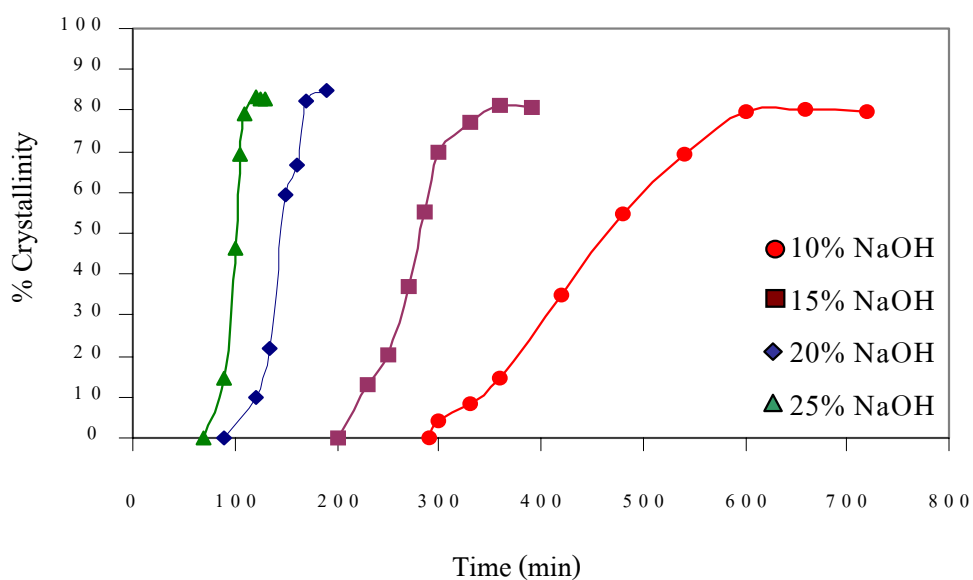


Figure 3.28 The percentage of crystallinity of zeolite Na-A obtained from the reaction of Narathiwat kaolinite activated at 700 °C with NaOH concentration of 10, 15, 20, and 25 % w/v and reaction temperature 70 °C.

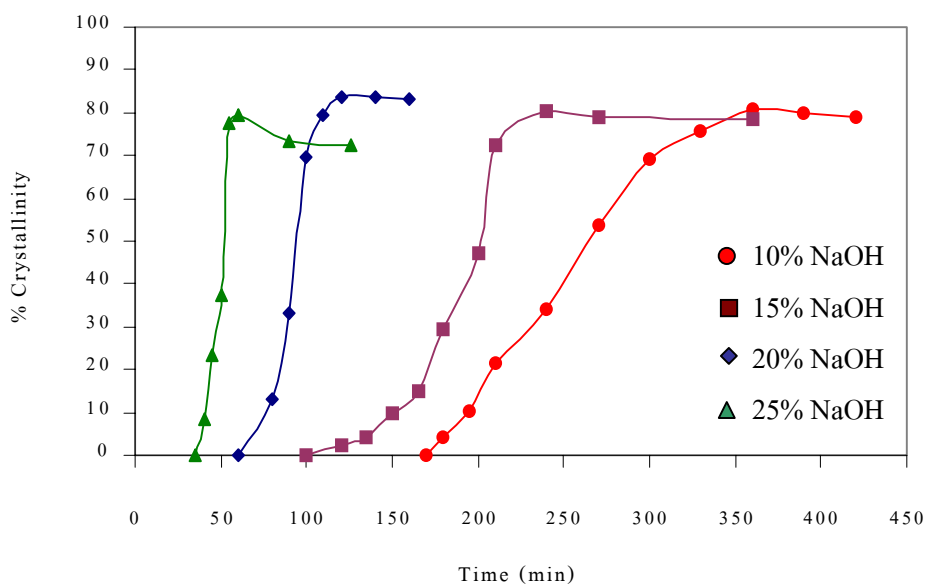


Figure 3.29 The percentage of crystallinity of zeolite Na-A obtained from the reaction of Narathiwat kaolinite activated at 700 °C with NaOH concentration of 10, 15, 20, and 25 % w/v and reaction temperature 80°C.

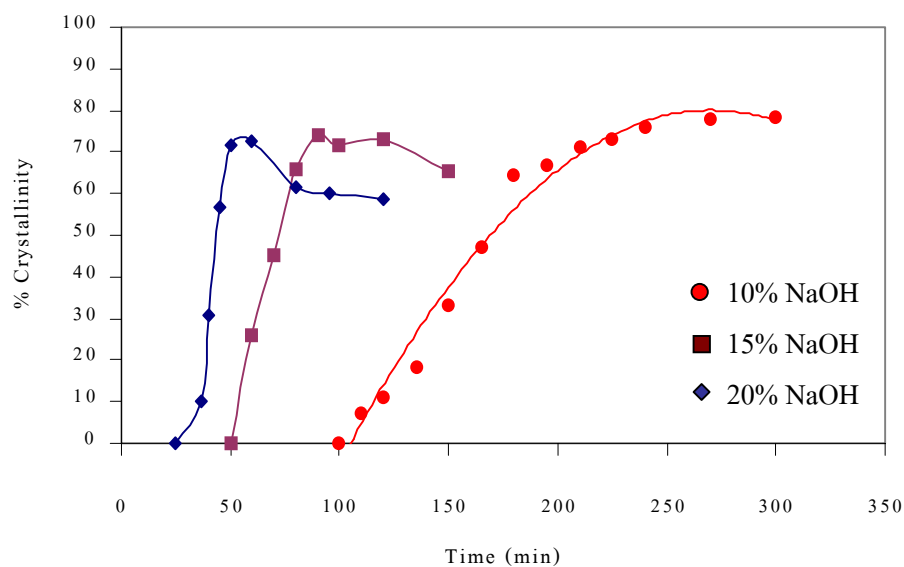


Figure 3.30 The percentage of crystallinity of zeolite Na-A obtained from the reaction of Narathiwat kaolinite activated at 700 °C with NaOH concentration of 10, 15, 20, and 25 % w/v and reaction temperature 90°C.

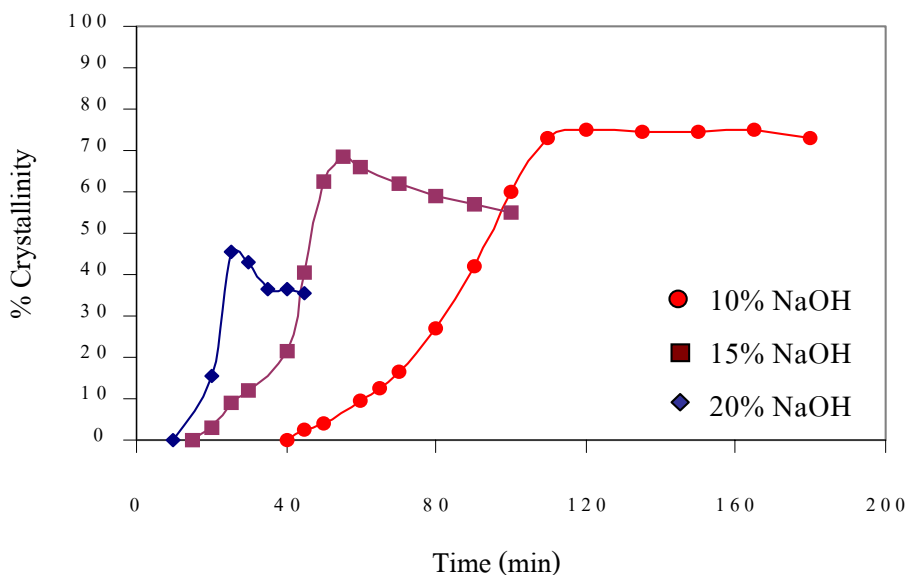


Figure 3.31 The percentage of crystallinity of zeolite Na-A obtained from the reaction of Narathiwat kaolinite activated at 700 °C with NaOH concentration of 10, 15, 20, and 25 % w/v and reaction temperature 100°C.

From crystallinity data, it may be concluded that both of the NaOH concentration and reaction temperature significantly influenced on the synthesis of zeolite Na-A from metakaolinite. The rate of crystallization was found to increase with NaOH concentration and reaction temperature. Simultaneously, the percentage of crystallinity of zeolite Na-A decreases at higher NaOH concentration and reaction temperature. Therefore, the NaOH concentration and reaction temperature are the important factors controlling the zeolite Na-A forming reaction.

XRD and IR technique were used to determine the percentage of crystallinity of zeolite Na-A at different stages of reactions. In general, both techniques give similar results thus confirming each other. To be precise, each technique has its own advantage and disadvantage compared to the other. IR would give an inaccurate crystallinity value at temperature 90°C and higher, due to the overlapping of absorption bands between zeolite Na-A and the other phase which is sodalite. However, the inductive period of crystal formation could be detected earlier by IR. For XRD technique, the crystallinity value could be measured at all range of temperatures

because of the lower effect on peaks overlapping, but it also insensitive to the detection of induction period.

From the crystalline curve of various experiment conditions, the percentage yields of zeolite Na-A are shown in table 3.5 for XRD data and table 3.6 for FTIR data. The suitable synthesis conditions were NaOH concentration of 10-15% and reaction temperature of 70-80°C which gave about 79-85% yield. In table 3.6, some of the IR data can not be obtained due to high intensity of sodalite absorption bands in those samples.

Table 3.5 The maximum yield of zeolite Na-A from various experiment conditions from XRD.

[NaOH] % w/v	Temp. (°C)							
	70 °C		80 °C		90 °C		100 °C	
	% yield	t (min)	% yield	t (min)	% yield	t (min)	% yield	t (min)
10 %	83	690	84	390	81	270	76	165
15%	79	440	84	300	80	100	74	55
20%	80	190	85	140	72	60	61	30
25%	80	125	74	60	58	45	46	25

Table 3.6 The maximum yield of zeolite Na-A from various experiment conditions from IR.

[NaOH] % w/v	Temp. (°C)							
	70 °C		80 °C		90 °C		100 °C	
	% yield	t (min)	% yield	t (min)	% yield	t (min)	% yield	t (min)
10 %	80	600	81	360	78	285	75	165
15%	81	360	81	315	74	100	68	55
20%	85	190	84	140	73	60	45	25
25%	83	120	80	60	-	-	-	-

Significantly at the 25% NaOH concentration and reaction temperature of 100 °C, a new phase, mixed with zeolite Na-A in the product, is observed. Figure 3.32 shows XRD pattern of the product. From XRD, the new phase was identified to be hydroxy-sodalite (SOD) at $2\theta = 14^\circ$ and 24.65° . This caused the crystallization percentage of zeolite Na-A to decrease at higher NaOH concentration.

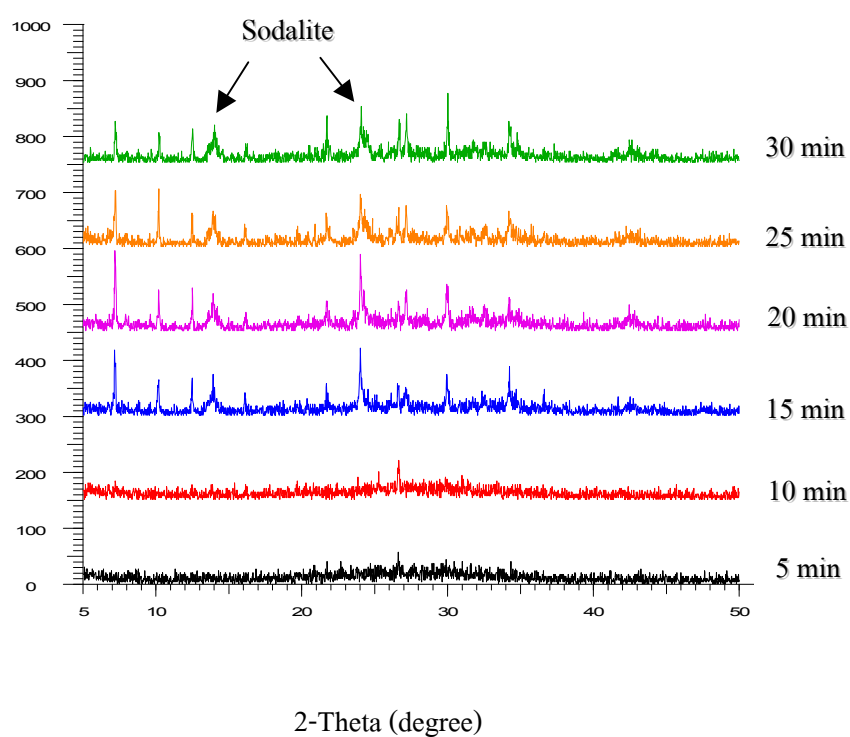


Figure 3.32 XRD pattern of the solid phase obtained in the synthesis of zeolite Na-A from Narathiwat kaolin activated at 700 °C with 25 % w/v NaOH at reaction temperature 100 °C. The sodalite peaks are indicated by arrows.

3.4 Kinetic study result

3.4.1 Determination of the Avrami exponent, n

By the technical limitation of IR, the data taken at high NaOH concentration will not be precise due to overlapping of different bands. Therefore, XRD was chosen to follow the crystal formation and find the kinetic parameters.

The kinetic analysis of zeolite formation was performed using Avrami method. In many cases, the Avrami equation can provide a good empirical fit of the kinetic curves. It can be used for the calculation of the rate constant and Avrami exponent. By using the equation (3.1)

$$\ln(-\ln(1-\alpha)) = n \ln t + \ln k \quad \dots(3.1).$$

α is the conversion factor representing the crystalline volume fraction developed at time t ranging from 0 to 1. The plot of $\ln(-\ln(1-\alpha))$ versus $\ln t$, would give the slope of the regression lines equal to the Avrami exponent n , which is related to the mechanism of reaction. Such plots are shown in figure 3.33 which were taken from XRD.

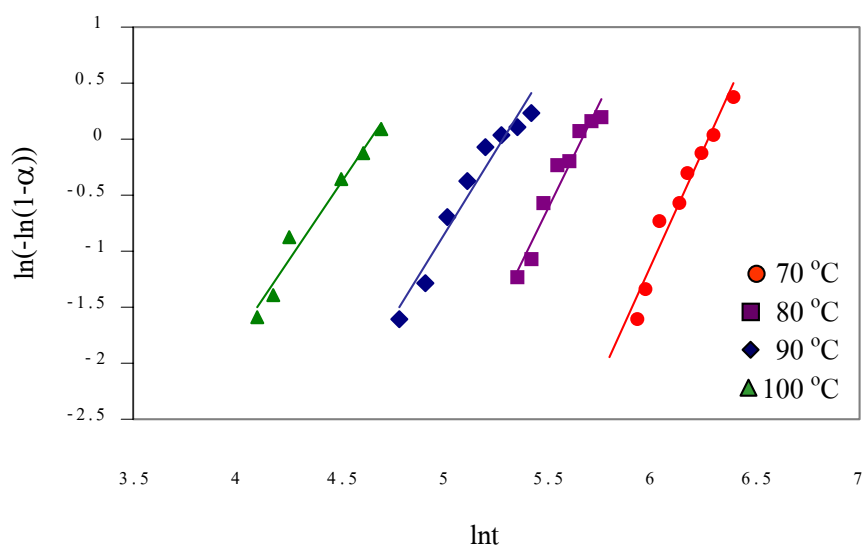


Figure 3.33 XRD results of the Plot for $\ln(-\ln(1-\alpha))$ versus $\ln t$ obtained in the synthesis of zeolite Na-A from Narathiwat kaolin activated at 700 °C with 10 % w/v NaOH.

From the plots, most of the data points tended to follow the Avrami model at the beginning of the plot. The values of n depended on the nature and conditions of crystal growth. Some deviations were seen late in the reaction with the lower slope value or indicated lower n value. This deviation implied more than one mechanism of the crystal formation. Avrami equation essentially describes the solid state reactions, however the Avrami equation is not always able to describe the rate process for several reasons such as solution-mediated processes (Gualtieri, A. et al., 1997).

In this work, it was assumed that the Avrami equation provides a simple means for rate constant determination for the series of crystallization under varying conditions. The Avrami coefficient, n , were deduced from the slope of plot of $\ln(-\ln(1-\alpha))$ versus $\ln t$. (α range within 0.1-0.7) and given in table 3.7 .

Table 3.7 The analytical result of the Avrami exponents for the growth of zeolite Na-A from Narathiwat kaolin activated at 700 °C at various conditions.

Temperature (°C)	[NaOH] 10% w/v		[NaOH] 15% w/v		[NaOH] 20% w/v	
	n	R	n	R	n	R
70	4.2	0.980	5.6	0.977	6.0	0.985
80	3.8	0.973	4.2	0.981	6.0	0.997
90	3.0	0.975	3.2	0.991	5.9	0.999
100	2.7	0.985	3.0	0.994	5.2	0.964

From table 3.7, at constant NaOH concentration, n had a tendency to decrease if the reaction temperature increased, possibly due to higher surface diffusion. At constant reaction temperature the n value increased when the NaOH concentration was increased, possibly due to higher rate of nucleation. The range of n values was found to be in between 3-6 which was similar to the values reported in the literatures (Gualtieri, A. et al., 1997 and Walton, R. I. et al., 2001).

Several researchers suggested various mechanisms to describe the varieties of the exponent n values. Subotic (1989) proposed that n tended to be 3 when zeolite was mostly formed by the growth of initial nuclei called homogeneous nuclei distributed through the liquid phase of the crystallizing systems at the beginning of the crystallization process.

Zhdanov (1990) found that the exponent n often greater than 4 when the nucleation rate increases during the autocatalytic stage of the crystallization process. Zhdanov explained the increase in the particles production rate, during the crystallization process by introducing the possibility of the formation of nuclei not only in the liquid phase but also quasi-crystalline phase (heterogeneous nucleation) released from the dissolution of the pre-existing short range ordered Si-Al polyhedra framework. The values of n depend on the ratio of the number of heterogeneous nuclei to the number of homogeneous nuclei (Subotic, B., 1989).

3.4.2 Determination of rate constant, k

The rate constant, k , from the hydrothermal operating at 70-100 °C can be deduced from the plot of conversion factor (α) and time as shown in figure 3.34. The values of k were obtained from the slope of the plot (α range within 0.1-0.7) (Gualtieri, A. et al., 1997) The resulting values of rate constant, k from various conditions of the experiment are reported in table 3.8.

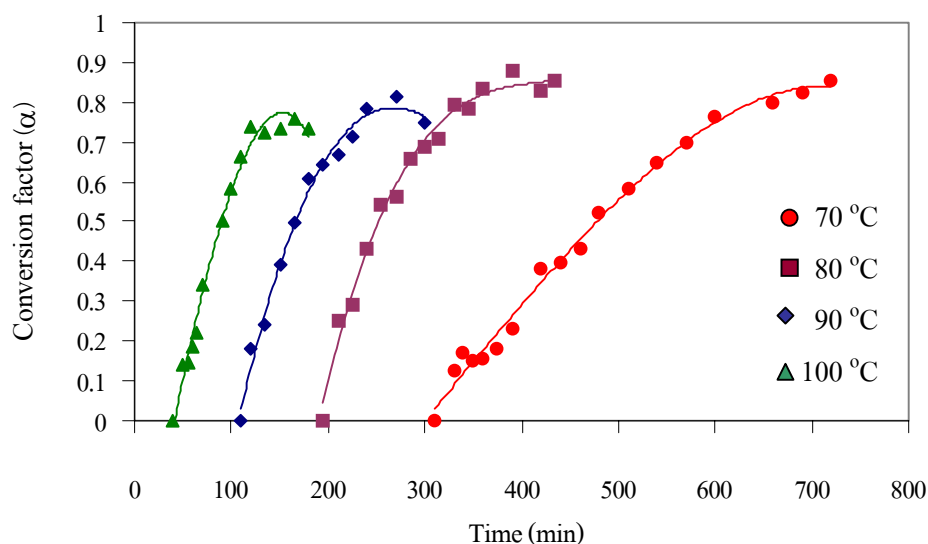


Figure 3.34 Plot of conversion factors and time for the hydrothermal experiment obtained from Narathiwat activated at 700 °C with 10 % NaOH at different reaction temperatures.

Table 3.8 The analytical result of the rate constant, k and fitting coefficient, R for the growth of zeolite Na-A from Narathiwat kaolin activated at 700 °C at various conditions.

Temperature (°C)	[NaOH] 10% w/v		[NaOH] 15% w/v		[NaOH] 20% w/v	
	k	R	k	R	k	R
70	0.0026	0.991	0.0054	0.986	0.0105	0.970
80	0.0049	0.983	0.0068	0.990	0.0190	0.995
90	0.0056	0.977	0.0181	0.964	0.0402	0.994
100	0.0091	0.994	0.0213	0.991	0.0496	0.975

From the values of the rate constants k obtained from the plot of conversion factor with time by Avrami equation, at constant NaOH concentration, k had a tendency to increase if the reaction temperature increased. At constant reaction temperature the k value increased when the NaOH concentration was increased. Similar trends were reported in the literature (Gualtieri, A. et al., 1997 and Walton, R. I. et al., 2001)

The rate constants k from various experiments were utilized in Arrhenius equation for the calculation of the activation energy (E_a).

3.4.3 Determination of activation energy (E_a) of zeolite Na-A crystallization

The activation energy, E_a , from thermodynamic point of view, can be used to determine the minimum energy needed for the crystallization. When comparing two processes, a lower value of E_a means it is easier for that process to occur. The activation energy could be varied depended on the process and mechanism.

Breck and Flanigen (1968) obtained 11 kcal/mol for the activation energy of crystallization of zeolite A. Zhdanov (1971) obtained 10.5 kcal/mol for the activation energy of crystallization of zeolite A. Culfas and Sand (1973) synthesized zeolite A in the temperature range 60-90 °C with the composition $2.5\text{Na}_2\text{O}-1.7\text{SiO}_2-\text{Al}_2\text{O}_3-150\text{H}_2\text{O}$ and reported activation energy of 19 kcal/mol for crystallization. Hu, H. C. et al., (1990) had the activation energy of

crystallization value of 10.9 kcal/mol for zeolite Na-A prepared from an amorphous sodium aluminosilicate gel. Guatieri, A. et al., (1997) synthesized zeolite Na-A from natural kaolinite activated at 800 °C at temperature between 70–110 °C and obtained the activation energy of crystallization to be 8.7 kcal/mol.

To find the activation energy, the rate constant, k are utilized in the Arrhenius equation as shown in equation (3.2).

$$k = A \exp(-E_a/RT) \quad \dots (3.2)$$

Taking the logarithms gives

$$\ln k = -E_a/RT + \ln A \quad \dots (3.3)$$

From the plot of the logarithm form $\ln k$ versus $1/T$, the calculation of the apparent activation energy (E_a) of the process can be obtained from the slope of the linear plot as shown in figures 3.35.

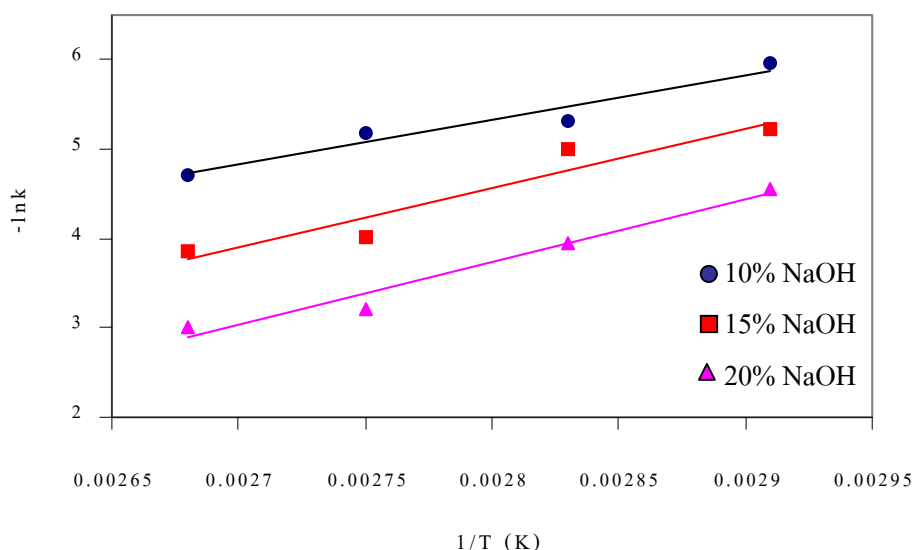


Figure 3.35 The XRD measurement result of $-\ln k$ versus $1/T$ obtained in the synthesis of zeolite Na-A from Narathiwat kaolin activated at 700 °C with 10, 15, and 20 % w/v NaOH at different reaction temperatures.

The resulting values of activation energy of crystallization Na-A from various conditions are reported in table 3.9.

Table 3.9 The analytical result of the apparent activation energy (E_a) and fitting coefficient (R) for the growth of zeolite Na-A from Narathiwat kaolin activated at 700 °C at various conditions.

	[NaOH] % w/v		
	10 %	15 %	20 %
E_a (kcal/mol)	9.9	13.0	13.8
R	0.985	0.955	0.987

It was expected that the value of E_a at 20% NaOH concentration will be lower since the apparent crystallization rate was faster. However, the value of E_a obtained from the experiment was higher than expected. Since there were many mechanisms involved in the crystal formation therefore, it was not straight forward to compare the values of E_a from different conditions.

From the data, the apparent activation energies obtained from various conditions are ranging from 9.9 to 13.8 kcal/mol which are in the range of the values reported in the literatures. At the NaOH concentration 10%, the crystallization of zeolite Na-A was mostly complete and high yield was obtained. This resulted in the lowest apparent E_a . At higher NaOH concentration, the formation of zeolite was less favorable by the competition formation of sodalite which was more stable at these conditions. Therefore the higher values of E_a were obtained.

As stated earlier, more than one process involved in the formation of zeolite Na-A crystals. Since the different process accounted for the nucleation of the crystals. Therefore, the activation energy of the nucleation (E_n) is different than the activation energy of crystallization (E_a). A similar method was used to determine E_n as discussed in the next section.

3.4.4 Activation energy, E_n of nucleation zeolite Na-A

Similar to the activation energy of crystallization, E_a , the activation energy of nucleation, E_n , determines the energy needed for the nucleation process. At the same condition, the lower value of E_n means the easier the nucleation can occur. However, the faster induction period does

not necessary mean the lower activation energy for nucleation. The activation energy could be also varied by many parameters such as the amount and type of impurities in the material, the synthesis condition etc. The activation energy of nucleation can be expressed in the Arrhenius-like form:

$$1/t_0 = B \exp(-E_n/RT) \quad \dots (3.5)$$

Taking the logarithms gives

$$-\ln t_0 = -E_n/RT + \ln B \quad \dots (3.6)$$

This method to determine the activation energy of nucleation was successfully applied by Joshi et al.(1990). The Arrhenius plot of logarithm of the induction periods (t_0) and $1/T$ for the calculation of activation energy, E_n of nucleation zeolite Na-A is shown in figure 3.36.

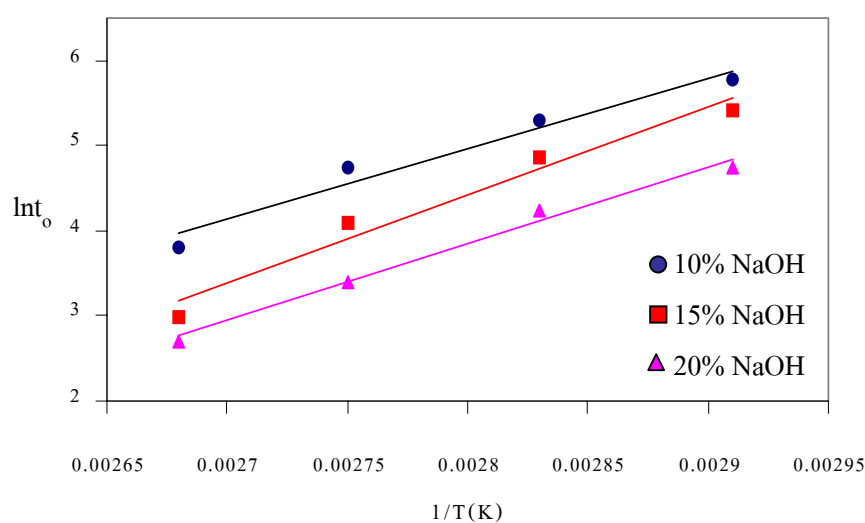


Figure 3.36 The plot of $\ln(t_0)$ versus $1/T$ obtained in the synthesis of zeolite Na-A from Narathiwat kaolin activated at 700°C with 10, 15, and 20 % w/v NaOH at different reaction temperatures.

The resulting values of activation energy of nucleation are given in table 3.10.

Table 3.10 Activation energy of the nucleation process calculated from the induction periods.

	[NaOH] 10% w/v	[NaOH] 15% w/v	[NaOH] 20% w/v
E_n (kcal/mol)	12.7	16.4	16.7
R	0.980	0.983	0.994

Due to limitation in sampling time, the induction period could not be measured at high precision, and only rough approximations can be made for the values of activation energy of nucleation. The activation energies of nucleation of zeolite Na-A (E_n), obtained from the experiment are in the range of 12.7-16.7 kcal/mol which is not far from 15.0 kcal/mol obtained by Hu and Lee (1990) and 16.2 kcal/mol obtained by Guatieri et al. (1997). The lower value of E_n of the reaction with NaOH 10% may imply that it was a suitable condition for the synthesis while the higher values of E_n at higher NaOH concentrations were related to the disturbance from the formation of sodalite and the faster consumption rate of secondary units as discussed earlier.

3.5 Ion exchange capability

Since the main feature of zeolite Na-A is the high selectivity of calcium ion exchange which made it popular in the applications. Therefore, an experiment was performed to test the ion exchange capacity of our synthetic product compared with resin which is one of the often used absorbent and with standard zeolite Na-A. The synthetic zeolite was obtained from the synthesis using Narathiwat kaolin activated at 700°C, 20%w/v NaOH and reaction temperature of 80°C. The ion exchange capacity was determined by comparing the concentration of Ca^{2+} left in the 100 ml of $CaCl_2$ solution with 1 g of the sample after allowing the process to continue for 3 days. The higher adsorption the lower Ca^{2+} left in the solution. The experiment was performed using Ca^{2+} concentration of 600, 1000, 1400 and 2000 ppm for the synthetic product and commercial resin (Amberlite IRN 160, particle size < 0.3 mm), 1000 and 2000 ppm for standard zeolite due to the limitation in the amount of material. The result is shown in table 3.11.

Table 3.11 Calcium ion exchanger capacity of the synthesis product, resin and standard zeolite-Na-A.

[Ca ²⁺] ppm	Adsorption (ppm)		
	Product	Resin	Standard Zeolite Na-A
600	593	589	-
1000	796	789	805
1400	811	834	-
2000	902	816	993

From the result, the synthetic zeolite Na-A product from this work performed well compared to commercial resin and standard zeolite. For 600 ppm solution, most of the Ca²⁺ ions were absorbed by the product and tend to reach some limit from 1000 ppm and higher concentration. Similar trend was also observed when using resin as the adsorbent. At 2000 ppm, a comparable adsorption capacity is obtained for the product and standard zeolite Na-A. Therefore, it may be concluded that our synthetic product has the ion exchange capability not far from the commercial standard zeolite Na-A.

Chapter IV

Conclusion

The formation of zeolite Na-A from natural kaolinites of Thailand collected from Lampang, Ranong and Narathiwat provinces has been studied. There were several factors that influenced on the formation of zeolite Na-A. It was confirmed that the composition of kaolin was one of the most important factor for the synthesis. Narathiwat and Ranong kaolin can be used in zeolite Na-A synthesis with good yields (>80%). On the other hand, the synthesis of zeolite Na-A from Lampang kaolin, which contained high composition of quartz, did not give a satisfactory result (~24%). The calcination of kaolin samples was the another important factor that influenced on the zeolite Na-A synthesis. Kaolin samples can be transformed into the amorphous phase called metakaolinite at the calcination temperature 600 °C or higher. Experimentally, the starting material with amorphous form was suitable for the synthesis. It was observed that, the rate of reaction increased along with increasing NaOH concentration and reaction temperature. At very high NaOH concentration (25% w/v) and reaction temperature (100°C), the percentage of crystallinity of zeolite Na-A decreased due to the competing formation of hydroxy-sodalite. The best condition (80-85% of crystallinity) was found to be Narathiwat kaolin activated at 700 °C with 10-15% w/v NaOH, and reaction temperature of 70-80 °C.

The kinetic data of the experiment extracted from Avrami and Arrhenius equations showed that the n values (related to the reaction mechanism) were in the range of 3-6. The k values increased with increased reaction temperature. The activation energies of crystallization and nucleation obtained from the experiment were 9.9-13.8 kcal/mol and 12.7-16.7 kcal/mol respectively. These analytical results compared well with the literatures. In conclusion, it was demonstrated that Thai kaolin could be used in the synthesis of zeolite Na-A with satisfactory and competitive results to the well-studied foreign materials.

There are some topics that may be interesting to be investigated furthermore such as the effects of impurity to the crystal formation, the relation of the synthesis condition to the particle size, the extraction of quartz from kaolin to increase yield, and the improvement of ion exchange capability.

References

- Antonic, T., Stubicar, N., and Subotic, B. (1997). Influence of gel properties on the crystallization of zeolites: part 1 influence of alkalinity during gel preparation on kinetics of nucleation of zeolite A. **Zeolite**. 18: 291-300.
- Barrer, R. M. (1978). **Zeolite and clay minerals as sorbent and molecular sieves**. London: Academic Press.
- Barrer, R. M. (1985). Synthesis of zeolites. In: Zeolites. Drzaj, B., Hocevar, S., Pejovnik, S. **Elsevier Science Publishers BV**: Amsterdam.
- Basaldella, E. I., and Tara, J. C. (1998). Modification of crystallite morphology during synthesis of LTA zeolite using triethanolamine as additive. **J. Mater. Letter** 34: 119-123.
- Beaty, R. D., and Kerber, J. D. (1993). **Concepts, Instrumentation and Techniques in atomic absorption spectrophotometry**. Perkin –Elmer Corporation, U. S. A.
- Bekkum, V. H., Cjansen, J., and Mflanigen, E. (1991). Zeolite and molecular sieves. **Introduction to zeolite science and practice**. 58: 13-33.
- Bongear, D., Geidel, E., and Smirnor, K. S. (2000). Vibrational spectra and structure of kaolinite: A computer simulation study. International zeolite Association. Elsevier. **B**. 104: 9210-9217.
- Breck, D. W., Eversole, W.G., Milton, R. M. Reed, T. B., and Thomas, T. L. (1956). The properties of a new synthetic zeolite, type A. **J. Chem. Soc.** 78: 5963-5971.
- Breck, D. W. (1974). **Zeolite molecular sieves: structure chemistry and use**. Willey. New York.
- Chandrasekhar, S., and Pramada, P. N. (1999). Investigation on the synthesis of zeolite Na-X from kerala kaolin. **J. of Porous Mater.** 6: 283-297.
- Chandrasekhar, S., and Pramada, P. N. (2001). Sintering behavior of calcium exchanged low silica zeolite synthesized from kaolin. **J. of Ceramic Inter.** 27: 105-114.
- Chang, H. L., and Shihg, W. H. (2000). Synthesis of zeolite A and X from fly ashes and their ion-exchange behavior with cobalt ions. **J. Ind. Eng. Chem. Res.** 39: 4185-4191.

- Demortier, A., Duhayon, C., Gobeltz, N., and Plelieur, J. (1999). Infrared evidence for the formation of an intermediate compound during the synthesis of zeolite Na-A from matakaolinite **Inter. J. Inorg. Mater.** 1: 129-134.
- Dutta, P. K., and Barco, B. D. (1985). Raman spectroscopic studies of zeolite framework. Hydrated zeolite A and the influence of cations. **J. Phys. Chem.** 89: 1861-1865.
- Dutta, P. K., and Shieh, D. C. (1986) Crystallization of zeolite A: A spectroscopic study. **J. Phys. Chem.** 90: 2331-2334.
- Dutta, P. K., and Barco, B. D. (1988). Raman spectroscopy of zeolite A: influence of Si/Al ratio. **J. Phys. Chem.** 92: 354-357.
- Dutta, P. K., and Twu, J. (1991). Influence of framework Si/Al ratio on the Raman spectra of faujasitic zeolite. **J. Phys. Chem.** 95:2498-2501.
- Dutta, P. K., and Robins, D. (1991). Synthesis of zeolite A from reactants enclosed in reverse micelles. **Langmuir.** 7: 1048-1050.
- Ejaz, T., Graham, P., and Jones, A. G. (1999). Solubility of zeolite A and its amorphous precursor under synthesis condition. **J. Chem. Eng.** 44: 574-576.
- Ellie, L., Nikolov, G.S., and Uzunova. (2000) DFT study of zeolite LTA structural fragment: Double four memberings of oxygen-bridged silicon and aluminum atom. **J. Phys. Chem.** 104: 5302-5306.
- Feijen, E. J. P., Martens, J. A. and Jacobs, P. A. (1994). **Zeolites and their mechanism of synthesis**, Zeolites and related microporous materials. Elsevier Science B. V. 84: 3-18.
- Ghosh, D., and Bhattacharyya, K. G. (2002). Adsorption of methylene blue on kaolinite, **J. Appl. Clay Sci.** 20: 295-300.
- Gora, L., Phillips, G. D., Streltzyk, K., and Thompson, R. W. (1997). **Zeolites.** 18:119-131.
- Grim, R. E. (1968). **Clay mineralogy, structure of clay mineral.** New York: McGraw-Hill. 57-66.
- Guatieri, A., Artioli, G. Hanson, J., and Norby, P. (1997). Kinetic of formation of zeolite Na-A [LTA] from kaolinite. **J. Phys. Chem. Mineral.** 24: 191-199.
- Guatieri, A., Artioli, G. Hanson, J., and Norby, P. (1997). Kinetic of formation of zeolite Na-A [LTA] from kaolinite. **J. Phys. Chem. Mineral.** 24: 191-199. Quoted in Joshi, P. N. et al. (1990). Crystallization kinetic of zeolite LTL. **Zeolite.** 10: 598-602.

- Hu, H. C., and Lee, T. Y. (1990). Synthesis kinetic of zeolite A. **J. Ind. Eng. Chem. Res.** 29: 749-754.
- Hu, H. C., and Lee, T. Y. (1990). Synthesis kinetic of zeolite A. **J. Ind. Eng. Chem. Res.** 29: 749-754. Quoted in Breck, D. W., Flanigen, E. M. (1968). **Molecular sieves**; Society of the Chemical Industrial: London.
- Hu, H. C., and Lee, T. Y. (1990). Synthesis kinetic of zeolite A. **J. Ind. Eng. Chem. Res.** 29: 749-754. Quoted in Zhdanov, S.P. (1971). **Some problems of zeolite crystallization**. In molecular sieve zeolite-I; Flanigen, E.M., Sand, L. B., Eds.; Advances in Chemistry 101; American Chemical Society: Washington, DC.
- Ikeda, T., Izumi, F., Kamiyama, T., and Kodaira, T. (1998). Structural study of sodium-type zeolite LTA by combination of rietveld and maximum-entropy method. **J. Chem. Mater.** 10: 3996-4004.
- Jenkins, R., and Synder, R. L. (1996). **Introduction to X-ray powder diffractometry**. 138: 1-202.
- Kacirek, H., and Lechert H. (1976). Rate of crystallization and a model for the growth of Na-Y zeolites. **J. Phys. Chem.** 80: 1291-1296.
- Kerr, G. T. (1966). Chemistry of crystalline aluminosilicate I. Factors affecting the formation of zeolite A. **J. Phys Chem.** 70: 1047-1050.
- Kosanovic, C., and Subotic, B. (1997). Invaliability of the particulate properties during the thermal treatment of potassium- exchanged zeolite A: Evidence for amorphous crystals. **Microporous Materials.** 12: 261-266.
- Madami, A., Azmar, A., Sanz, J., and Serratos, J. M. (1990). ^{29}Si and ^{27}Al NMR study of zeolite formation from alkali-leached kaolinites. Influence of thermal preactivation. **J. Phys. Chem.** 94: 760-765.
- McNid, B. D., Loos, K. R., and Pott, G.T. (1972). Spectroscopic study of zeolite synthesis. **J. Phys. Chem.** 76: 3388-3390.
- Meier, W. M., Baerlocher, C., and Olson, D. H. (1996). **Atlas of zeolite structure types**. International zeolite Association. Elsevier. 130-189.
- Mintova, S., Olson, N. H., and Valtcher, V. (1999). Mechanism of zeolite A nanocrystal growth from colloids at room temperature. **Science.** 283: 958-960.

- Muller, J. C. M., Hakvoort, G., and Jansen, J.C. (1998). DSC and TG study of water adsorption and desorption on zeolite Na-A. **J. Thermal. Anal.** 53: 258-261.
- Murayama, N., Shibata, J., and Yamamoto, H. (2002). Mechanism of zeolite synthesis from coal fly ash by alkali hydrothermal reaction. **J. Miner. Process.** 64: 1-17.
- Norby, P. C. (1997). Hydrothermal conversion of zeolite: An in situ synchrotron x-ray powder diffraction study. **J. Am. Chem. Soc.** 119: 5215-5225.
- Qiu, P., Balog, P. S., Huang, Y., and Secco, R.A. (1999). Effect of multi-stage dehydration on electrical conductivity of zeolite A. **Solid State Ionics.** 118: 281-285.
- Reed, T. B., and Breck, D. W. (1956). **Crystalline zeolite. II Crystal structure of synthetic zeolite type A linde.** Air product company a division of Union Carbide and Carbon Corporation. 78: 5972-5977.
- Rocha, J., and Kliniowski, J. (1991). Synthesis of Zeolite Na-A from metakaolinite revisited. **Faraday.** 87: 3091-3097.
- Rocha, J. (1999). Single and Triple-Quantum ^{27}Al MAS NMR study of the thermal transformation of kaolinite. **J. Phys. Chem. B.** 103:9801-9804.
- Ruiz, R., Benito, I., Blanco, C., Gonzalez, F., Lopez, J.L., and Pesquera, C. (1997). **Appl. Clay. Sci.** 12:73.
- Shamon, S.R., and Metiu, H. (2001). The water molecule in $\text{Na}_6[\text{AlSiO}_4]_6$ sodalite. **J. Phys. Chem. B.** A-J.
- Smirnov, K.S., and Bougeard, D. (1993). Molecular dynamics study of the vibrational spectra of siliceous zeolites built from sodalite cages. **J. Phys. Chem.** 97: 9434-9440.
- Szostak, R. (1992). **Linde type A. Handbook of molecular sieve,** 258-261.
- Treacy, M. M., Ballmoos, R. V., and Higgins, J. B. (1996). **Collection of simulated XRD powder pattern for zeolite.** International zeolite Association. Elsevier. 500-581
- Velde, B. (1992). **Clay mineral structure, Introduction of Clay minerals.**
- Walton, R.I., Milange, F., O'Hare, D., Davies, A.T., Sankar, G., and Catlow, C.R.A. (2001). An in situ energy dispersive X-ray diffraction study of the hydrothermal crystallization of zeolite A., 1. Influence of reaction conditions and transformation into sodalite, **J. Phys. Chem. B.** 105: 83-90.

- Wang, J., and Tomita, A. (1997). Hydrothermal reaction of kaolinite with calcium hydroxide and dissolution of reaction product in hydrochloric acid. **J. Ind. Eng. Chem. Res.** 36:5258-5264.
- Yang, S., Evmiridis, N.P., and Vlessidiss, A.G. (1997). Influence of gel composition and crystallization condition on the conventional synthesis of zeolite. **J. Ind. Eng. Chem. Res.** 36: 1622-1631.
- Zhdanov, S. P., Feoktistova, N. N., and Khvoshchev, S. S. (1990). **Crystallization, Synthetic zeolites.** Gordon and Breach Science. New york. 1: 26-57.
- Zhu, G., Qui, S., Sakamoto, Y., Terasaki, O., Xiao, F., Xu, R., and Yu, J. (1998). Synthesis and characterization of high quality zeolite LTA and FAU single nanocrystals. **J. Chem. Mater.** 10: 1483-1486.

Appendix A

Atlas of zeolite structure types

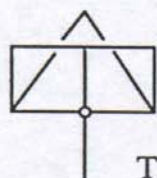
LTA

LINDE TYPE A

Pm3m

Framework density: 12.9 T/1000 Å³

Loop configuration
of T-atoms:



Coordination sequences: T(24) 4 9 17 28 42 60 81 105 132 162

Channels: <100> 8 4.1***

Type material: **Linde Type A** {Na₁₂[Al₁₂Si₁₂O₄₈] · 27 H₂O}₈
cubic, Fm $\bar{3}$ c, a=24.6 Å^(1,2)
(pseudocell, Pm3m, a'=12.3 Å)

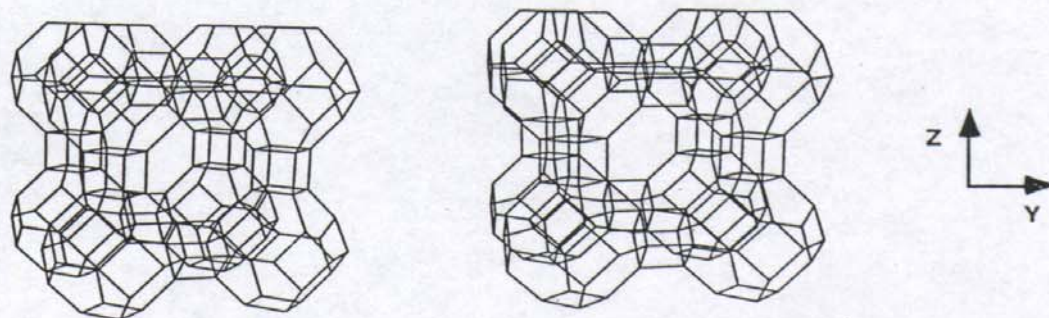
Isotypic framework structures:	Alpha ⁽³⁾	SAPO-42 ⁽⁸⁾
	Gallogermanate LTA ⁽⁴⁾	ZK-4 ⁽⁹⁾
	Gallophosphate LTA ⁽⁵⁾	ZK-21 ⁽¹⁰⁾
	LZ-215 ⁽⁶⁾	ZK-22 ⁽¹⁰⁾
	N-A ⁽⁷⁾	

References:

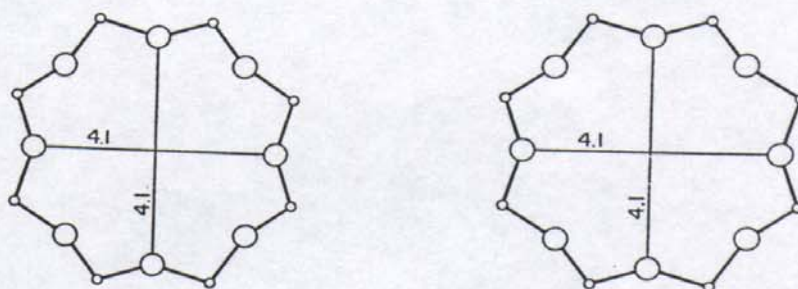
- (1) T. B. Reed and D. W. Breck, *J. Am. Chem. Soc.* **78**, 5972 (1956).
- (2) V. Gramlich and W. M. Meier, *Z. Kristallogr.* **133**, 134 (1971).
- (3) R. L. Wadlinger, E. J. Rosinski and C. J. Plank, U.S. Patent 3,375,205 (1968).
- (4) R. M. Barrer, J. W. Baynham, F. W. Bultitude and W. M. Meier, *J. Chem. Soc.* **1959**, 195 (1959).
- (5) A. Simmen, J. Patarin and Ch. Baerlocher, *Proc. 9th IZC, Montreal, Butterworth-Heinemann* (1993) p. 433.
- (6) D. W. Breck and G. W. Skeels, US Patent 4,503,023 (1985).
- (7) R. M. Barrer and P. J. Denny, *J. Chem. Soc.* **1961**, 971 (1961).
- (8) B. M. Lok, C. A. Messina, R. L. Patton, R. T. Gajek, T. F. Cannan and E. M. Flanigen, *J. Am. Chem. Soc.* **106**, 6092 (1984).
- (9) G. T. Kerr, *Inorg. Chem.* **5**, 1537 (1966).
- (10) G. H. Kuehl, *Inorg. Chem.* **10**, 2488 (1971).

24 T(m)

LTA



framework viewed along [100]

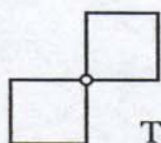


8-ring viewed along [100]

SOD**SODALITE** **$Im\bar{3}m$**

Framework density: 17.2 T/1000 Å³

**Loop configuration
of T-atoms:**



Coordination sequences: T(12) 4 10 20 34 52 74 100 130 164 202

Channels: apertures formed by 6-rings only

Type material: Sodalite Na₆[Al₆Si₆O₂₄] · 2 NaCl
cubic, $P\bar{4}3n$, $a=8.9$ Å^(1,2)

Framework description: ABC sequence of 6-rings

**Isotypic framework
structures:**

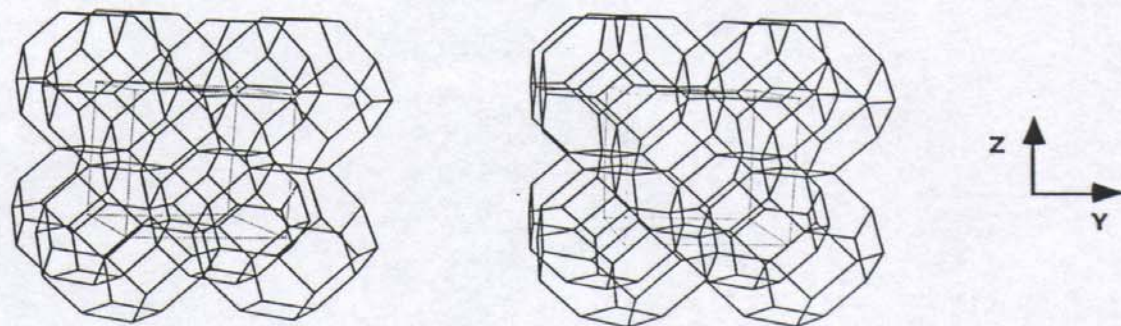
AlPO₄-20^(3,4)^a
Aluminate SOD⁽⁵⁾
Basic sodalite⁽⁶⁾
Beryllarsenate SOD⁽⁷⁾
Beryllphosphate SOD⁽⁷⁾
Beryllsilicate SOD⁽⁸⁾
Bicchulite⁽⁹⁾
Danalite⁽¹⁰⁾
G⁽¹¹⁾
Gallosilicate SOD⁽¹²⁾
Genthelvite⁽¹³⁾

Hauyn⁽¹⁴⁾
Helvin⁽¹⁰⁾
Hydroxo sodalite⁽¹⁵⁾
Nosean⁽¹⁶⁾
Silica sodalite⁽¹⁷⁾
TMA sodalite⁽¹⁸⁾
Tugtupite⁽¹⁹⁾
Zincoarsenate SOD⁽²⁰⁾
Zincophosphate SOD⁽²⁰⁾
plus other compositional
variants

^aplus numerous compositional variants⁽¹⁷⁾

12 T($\bar{4}2m$)

SOD



framework viewed along [100]

References:

- (1) L. Pauling, *Z. Kristallogr.* **74**, 213 (1930).
- (2) J. Loens and H. Schulz, *Acta Cryst.* **23**, 434 (1967).
- (3) S. T. Wilson, B. M. Lok, C. A. Messina, T. R. Cannan and E. M. Flanigen, *J. Am. Chem. Soc.* **104**, 1146 (1982).
- (4) E. M. Flanigen, B. M. Lok, R. L. Patton and S. T. Wilson, *Proc. 7th IZC, Tokyo* (Kodansha and Elsevier, 1986) p. 103.
- (5) W. Depmeier, *Acta Cryst.* **C40**, 226 (1984).
- (6) (a) R. M. Barrer and E. A. D. White, *J. Chem. Soc.* **1951**, 1167 (1951). (b) I. Hassan and H. D. Grundy, *Acta Cryst.* **C39**, 3 (1983).
- (7) T. E. Gier, W. T. A. Harrison and G. D. Stucky, *Angew. Chem. Int. Ed. Engl.* **30**, 1169 (1991).
- (8) S.E. Dann and M.T. Weller, *Inorg. Chem.* **35**, 555 (1996).
- (9) K. Sahl and N. D. Chatterjee, *Z. Kristallogr.* **146**, 35 (1977).
- (10) J. J. Glass, R. H. Jahns and R. E. Stevens, *Am. Min.* **29**, 163 (1944).
- (11) T. N. Shishakova and M. M. Dubinin, *Izv. Akad. Nauk SSSR*, **1965**, 1303 (1965).
- (12) L. B. McCusker, W. M. Meier, K. Suzuki and S. Shin, *Zeolites* **6**, 388 (1986).
- (13) S. Merlino, *Feldspars and Feldspathoids* (W. L. Brown ed., Reidel, Dordrecht, 1984) p. 460.
- (14) J. Loens and H. Schulz, *N. Jb. Min. Abh.* **109**, 201 (1968).
- (15) J. Felsche, S. Luger and Ch. Baerlocher, *Zeolites* **6**, 367 (1986).
- (16) H. Schulz and H. Saalfeld, *Tschemm. Min. Petr. Mitt.* **10**, 225 (1965).
- (17) D. M. Bibby and M. P. Dale, *Nature* **317**, 157 (1985).
- (18) Ch. Baerlocher and W. M. Meier, *Helv. Chim. Acta* **52**, 1853 (1969).
- (19) H. Sorensen, *Am. Mineral.* **48**, 1178 (1963).
- (20) T. N. Nenoff, W. T. A. Harrison, T. E. Gier and G. D. Stucky, *J. Am. Chem. Soc.* **113**, 378 (1991).

Appendix B

Simulated XRD powder patterns for zeolites

LTA

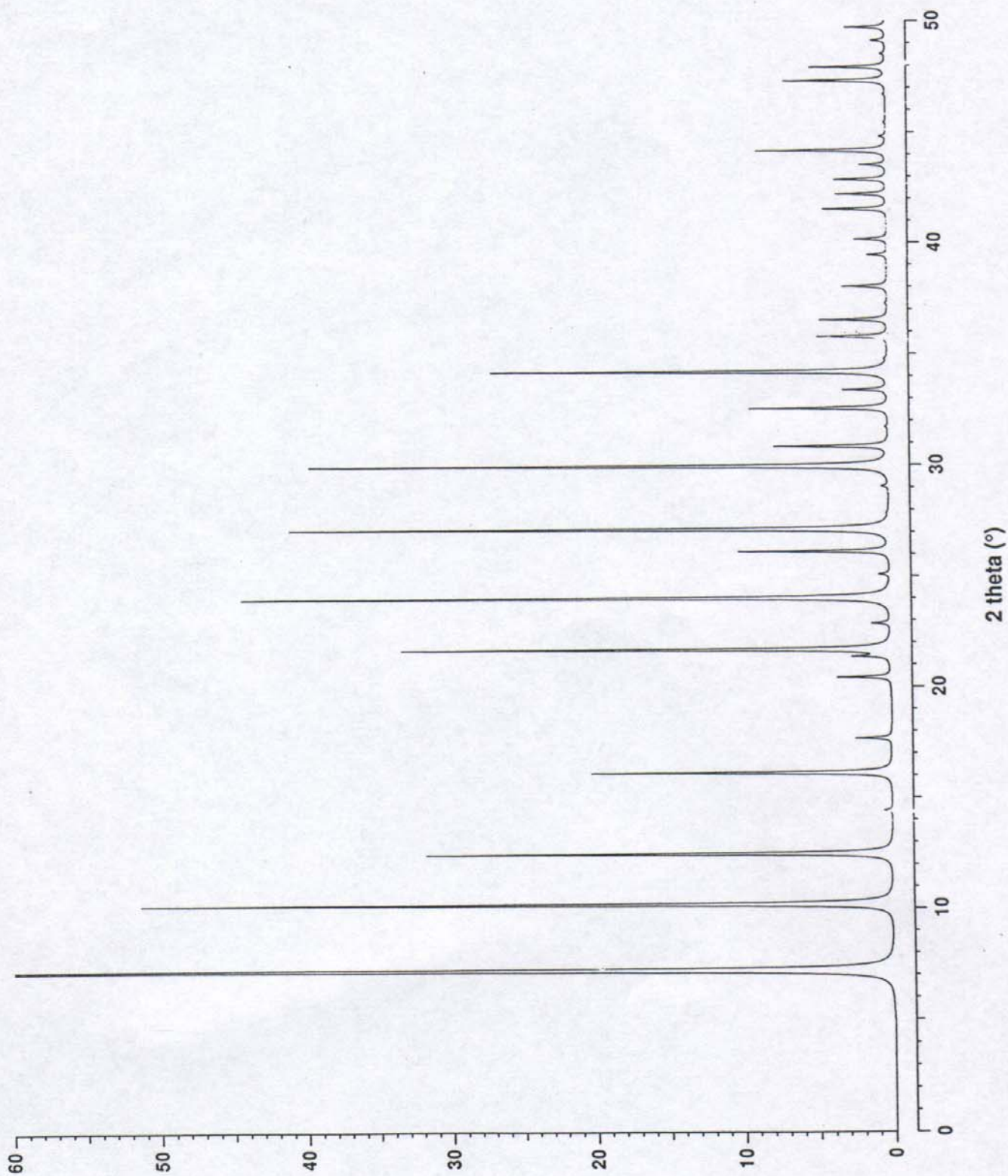
Hydrated Linde Type A

COMPOSITION: $\text{Na}_{96}(\text{Si}_{96}\text{Al}_{96}\text{O}_{384}) \cdot 216\text{H}_2\text{O}$ CRYSTAL DATA: $Fm\bar{3}c$ (No. 226)
 $a = 24.61 \text{ \AA}$ $b = 24.61 \text{ \AA}$ $c = 24.61 \text{ \AA}$
 $\alpha = 90^\circ$ $\beta = 90^\circ$ $\gamma = 90^\circ$
REFERENCE: V. Gramlich and W. M. Meier,
Z. Kristallogr. 133, 134-149 (1971).

<i>h</i>	<i>k</i>	<i>l</i>	2θ	<i>d</i>	<i>M</i>	<i>I</i> _{rel}	<i>h</i>	<i>k</i>	<i>l</i>	2θ	<i>d</i>	<i>M</i>	<i>I</i> _{rel}	<i>h</i>	<i>k</i>	<i>l</i>	2θ	<i>d</i>	<i>M</i>	<i>I</i> _{rel}
2	0	0	7.18	12.305	6	100.0	6	6	0	30.83	2.900	12	2.3	8	6	6	42.85	2.110	24	2.3
2	2	0	10.17	8.701	12	51.3	8	2	2	30.83	2.900	24	5.4	10	6	0	42.85	2.110	24	1.2
2	2	2	12.46	7.104	8	31.8	6	6	2	31.70	2.823	24	0.2	10	6	2	43.51	2.080	48	1.8
4	0	0	14.40	6.153	6	0.5	8	4	0	32.54	2.752	24	9.3	8	8	4	44.16	2.051	24	0.9
4	2	0	16.11	5.503	24	20.3	8	4	2	33.37	2.685	48	3.0	12	0	0	44.16	2.051	6	7.8
4	2	2	17.65	5.024	24	2.4	6	6	4	34.18	2.623	24	27.1	12	2	0	44.80	2.023	24	0.5
4	4	0	20.41	4.350	12	3.6	9	3	1	34.77	2.580	48	0.1	12	2	2	45.44	1.996	24	0.1
5	3	1	21.36	4.160	48	2.1	8	4	4	35.75	2.512	24	4.7	12	4	0	46.69	1.946	24	0.2
4	4	2	21.67	4.102	24	22.8	8	6	0	36.51	2.461	24	0.4	8	8	6	47.30	1.922	24	4.2
6	0	0	21.67	4.102	6	10.6	10	0	0	36.51	2.461	6	4.1	10	8	0	47.30	1.922	24	2.3
6	2	0	22.85	3.891	24	1.2	10	2	0	37.26	2.413	24	0.1	12	4	2	47.30	1.922	48	0.3
6	2	2	23.99	3.710	24	44.3	6	6	6	38.00	2.368	8	1.4	10	8	2	47.91	1.899	48	5.1
4	4	4	25.07	3.552	8	0.7	10	2	2	38.00	2.368	24	1.6	10	6	6	48.51	1.877	24	0.3
6	4	0	26.11	3.413	24	10.1	8	6	4	39.43	2.285	48	1.0	12	4	4	49.11	1.855	24	0.9
6	4	2	27.11	3.289	48	41.0	10	4	0	39.43	2.285	24	0.3	10	8	4	49.70	1.834	48	1.8
8	0	0	29.03	3.076	6	0.4	10	4	2	40.14	2.247	48	2.2	12	6	0	49.70	1.834	24	0.9
6	4	4	29.94	2.984	24	19.7	8	8	0	41.51	2.175	12	4.3							
8	2	0	29.94	2.984	24	19.9	10	4	4	42.19	2.142	24	3.4							

Hydrated Linde Type A

LTA



LTA

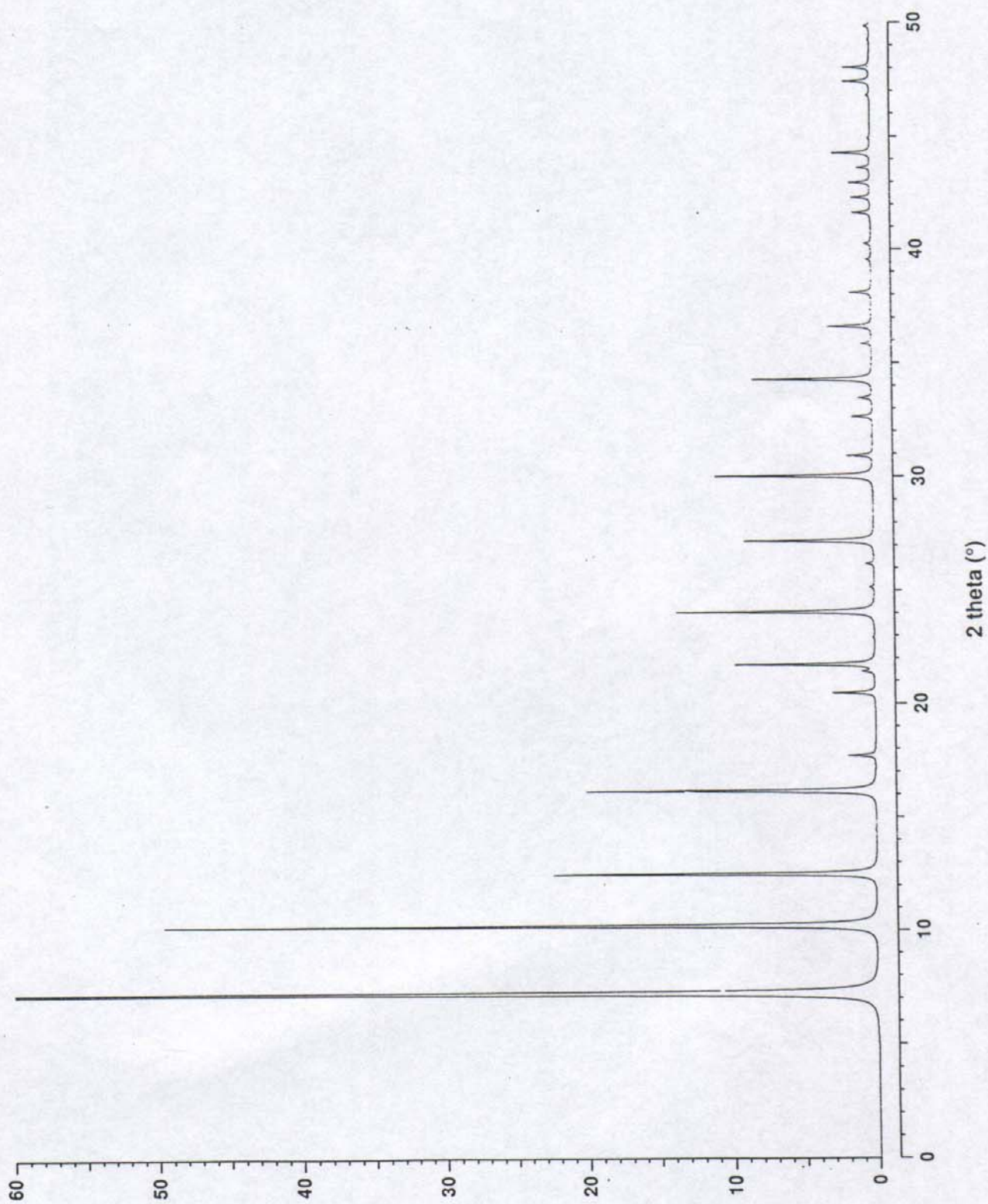
Dehydrated Linde Type A

COMPOSITION: $\text{Na}_{91.7}(\text{Si}_{96}\text{Al}_{96}\text{O}_{384})$ CRYSTAL DATA: $Fm\bar{3}c$ (No. 226)
 $a = 24.555 \text{ \AA}$ $b = 24.555 \text{ \AA}$ $c = 24.555 \text{ \AA}$
 $\alpha = 90^\circ$ $\beta = 90^\circ$ $\gamma = 90^\circ$
REFERENCE: J. J. Pluth and J. V. Smith,
J. Am. Chem. Soc. 102, 4704-4708 (1980).

<i>h</i>	<i>k</i>	<i>l</i>	2θ	<i>d</i>	<i>M</i>	<i>I</i> _{rel}	<i>h</i>	<i>k</i>	<i>l</i>	2θ	<i>d</i>	<i>M</i>	<i>I</i> _{rel}	<i>h</i>	<i>k</i>	<i>l</i>	2θ	<i>d</i>	<i>M</i>	<i>I</i> _{rel}
2	0	0	7.20	12.278	6	100.0	6	4	4	30.01	2.978	24	4.6	8	8	0	41.61	2.170	12	1.3
2	2	0	10.19	8.681	12	49.6	8	2	0	30.01	2.978	24	6.4	10	4	4	42.29	2.137	24	1.3
2	2	2	12.49	7.088	8	22.4	6	6	0	30.90	2.894	12	0.6	8	6	6	42.95	2.106	24	1.0
4	2	0	16.14	5.491	24	20.1	8	2	2	30.90	2.894	24	1.2	10	6	0	42.95	2.106	24	0.5
4	2	2	17.69	5.012	24	1.9	8	4	0	32.62	2.745	24	1.4	10	6	2	43.61	2.075	48	0.9
4	4	0	20.46	4.341	12	3.0	8	4	2	33.45	2.679	48	1.0	8	8	4	44.26	2.046	24	0.5
5	3	1	21.41	4.151	48	0.8	6	6	4	34.26	2.618	24	8.4	12	0	0	44.26	2.046	6	2.2
4	4	2	21.72	4.093	24	8.4	8	4	4	35.83	2.506	24	0.8	12	2	0	44.91	2.018	24	0.1
6	0	0	21.72	4.093	6	1.3	10	0	0	36.59	2.455	6	3.0	12	4	0	46.80	1.941	24	0.2
6	2	0	22.91	3.882	24	0.1	6	6	6	38.08	2.363	8	1.3	8	8	6	47.41	1.917	24	1.2
6	2	2	24.04	3.702	24	13.7	10	2	2	38.08	2.363	24	0.2	10	8	0	47.41	1.917	24	0.6
4	4	4	25.13	3.544	8	0.3	8	6	4	39.53	2.280	48	0.2	10	8	2	48.02	1.894	48	1.8
6	4	0	26.17	3.405	24	0.6	10	4	0	39.53	2.280	24	0.1	10	8	4	49.82	1.830	48	0.4
6	4	2	27.18	3.281	48	9.0	10	4	2	40.23	2.242	48	0.5							

Dehydrated Linde Type A

LTA



SOD

Sodalite octahydrate

COMPOSITION: $\text{Na}_6(\text{Si}_6\text{Al}_6\text{O}_{24}) \cdot 8\text{H}_2\text{O}$

CRYSTAL DATA: $P\bar{4}3n$ (No. 218)

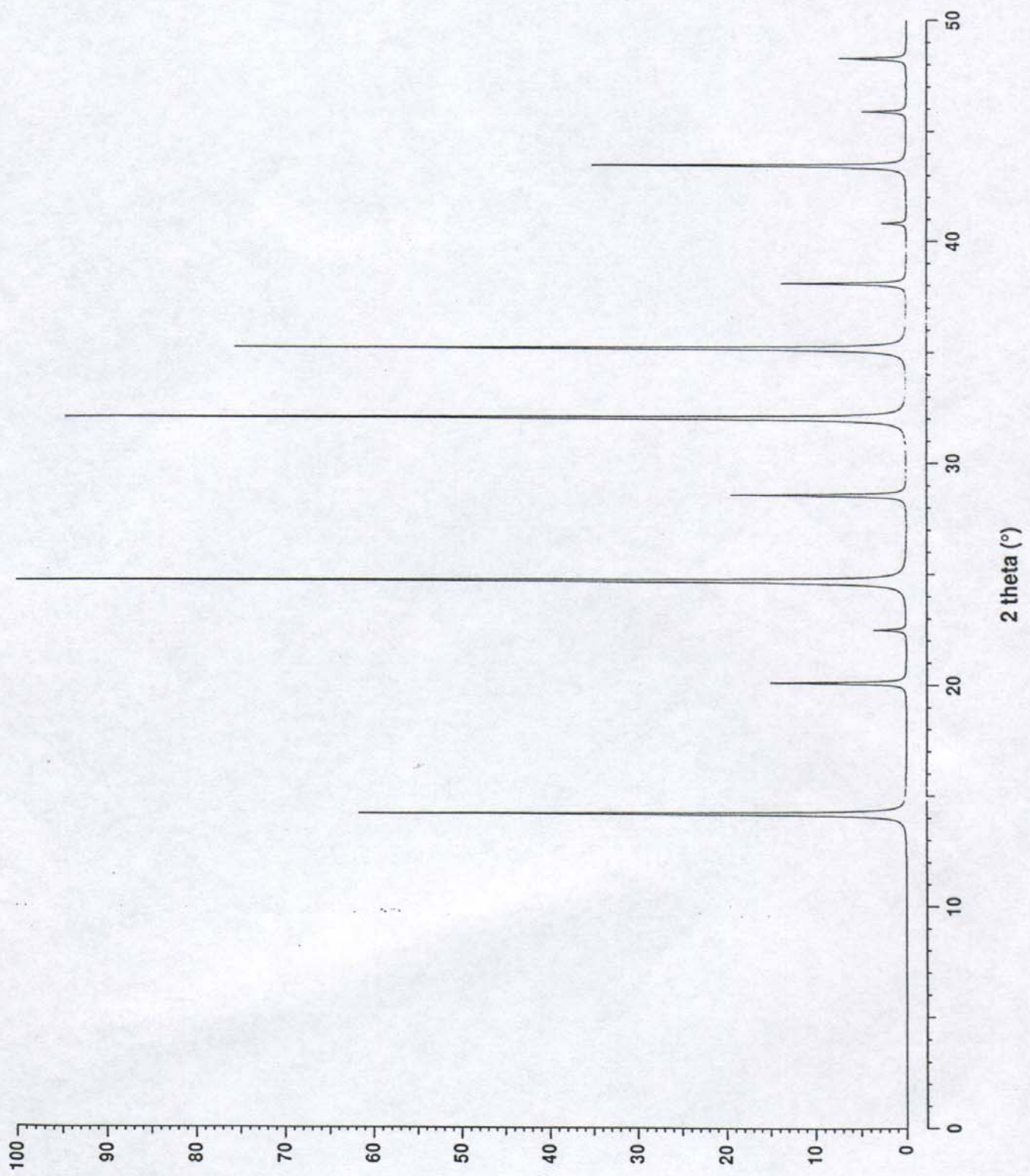
$a = 8.848 \text{ \AA}$ $b = 8.848 \text{ \AA}$ $c = 8.848 \text{ \AA}$
 $\alpha = 90^\circ$ $\beta = 90^\circ$ $\gamma = 90^\circ$

REFERENCE: J. Felsche, S. Luger and Ch. Baerlocher,
 Zeolites 6, 367-372 (1986).

<i>h</i>	<i>k</i>	<i>l</i>	2θ	<i>d</i>	<i>M</i>	<i>I</i> _{rel}	<i>h</i>	<i>k</i>	<i>l</i>	2θ	<i>d</i>	<i>M</i>	<i>I</i> _{rel}	<i>h</i>	<i>k</i>	<i>l</i>	2θ	<i>d</i>	<i>M</i>	<i>I</i> _{rel}	
1	1	0	14.16	6.257	12	61.8	3	1	0	31.99	2.798	24	94.6	4	1	1	43.39	2.086	24	19.6	
2	0	0	20.07	4.424	6	15.1	2	2	2	35.13	2.554	8	75.7	4	2	0	45.86	1.978	24	4.9	
2	1	0	22.47	3.957	24	3.6	3	2	1	38.05	2.365	48	13.9	4	2	1	47.06	1.931	48	0.1	
2	1	1	24.65	3.612	24	100.0	4	0	0	40.79	2.212	6	2.7	3	3	2	48.24	1.886	24	7.5	
2	2	0	28.53	3.128	12	19.6	3	3	0	43.39	2.086	12	15.8								

Sodalite octahydrate

SOD



Appendix C

XRD powder patterns of the synthesis products

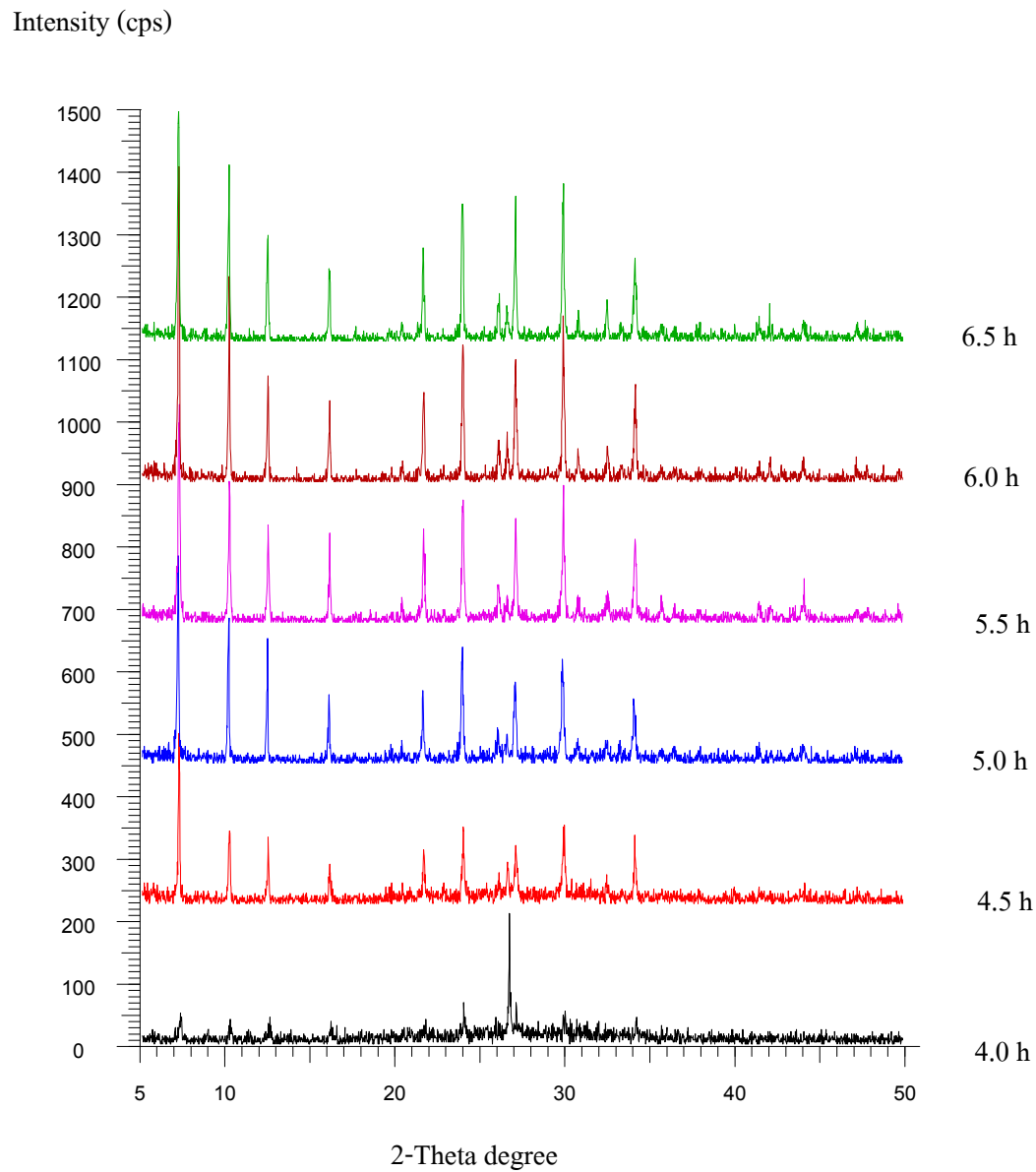


Figure A1 XRD powder patterns of the solid phases obtained in the synthesis of Narathiwat kaolin activated at 700°C with 15 % w/v NaOH concentration and reaction temperature 70°C for various times

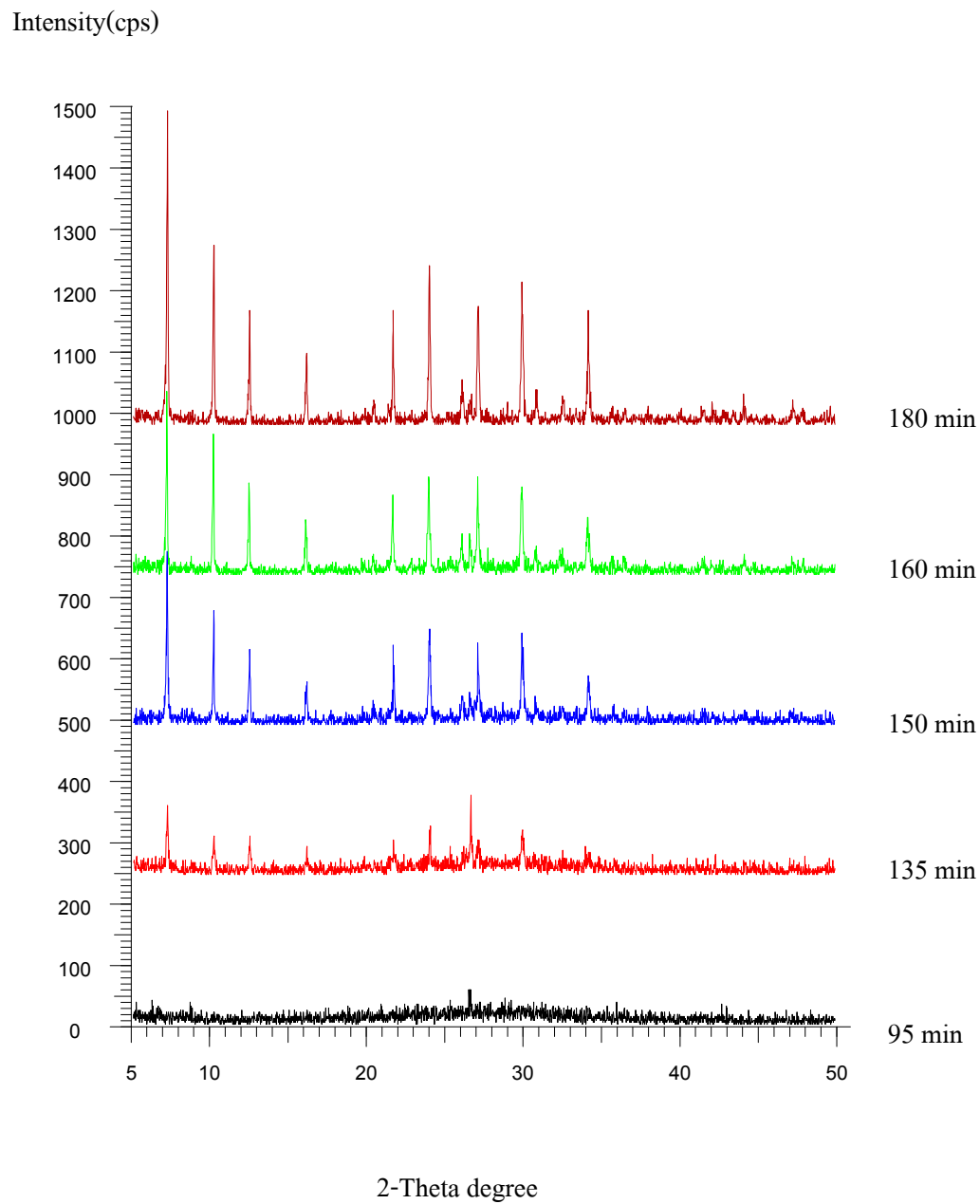


Figure A2 XRD powder patterns of the solid phases obtained in the synthesis of Narathiwat kaolin activated at 700°C with 20 % w/v NaOH concentration and reaction temperature 70°C for various times

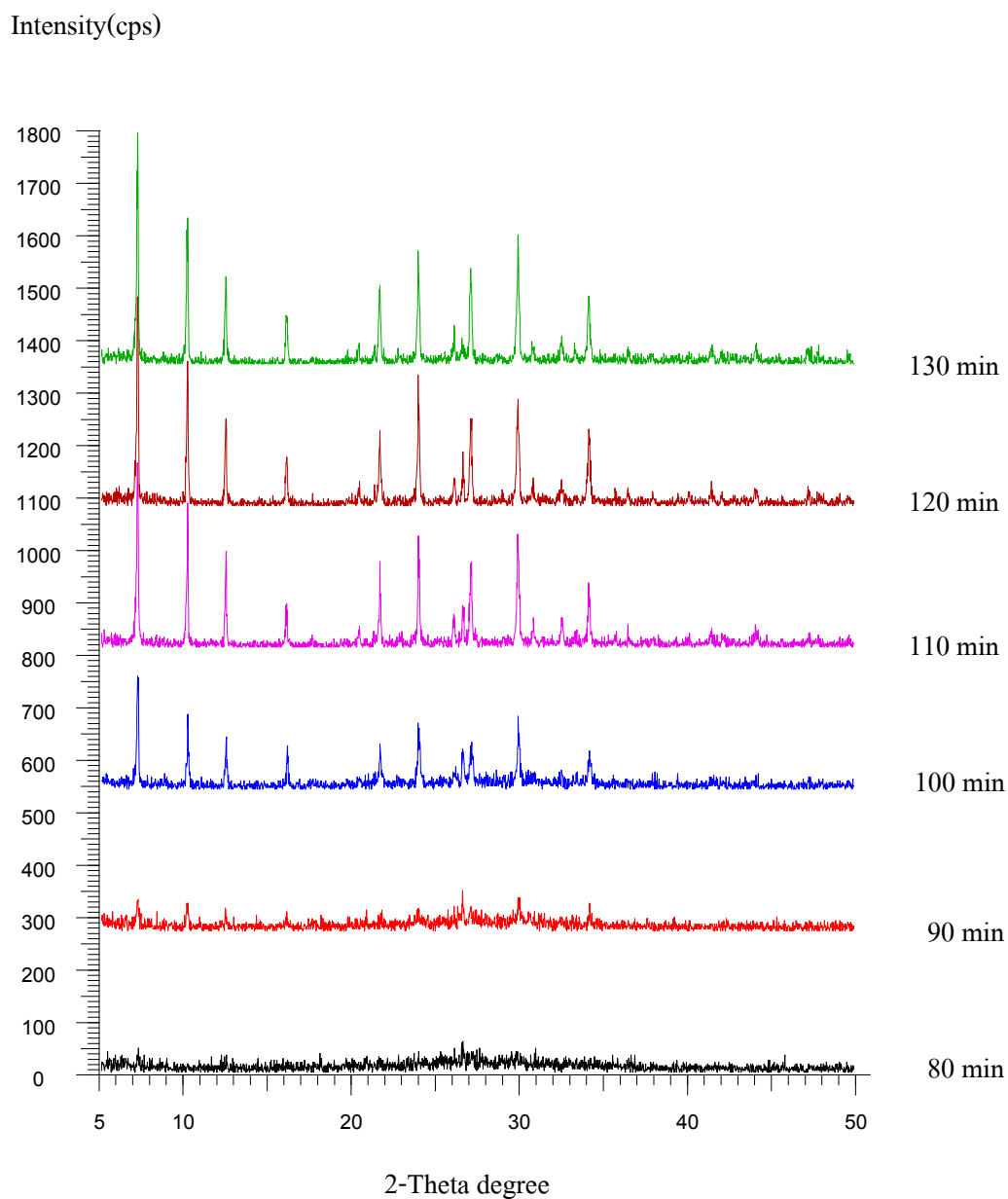


Figure A3 XRD powder patterns of the solid phases obtained in the synthesis of Narathiwat kaolin activated at 700°C with 25 % w/v NaOH concentration and reaction temperature 70°C for various times

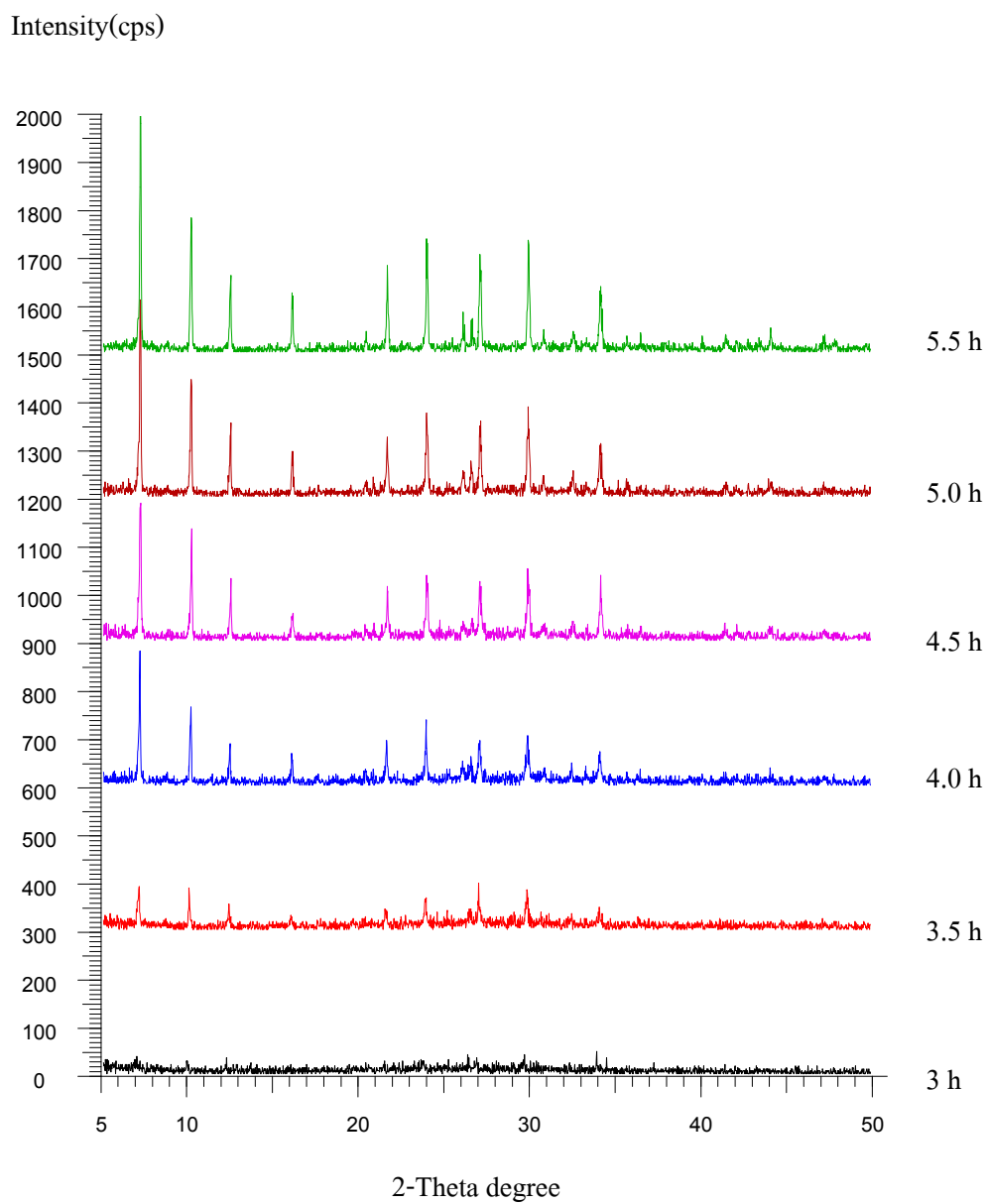


Figure A4 XRD powder patterns of the solid phases obtained in the synthesis of Narathiwat kaolin activated at 700⁰C with 10 % w/v NaOH concentration and reaction temperature 80⁰C for various times

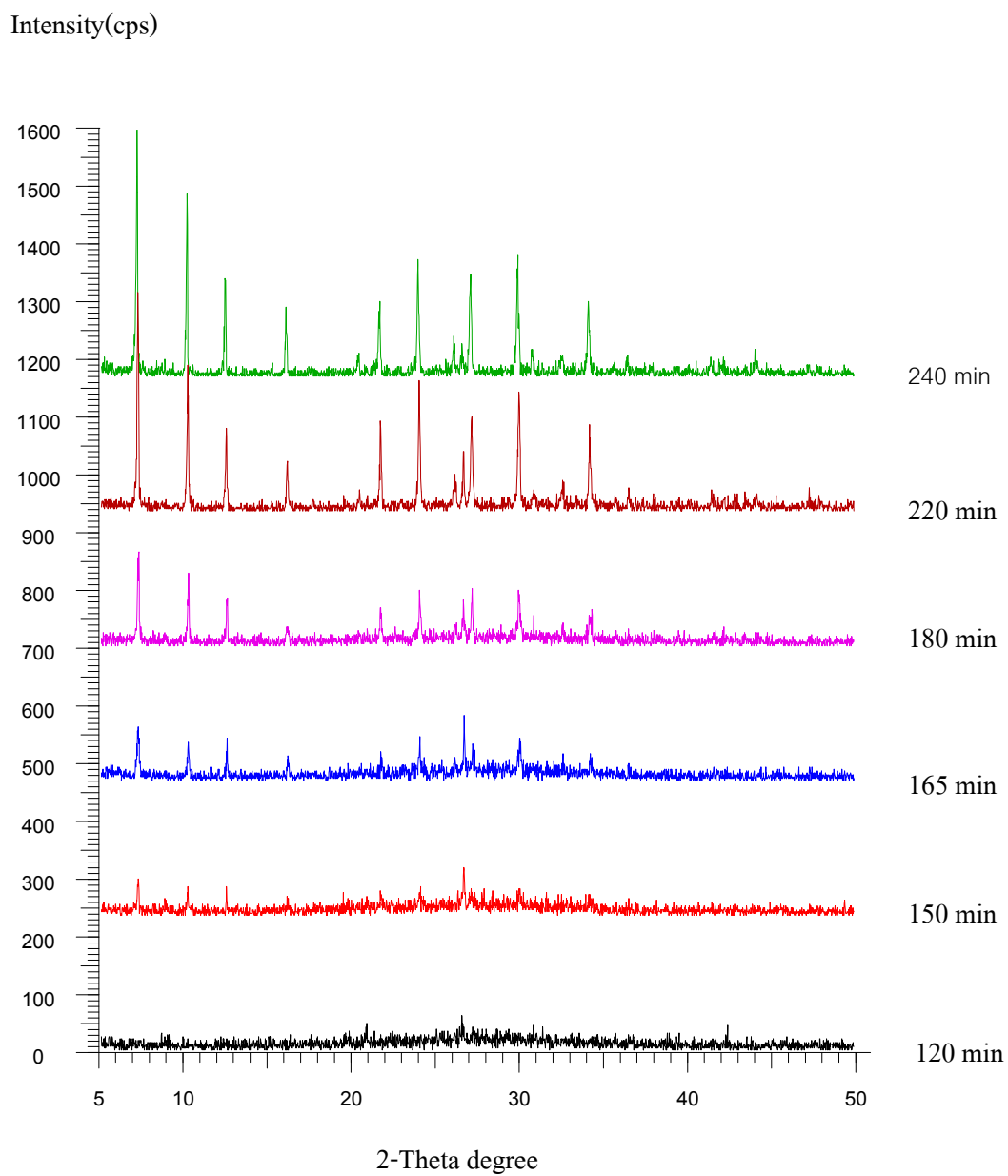


Figure A5 XRD powder patterns of the solid phases obtained in the synthesis of Narathiwat kaolin activated at 700⁰C with 15 % w/v NaOH concentration and reaction temperature 80⁰C for various times

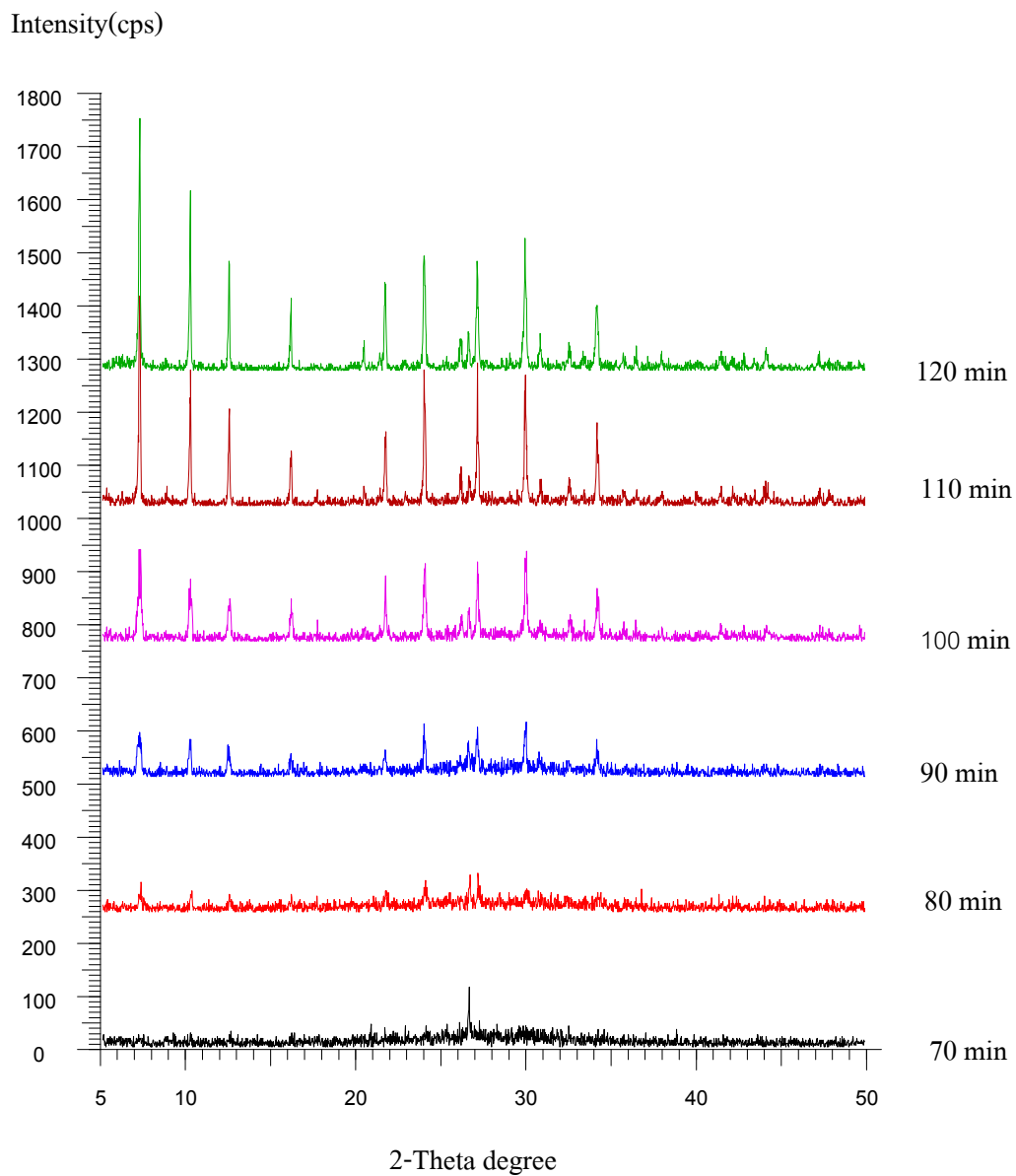


Figure A6 XRD powder patterns of the solid phases obtained in the synthesis of Narathiwat kaolin activated at 700⁰C with 20 % w/v NaOH concentration and reaction temperature 80⁰C for various times

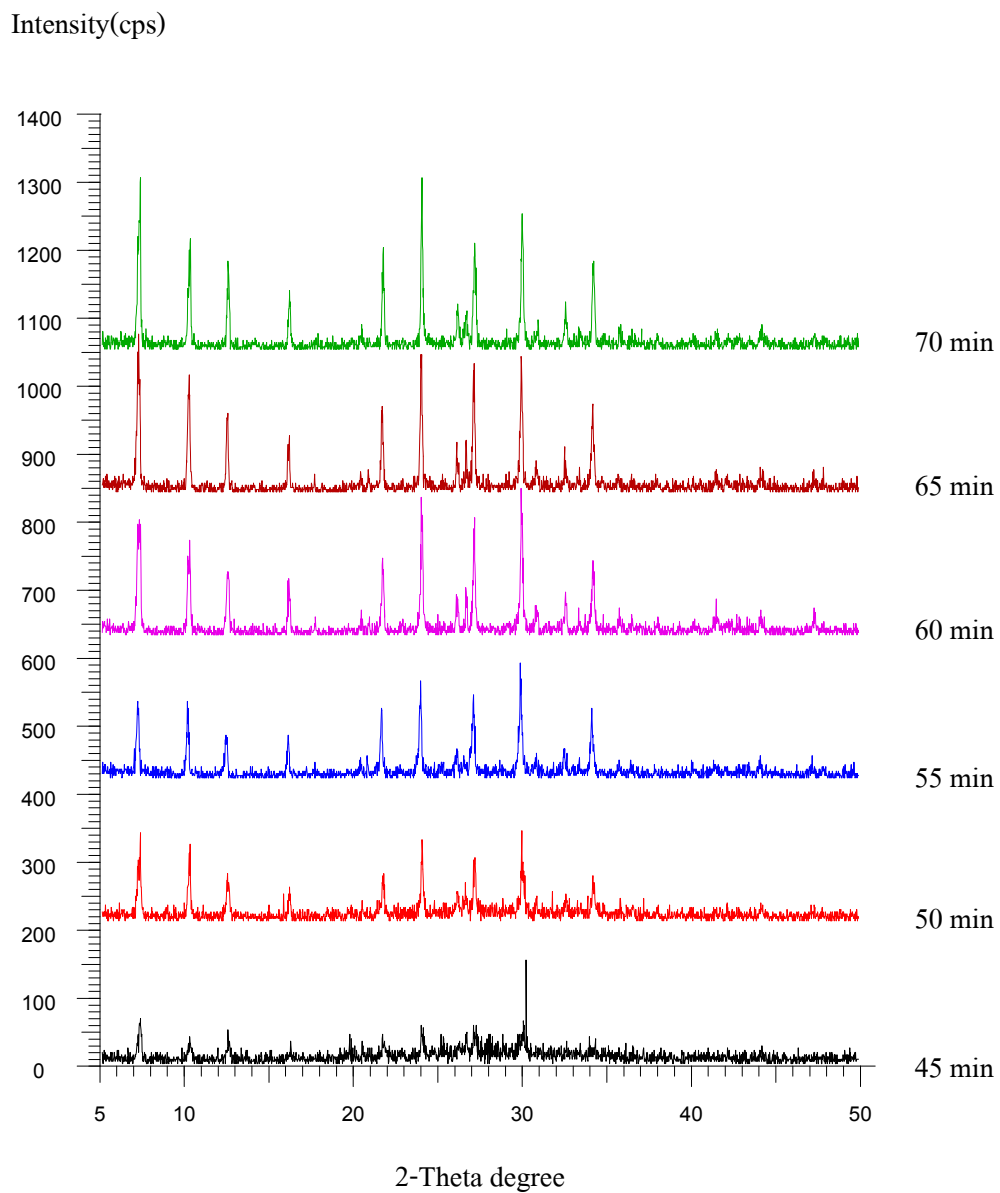


Figure A7 XRD powder patterns of the solid phases obtained in the synthesis of Narathiwat kaolin activated at 700°C with 25 % w/v NaOH concentration and reaction temperature 80°C for various times

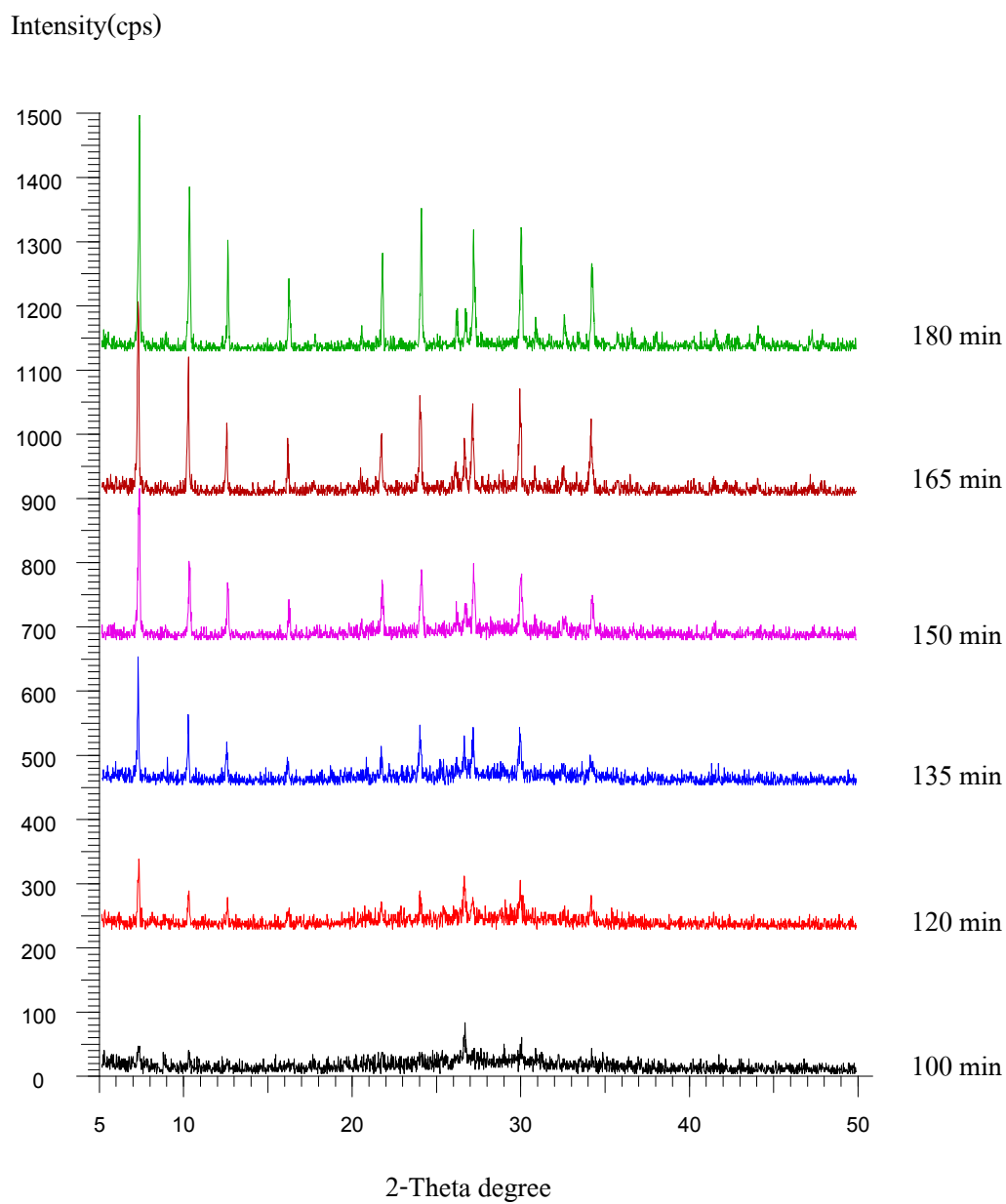


Figure A8 XRD powder patterns of the solid phases obtained in the synthesis of Narathiwat kaolin activated at 700°C with 10 % w/v NaOH concentration and reaction temperature 90°C for various times

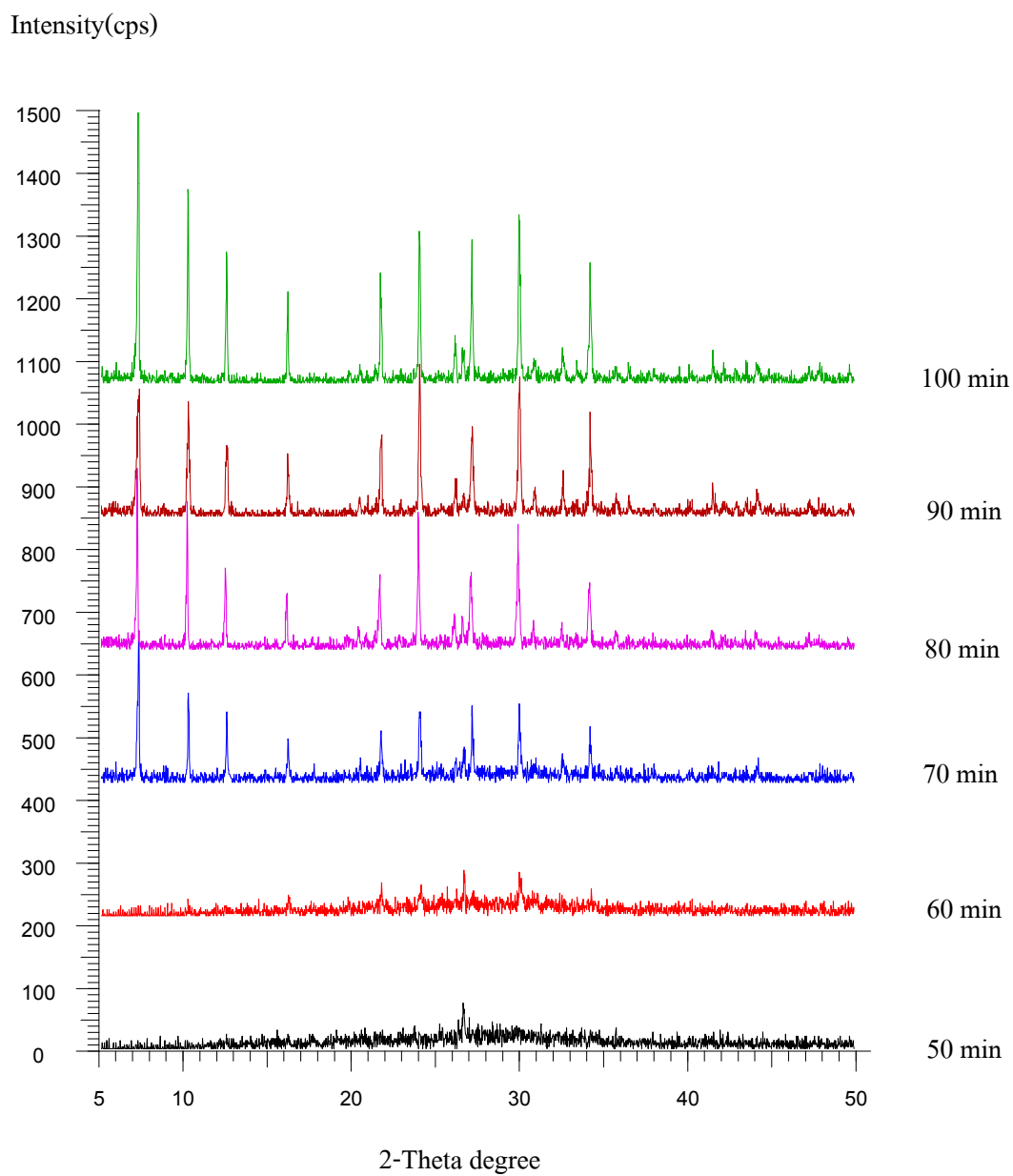


Figure A9 XRD powder patterns of the solid phases obtained in the synthesis of Narathiwat kaolin activated at 700⁰C with 15 % w/v NaOH concentration and reaction temperature 90⁰C for various times

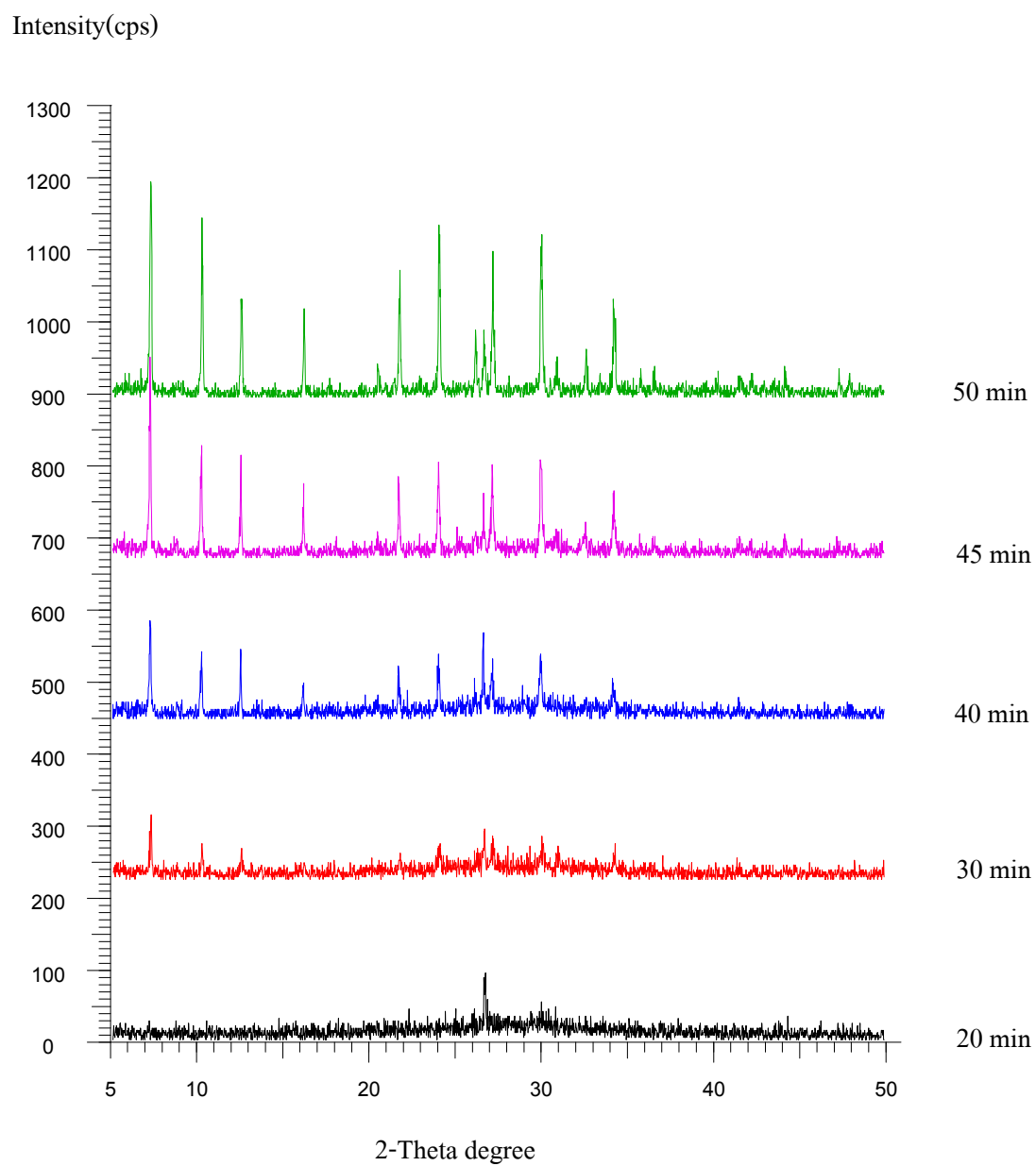


Figure A10 XRD powder patterns of the solid phases obtained in the synthesis of Narathiwat kaolin activated at 700⁰C with 20 % w/v NaOH concentration and reaction temperature 90⁰C for various times

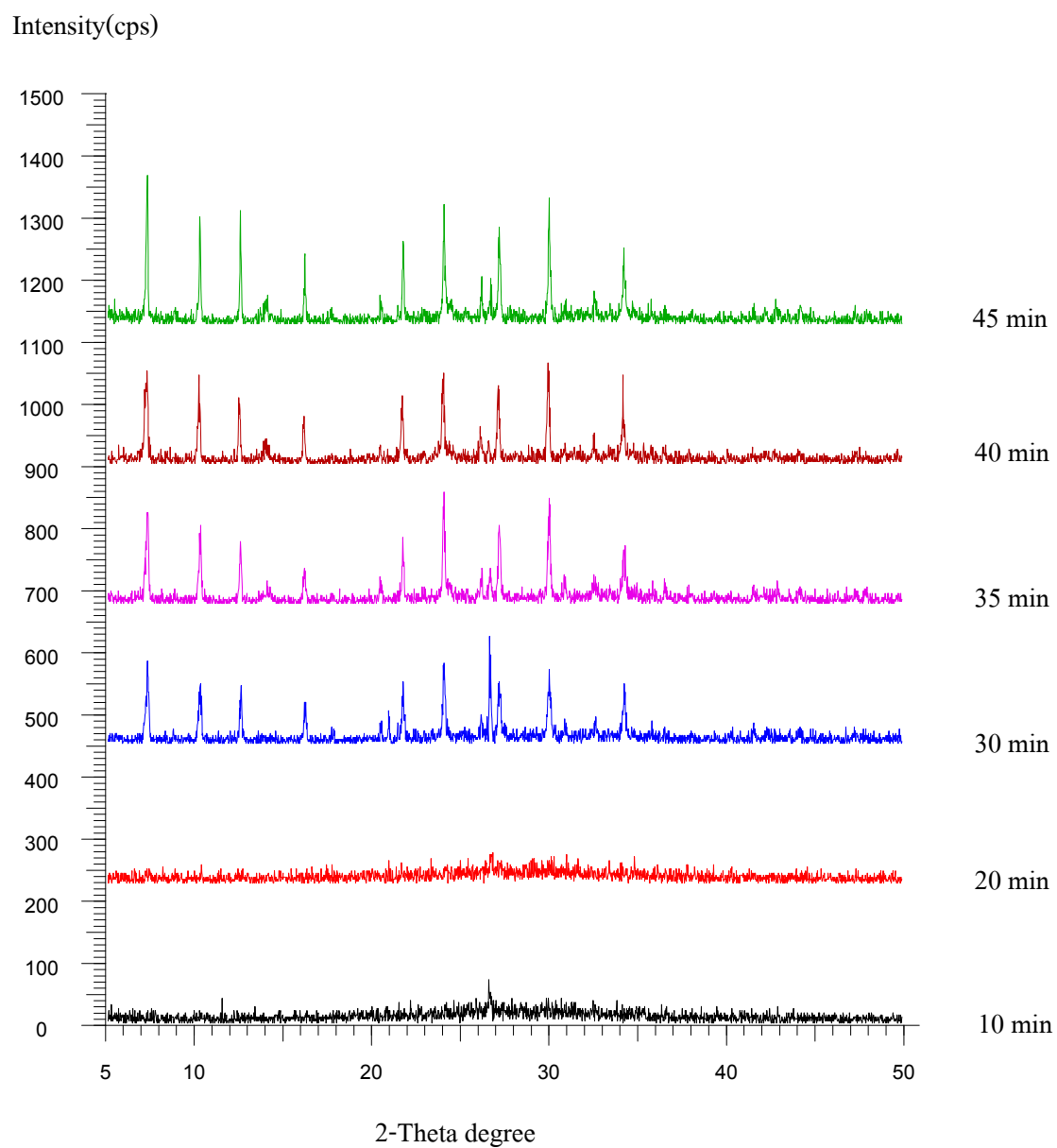


Figure A11 XRD powder patterns of the solid phases obtained in the synthesis of Narathiwat kaolin activated at 700⁰C with 25 % w/v NaOH concentration and reaction temperature 90⁰C for various times

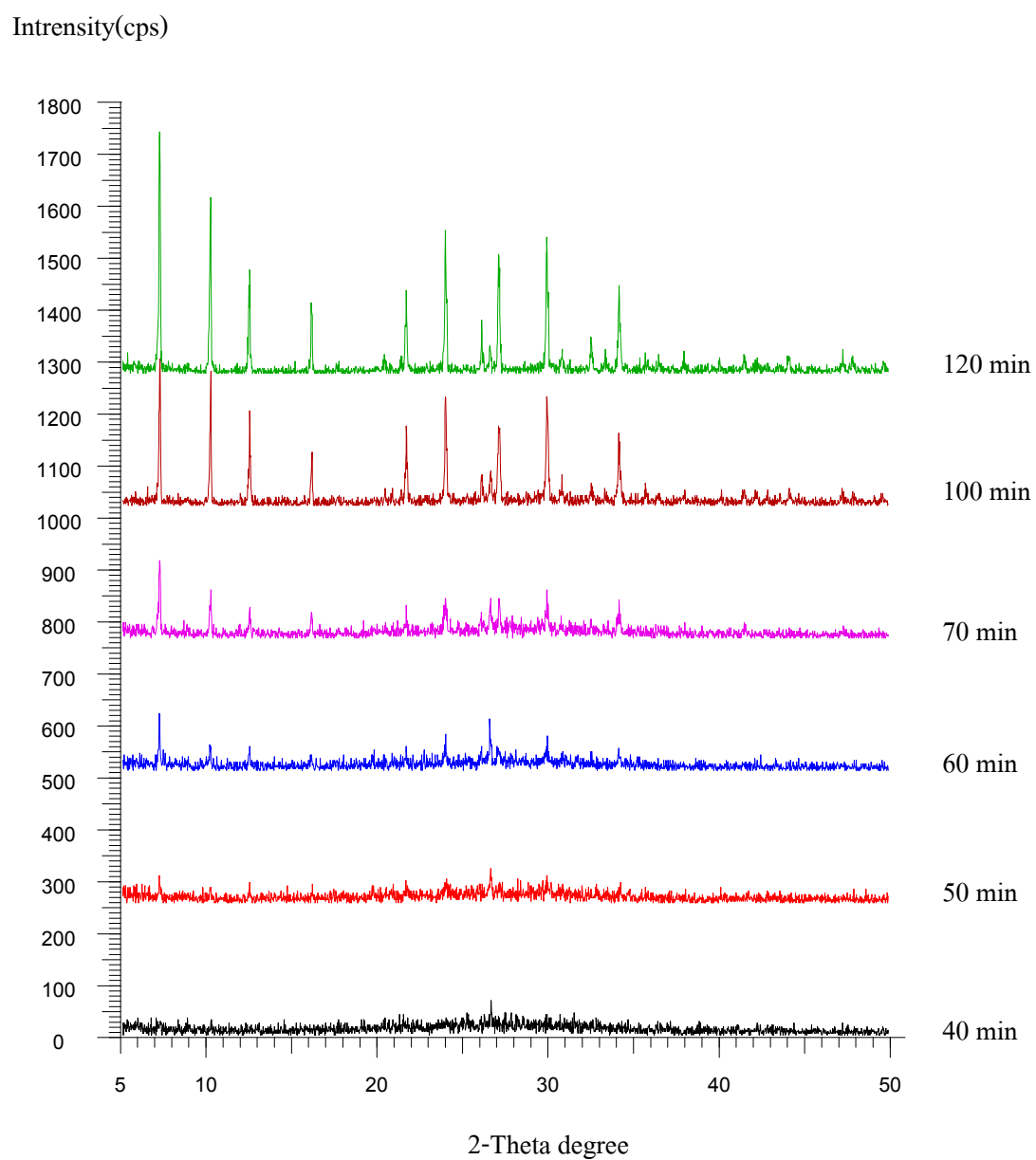


Figure A12 XRD powder patterns of the solid phases obtained in the synthesis of Narathiwat kaolin activated at 700⁰C with 10 % w/v NaOH concentration and reaction temperature 100⁰C for various times

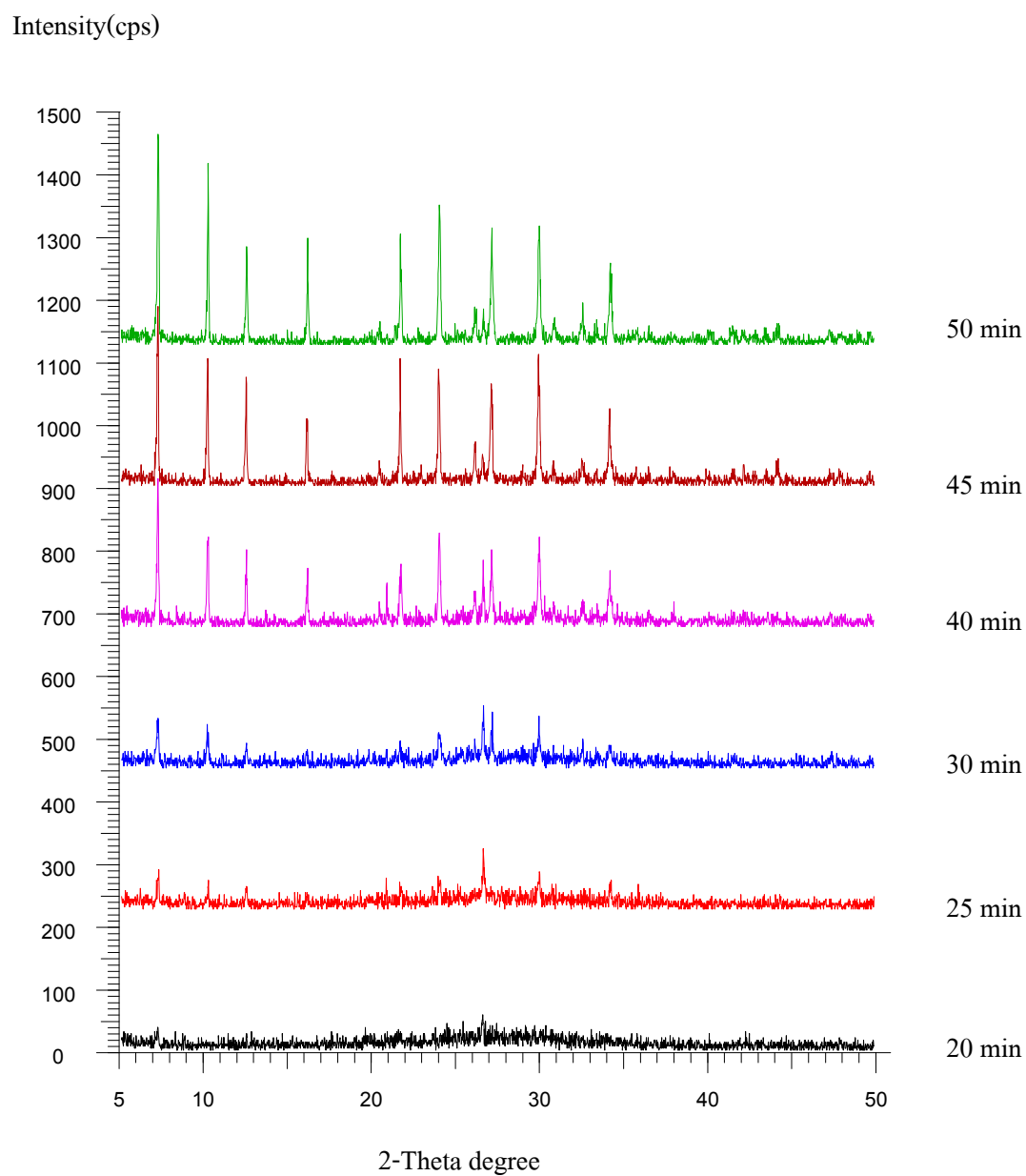


Figure A13 XRD powder patterns of the solid phases obtained in the synthesis of Narathiwat kaolin activated at 700⁰C with 15 % w/v NaOH concentration and reaction temperature 100⁰C for various times

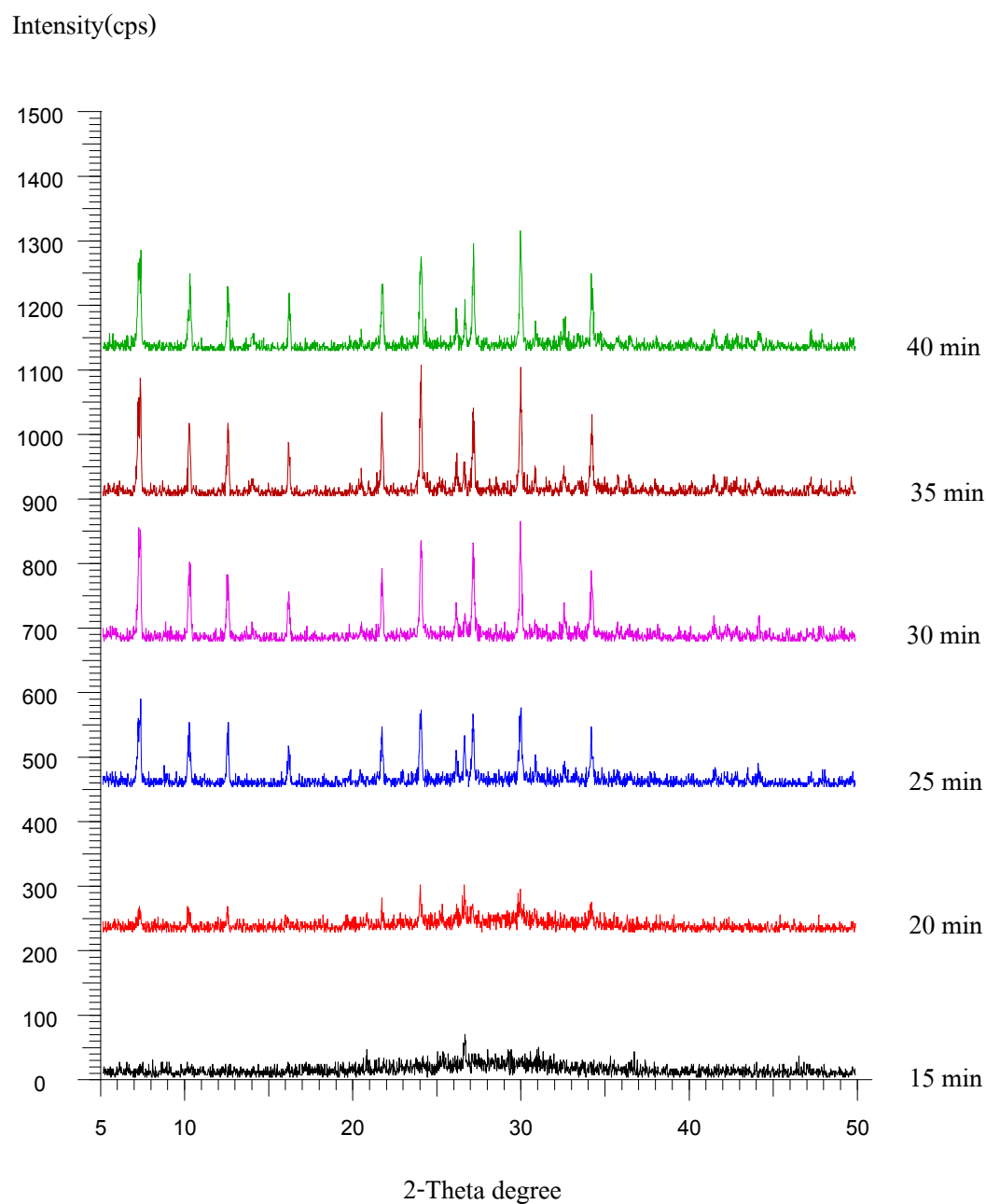


Figure A14 XRD powder patterns of the solid phases obtained in the synthesis of Narathiwat kaolin activated at 700°C with 20 % w/v NaOH concentration and reaction temperature 100°C for various times

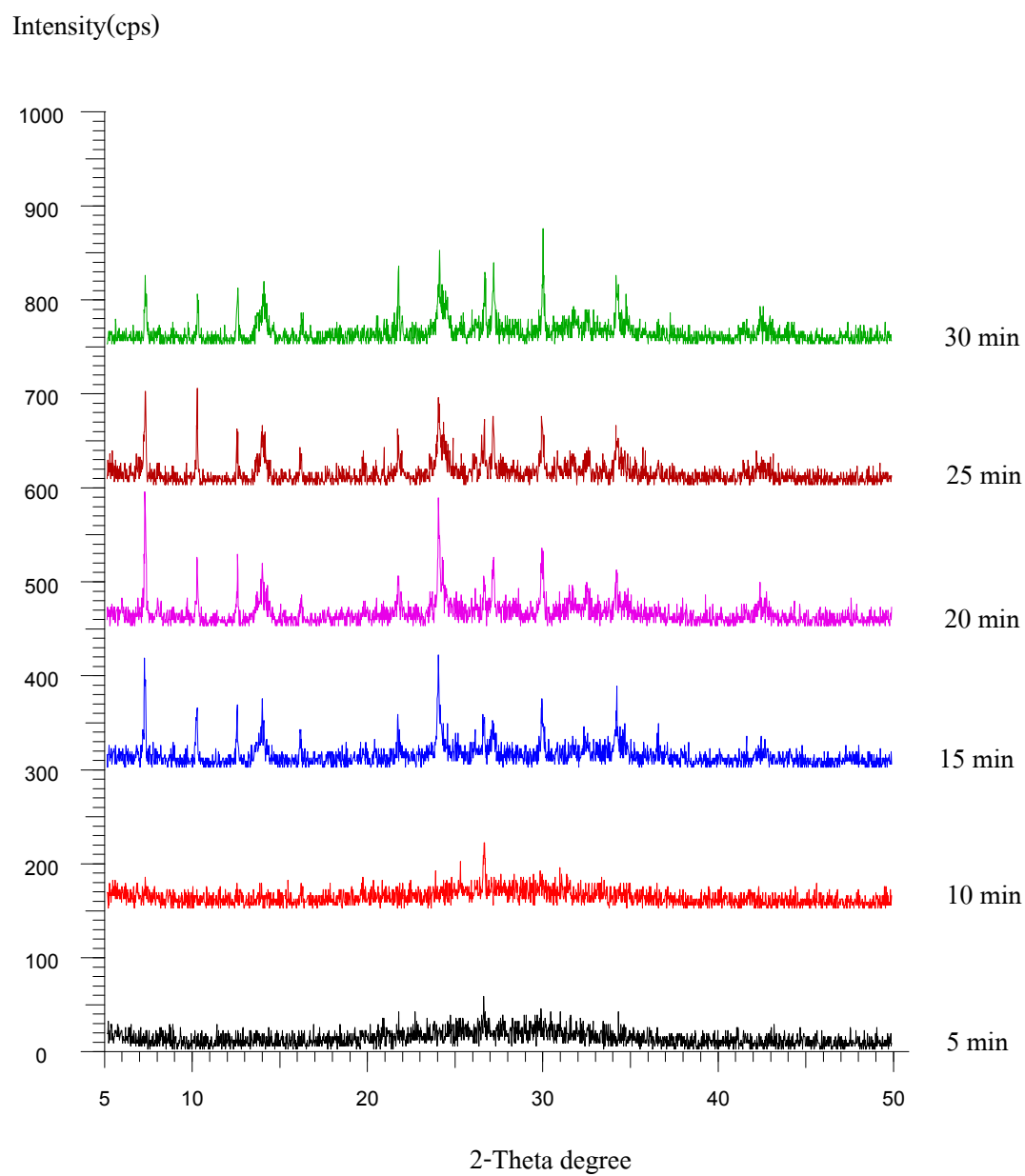


Figure A15 XRD powder patterns of the solid phases obtained in the synthesis of Narathiwat kaolin activated at 700⁰C with 25 % w/v NaOH concentration and reaction temperature 100⁰C for various times

Curriculum Vitae

JANJIRA WONGWIWATTANA

Born: June 27, 1971, Nakhon Ratchasima

Citizenship: Thailand

Education

1989-1992 B.Sc. Chemistry
 Khon kaen University, Khon kaen, Thailand

Experience

1993-1995 Scientist, Department of Fuel
 Ministry of Commercial

1995-1998 Scientist, Department of Pollutant Control
 Ministry of Science and Technology

1998-Present Scientist, Center for Scientific and Technological Equipment
 Suranaree University of Technology

Presentation

“Synthesis and Kinetic study of Zeolite Na-A from Thai Kaolin”, (with Kunwadee Rangriwatananon), The 3rd National Symposium on Graduated Research, 18-19 July 2002, Suranaree University of Technology, Thailand.